HYDRODYNAMIC, SURVEY AND SEDIMENT DATA COLLECTION BOMBAY HOOK NATIONAL WILDLIFE REFUGE, DELAWARE

Mithun Deb[1], Ali Abdolali[2,3], Conor McDowell[4], James T. Kirby[1], Chris Sommerfield[4], and Fengyan Shi[1]

[1]Center for Applied Coastal Research, Department of Civil and Environmental Engineering, University of Delaware, Newark, DE 19716 USA

[2]NWS/NCEP/Environmental Modeling Center, National Oceanic and Atmospheric Administration (NOAA), College Park MD 20740 USA

[3]University Corporation for Atmospheric Research (UCAR), Boulder, CO 80301 USA

[4]College of Earth, Ocean and Environment, University of Delaware, Lewes, DE USA

RESEARCH REPORT NO. CACR-18-03

RESEARCH SUPPORTED BY THE NATIONAL FISH AND WILDLIFE FOUNDATION, GRANT #43752

CENTER FOR APPLIED COASTAL RESEARCH

University of Delaware

Newark, DE 19716

Abstract

This report describes the collection of data in support of the development and validation of a 3D numerical code for simulating hydrodynamic and sediment processes in Bombay Hook National Wildlife Refuge, Delaware. The hydrodynamic data consisted of water level measurements, high frequency pressure measurements for surface wave estimation, and current profiling. Surveying was conducted to obtain ground truth measurements of marsh surface elevation to use in vegetation bias correction, and surveys of channels within the marsh system. Additional work on collection of sediment cores and analysis of sediment accretion rates is described separately by McDowell (2017). Modeling results are reported in Deb et al (2018).

Contents

1 Water level data **1**

1.1 Barometric pressure 1

1.2 Water level sensors deployed on the marsh platform 2

1.2.1 Onset Hobo gauge 2

1.2.2 Hobo deployments and data files 2

1.2.3 Data processing 3

2 High frequency pressure measurements in Money Marsh **11**

2.1 RBRsolo D pressure gauges 11

2.2 Instrument deployment and location 11

2.3 Data collection 12

2.4 RBRsolo data 13

2.4.1 RBRsolo filenames and deployment period 13

2.4.2 Data processing 13

3 Current data **40**

3.1 Aquadopp profiler 40

3.1.1 Data processing 40

4 Bathymetric/topographic data **65**

5 Survey data **65**

5.1 Marsh platform surveys 65

5.2 Survey of marsh channels 68

6 Sediment coring and accretion analysis. 74

A Technical specifications of Onset Hobo tide gauge 74

B Technical specifications of RBRsolo wave gauge 75

C Technical specifications of Aquadopp current profiler 76

List of Figures

1 Barometric pressure data (in dBar) from April - October, 2015 [filename: `Barometric.mat`] 1

2 Hobo deployment locations, May - October 2015 3

3 (a) Hobo raw pressure p_m^1 (Kpa), (b) calculated water surface elevation η^1 (m), (c) temperature (°C) at location 1 from May-July 2015. 4

4 (a) Hobo raw pressure p_m^1 (Kpa), (b) calculated water surface elevation η^1 (m), (c) temperature (°C) at location 1 from July-October 2015. 5

5 (a) Hobo raw pressure p_m^2 (Kpa), (b) calculated water surface elevation η^2 (m), (c) temperature (°C) at location 2 from May-July 2015. 5

6 (a) Hobo raw pressure p_m^2 (Kpa), (b) calculated water surface elevation η^2 (m), (c) temperature (°C) at location 2 from July-October 2015. 6

7 (a) Hobo raw pressure p_m^3 (Kpa), (b) calculated water surface elevation η^3 (m), (c) temperature (°C) at location 3 from May-July 2015. 6

8 (a) Hobo raw pressure p_m^3 (Kpa), (b) calculated water surface elevation η^3 (m), (c) temperature (°C) at location 3 from July-October 2015. 7

9 (a) Hobo raw pressure p_m^4 (Kpa), (b) calculated water surface elevationη^4 (m), (c) temperature (°C) at location 4 from May-July 2015. 7

10 (a) Hobo raw pressure p_m^4 (Kpa), (b) calculated water surface elevation η^4 (m), (c) temperature (°C) at location 4 from July-October 2015. 8

11 (a) Hobo raw pressure p_m^5 (Kpa), (b) calculated water surface elevation η^5 (m), (c) temperature (°C) at location 5 from May-July 2015. 8

12 (a) Hobo raw pressure p_m^5 (dKpa), (b) calculated water surface elevation η^5 (m), (c) temperature (°C) at location 5 from July-October 2015. 9

13 (a) Hobo raw pressure p_m^6 (Kpa), (b) calculated water surface elevation η^6 (m), (c) temperature (°C) at location 6 from May-July, 2015. 9

14 (a) Hobo raw pressure p_m^6 (Kpa), (b) calculated water surface elevation η^6 (m), (c) temperature (°C) at location 6 from July-October 2015. 10

15 RBR pressure sensor mounted on expanded metal grating. 12

16 Pressure gauge positions in the Money Marsh tidal flat. 13

17 RBRsolo wave gauge raw pressure data at location 1 and 2 from March 31 - April 23, 2015 [filenames: `RBR1_20150423.mat` & `RBR2_20150423.mat`] 15

18 RBRsolo wave gauge raw pressure data at location 1 and 2 from April 23 - May 15, 2015 [filenames: `RBR1_20150515.mat` & `RBR2_20150515.mat`] 16

19 RBRsolo wave gauge raw pressure data at location 1 and 2 from May 15 - June 3, 2015 [filenames: `RBR1_20150603.mat` & `RBR2_20150603.mat`] 17

20 RBRsolo wave gauge raw pressure data at location 1 and 2 from June 3 - June 24, 2015 [filenames: `RBR1_20150624.mat` & `RBR2_20150624.mat`] 18

21 RBRsolo wave gauge raw pressure data at location 1 and 2 from June 24 - July 14, 2015 [filenames: `RBR1_20150714.mat` & `RBR2_20150714.mat`] 19

22 RBRsolo wave gauge raw pressure data at location 1 and 2 from July 14 - August 4, 2015 [filenames: `RBR1_20150804.mat` & `RBR2_20150804.mat`] 20

23 RBRsolo wave gauge raw pressure data at location 1 and 2 from August 4 - August 28, 2015 [filenames: `RBR1_20150828.mat` & `RBR2_20150828.mat`] 21

24 RBRsolo wave gauge raw pressure data at location 1 and 2 from August 28 - September 21, 2015 [filenames: `RBR1_20150921.mat` & `RBR2_20150921.mat`] 22

25 RBRsolo wave gauge raw pressure data at location 1 and 2 from September 21 - October 16, 2015 [filenames: `RBR1_20151016.mat` & `RBR2_20151016.mat`] 23

26 RBRsolo wave gauge raw pressure data at location 1 and 2 from October 16 - November 17, 2015 [filenames: `RBR1_20151117.mat` & `RBR2_20151117.mat`] 24

27 RBRsolo wave gauge raw pressure data at location 1 and 2 from December 9, 2015 - January 8, 2016 [filenames: `RBR1_20160108.mat` & `RBR2_20160108.mat`] 25

28 (a) Significant wave height, Hs (m) and Peak wave period, Tp (s) calculated using the linear wave theory and spectral analysis at location 1 from March 31 - April 23, 2015 (b) Histogram of the wind wave properties. [filename: `RBR1_20150423.mat`] . . 26

29 (a) Significant wave height, Hs (m) and Peak wave period, Tp (s) calculated using the linear wave theory and spectral analysis at location 1 from April 23 - May 15, 2015 (b) Histogram of the wind wave properties. [filename: `RBR1_20150515.mat`] . . 27

30 (a) Significant wave height, Hs (m) and Peak wave period, Tp (s) calculated using the linear wave theory and spectral analysis at location 1 from June 3 - June 24, 2015 (b) Histogram of the wind wave properties. [filename: `RBR1_20150624.mat`] 28

31 (a) Significant wave height, Hs (m) and Peak wave period, Tp (s) calculated using the linear wave theory and spectral analysis at location 1 from June 24 - July 14, 2015 (b) Histogram of the wind wave properties. [filename: `RBR1_20150714.mat`] . . 29

32 (a) Significant wave height, Hs (m) and Peak wave period, Tp (s) calculated using the linear wave theory and spectral analysis at location 1 from July 14 - August 4, 2015 (b) Histogram of the wind wave properties. [filename: `RBR1_20150804.mat`] . . 30

33 (a) Significant wave height, Hs (m) and Peak wave period, Tp (s) calculated using the linear wave theory and spectral analysis at location 1 from August 4 - August 28, 2015 (b) Histogram of the wind wave properties. [filename: `RBR1_20150828.mat`] 31

34 (a) Significant wave height, Hs (m) and Peak wave period, Tp (s) calculated using the linear wave theory and spectral analysis at location 1 from August 28 - September 21, 2015 (b) Histogram of the wind wave properties. [filename: `RBR1_20150921.mat`] 32

35 (a) Significant wave height, Hs (m) and Peak wave period, Tp (s) calculated using the linear wave theory and spectral analysis at location 2 from March 31 - April 23, 2015 (b) Histogram of the wind wave properties. [filename: `RBR2_20150423.mat`] . . 33

36 (a) Significant wave height, Hs (m) and Peak wave period, Tp (s) calculated using the linear wave theory and spectral analysis at location 2 from June 3 - June 24, 2015 (b) Histogram of the wind wave properties. [filename: `RBR2_20150624.mat`] 34

37 (a) Significant wave height, Hs (m) and Peak wave period, Tp (s) calculated using the linear wave theory and spectral analysis at location 2 from June 24 - July 14, 2015 (b) Histogram of the wind wave properties. [filename: `RBR2_20150714.mat`] . . 35

38 (a) Significant wave height, Hs (m) and Peak wave period, Tp (s) calculated using the linear wave theory and spectral analysis at location 2 from July 14 - August 4, 2015 (b) Histogram of the wind wave properties. [filename: `RBR2_20150804.mat`] . . 36

39 (a) Significant wave height, Hs (m) and Peak wave period, Tp (s) calculated using the linear wave theory and spectral analysis at location 2 from August 4 - August 28, 2015 (b) Histogram of the wind wave properties. [filename: `RBR2_20150828.mat`] 37

40 (a) Significant wave height, Hs (m) and Peak wave period, Tp (s) calculated using the linear wave theory and spectral analysis at location 2 from August 28 - September 17, 2015 (b) Histogram of the wind wave properties. [filename: `RBR2_20150921.mat`] 38

41 (a) Significant wave height, Hs (m) and Peak wave period, Tp (s) calculated using the linear wave theory and spectral analysis at location 2 from September 21 - October 16, 2015 (b) Histogram of the wind wave properties. [filename: `RBR2_20151016.mat`] 39

42 Position and orientation of the Aquadopp HR-profiler at location A during deployment and retrieval [filename: `AquaA_20150612.csv`] 42

43 Aquadopp HR-profiler Heading, Pitch and Roll at location A during April 16 - June 12, 2015 42

44 Pressure and temperature variation at location A. We can notice that the instrument shifted several times from its origin. Hence, the recorded data is separated into four segments in the following figures. 43

45 Depth varying velocity (in m/s) [on the left], and depth averaged velocity and pressure (in dBar, blue line) [on the right] for segment 1 (location A) 44

46 Direction and magnitude of depth averaged velocity (in m/s) [on the left], Histogram of the flow velocity and direction [on the right] for segment 1 (location A). 44

47 Depth varying velocity (in m/s) [on the left], and depth averaged velocity and pressure (in dBar, blue line) [on the right] for segment 2 (location A). 45

48 Direction and magnitude of depth averaged velocity (in m/s) [on the left], Histogram of the flow velocity and direction [on the right] for segment 2 (location A) 45

49 Depth varying velocity (in m/s) [on the left], and depth averaged velocity and pressure (in dBar, blue line) [on the right] for segment 3 (location A) 46

50 Direction and magnitude of depth averaged velocity (in m/s) [on the left], Histogram of the flow velocity and direction [on the right] for segment 3 (location A) 46

51 Depth varying velocity (in m/s) [on the left], and depth averaged velocity and pressure (in dBar, blue line) [on the right] for segment 4 (location A) 47

52 Direction and magnitude of depth averaged velocity (in m/s) [on the left], Histogram of the flow velocity and direction [on the right] for segment 4 (location A) 47

53 Position and orientation of the Aquadopp HR-profiler at location B during deployment and retrieval [filename: `AquaB_20150612.csv`] 48

54 Aquadopp HR-profiler Heading, Pitch and Roll at location B during April 16 - June 12, 2015 48

55 Pressure and temperature variation at location B. We can notice that the instrument shifted several times from its origin. Hence, the recorded data is separated into two segments in the following figures. 49

56 Depth varying velocity (in m/s) [upper subplot], and depth averaged velocity and pressure (in dBar, blue line) [lower subplot] for segment 1 (location B) 50

57 Direction and magnitude of depth averaged velocity (in m/s) [on the left], Histogram of the flow velocity and direction [on the right] for segment 1 (location B) 50

58 Depth varying velocity (in m/s) [upper subplot], and depth averaged velocity and pressure (in dBar, blue line) [lower subplot] for segment 2 (location B) 51

59 Direction and magnitude of depth averaged velocity (in m/s) [on the left], Histogram of the flow velocity and direction [on the right] for segment 2 (location B) 51

60 Position and orientation of the Aquadopp HR-profiler at location C during deployment and retrieval [filename: `AquaC_20150612.csv`] 52

61 Aquadopp HR-profiler Heading, Pitch and Roll at location C during April 16 - June 12, 2015 52

62 Pressure and temperature variation at location C. We can notice that the instrument shifted several times from its origin. Hence, the recorded data is separated into two segments in the following figures. 53

63 Depth varying velocity (in m/s) [on the left], and depth averaged velocity and pressure (in dBar, blue line) [on the right] for segment 1 (location C) 54

64 Direction and magnitude of depth averaged velocity (in m/s) [on the left], Histogram of the flow velocity and direction [on the right] for segment 1 (location C) 54

65 Depth varying velocity (in m/s) [upper subplot], and depth averaged velocity and pressure (in dBar, blue line) [lower subplot] for segment 2 (location C) 55

66 Direction and magnitude of depth averaged velocity (in m/s) [on the left], Histogram of the flow velocity and direction [on the right] for segment 2 (location C) 55

67 Position and orientation of the Aquadopp HR-profiler at location D during deployment and retrieval [filename: `AquaD_20150612.csv`] 56

68 Aquadopp HR-profiler Heading, Pitch and Roll at location D during April 16 - June 12, 2015 56

69 Pressure and temperature variation at location D. The recorded data is separated into multiple segments in the following figures. 57

70 Depth varying velocity (in m/s) [upper subplot], and depth averaged velocity and pressure (in dBar, blue line) [lower subplot] from April 16 - May 1, 2015 (location D) 58

71 Depth varying velocity (in m/s) [upper subplot], and depth averaged velocity and pressure (in dBar, blue line) [lower subplot] from May 1 - May 15, 2015 (location D) 58

72 Depth varying velocity (in m/s) [upper subplot], and depth averaged velocity and pressure (in dBar, blue line) [lower subplot] from May 15 - May 29, 2015 (location D) 59

73 Depth varying velocity (in m/s) [upper subplot], and depth averaged velocity and pressure (in dBar, blue line) [lower subplot] from May 29 - June 12, 2015 (location D) 59

74 Direction and magnitude of depth averaged velocity (in m/s) [on the left], Histogram of the flow velocity and direction [on the right] (location D) 60

75 Position and orientation of the Aquadopp HR-profiler at location E during deployment and retrieval [filename: `AquaE_20150612.csv`] 61

76 Aquadopp HR-profiler Heading, Pitch and Roll at location E during April 16 - June 12, 2015 61

77 Pressure and temperature variation at location E. We can notice that the instrument shifted several times from its origin. Hence, the recorded data is separated into two segments in the following figures. 62

78 Depth varying velocity (in m/s) [upper subplot], and depth averaged velocity and pressure (in dBar, blue line) [lower subplot] for segment 1 (location E) 63

79 Direction and magnitude of depth averaged velocity (in m/s) [on the left], Histogram of the flow velocity and direction [on the right] for segment 1 (location E) 63

80 Depth varying velocity (in m/s) [upper subplot], and depth averaged velocity and pressure (in dBar, blue line) [lower subplot] for segment 2 (location E) 64

81 Direction and magnitude of depth averaged velocity (in m/s) [on the left], Histogram of the flow velocity and direction [on the right] for segment 2 (location E) 64

82 Marsh elevation survey track lines. Here, red represents survey points on the open marsh platform and yellow represents on marsh enclosed by impoundments. Data set filename: marsh_survey.csv and column header in the .csv file: Longitude (dec deg) | Latitude (dec deg) | Depth (m) | Longitude (UTM) | Latitude (UTM) | Zone . 66

83 Bathymetric survey track lines 70

84 Original bathymetric data: a) Horizontal view, c) transect; Modified bathymetric data b) Horizontal view, d) transect 71

85 Original Bathymetric data, interpolated within channel boundaries 72

86 Modified Bathymetric data, interpolated within channel boundaries 73

1 Water level data

We deployed different types of pressure measurement devices in the mudflat and marsh platform to evaluate the hydrodynamics of the Bombay Hook National Wildlife Refuge (BHNWR) wetland system. Collected raw pressure datasets were then processed to obtain water surface elevation. Brief description about the pressure gauges and data post-processing are presented in the following sections.

1.1 Barometric pressure

Barometric pressure data has been collected from an atmospheric gauge in BHNWR, maintained by the Department of Natural Resources and Environmental Control (DNREC), State of Delaware. This data is used for atmospheric pressure correction of the measurement devices deployed on the mudflat and marsh platform. The data for the period of April - October 2015 is illustrated in Figure 1.

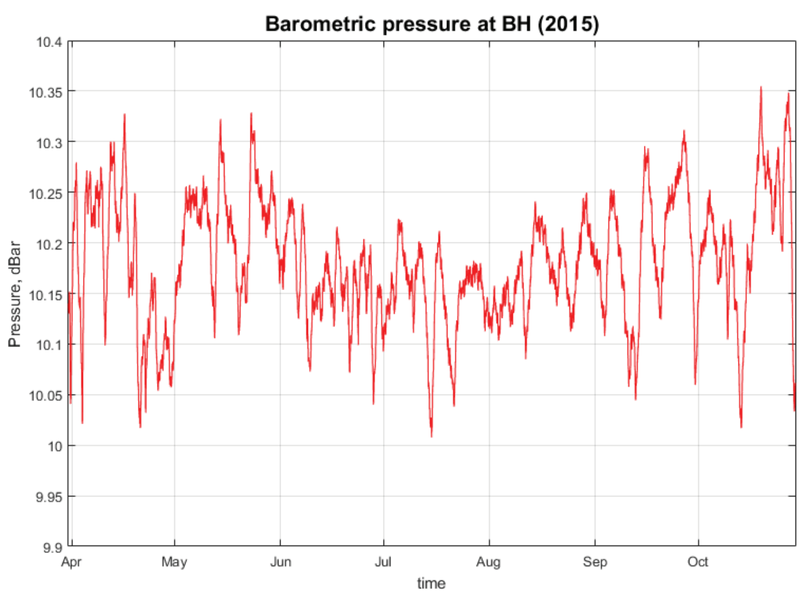

Figure 1: Barometric pressure data (in dBar) from April - October, 2015 [filename: `Barometric.mat`]

Gauge	Location (° N)	Location (° E)	Elevation z^n (m NAVD88)	5/27/15 - 7/26/15	7/26/15 - 10/6/15
1	39.247685	-75.464983)	0.68	hobo_1_07_2015.xlsx	hobo_1_10_2015.xlsx
2	39.248447	-75.463678)	0.75	hobo_2_07_2015.xlsx	hobo_2_10_2015.xlsx
3	39.249209	-75.462385)	0.67	hobo_3_07_2015.xlsx	hobo_3_10_2015.xlsx
4	39.250308	-75.461167)	0.75	hobo_4_07_2015.xlsx	hobo_4_10_2015.xlsx
5	39.250751	-75.459753)	0.74	hobo_5_07_2015.xlsx	hobo_5_10_2015.xlsx
6	39.251295	-75.458818)	0.51	hobo_6_07_2015.xlsx	hobo_6_10_2015.xlsx

Table 1: Deployment locations, surveyed gauge elevations, and data files for Hobo water level loggers.

1.2 Water level sensors deployed on the marsh platform

1.2.1 Onset Hobo gauge

Six Onset Hobo U20 water-level loggers were deployed continuously on the marsh platform to measure inundation depths during high tide or surge conditions. This small submersible pressure logger is capable of recording about 22,000 pressure and temperature samples at rates up to 1 Hz. Technical specification of the instrument along with the file type and structure is briefly described in Appendix A.

1.2.2 Hobo deployments and data files

The deployment locations for the six Hobo gauges are shown graphically in Figure 2 and listed in Table 1 along with filenames for stored data. Filenames are constructed as "hobo_n_mm_yyyy.xlsx", where "n" is gauge number 1-6, "mm" is the month of collection (here 07 for July or 10 for October) and "yyyy" is year (here 2015).

Figure 2: Hobo deployment locations, May - October 2015

1.2.3 Data processing

The raw pressure data $p_m^n(t)$ recorded by Hobo gauge n is in kilo-pascals (KPa). The barometric pressure $p_b(t)$ is removed, and the data is then converted to Pascals by multiplying by 1000, and divided by specific weight ρg (where water density ρ is assumed equal to 1025 kg/m^3 and $g = 9.80621 m/s^2$ is gravitational acceleration) to obtain water inundation depth $h^n(t)$ in meters. Water surface $\eta^n(t)$ at each gauge is then calculated by adding the surveyed gauge elevation z^n (in m NAVD88, listed in Table 1 and 2) to the calculated h^n.

$$\eta^n = z^n + h^n = z^n + 1000(p_m^n - p_b)/\rho g \tag{1}$$

Figures 3 - 14 show plots of (a) raw pressure (in Kpa), (b) calculated water surface elevation, and (c) temperature for each gauge for the two deployment periods.

Gauge	Location (° N)	Location (° E)	Elevation z^n (m NAVD88)	5/27/15 - 10/6/15
1	39.247685	-75.464983)	0.68	Hobo1Final.mat
2	39.248447	-75.463678)	0.75	Hobo2Final.mat
3	39.249209	-75.462385)	0.67	Hobo3Final.mat
4	39.250308	-75.461167)	0.75	Hobo4Final.mat
5	39.250751	-75.459753)	0.74	Hobo5Final.mat
6	39.251295	-75.458818)	0.51	Hobo6Final.mat

Table 2: Deployment locations, surveyed gauge elevations, and water inundation depth $h^n(t)$ data files for the entire survey period (Here, we have combined our previously mentioned two deployment datasets. Column header in the .mat file: Time | Water depth (meters) | Temperature (°C))

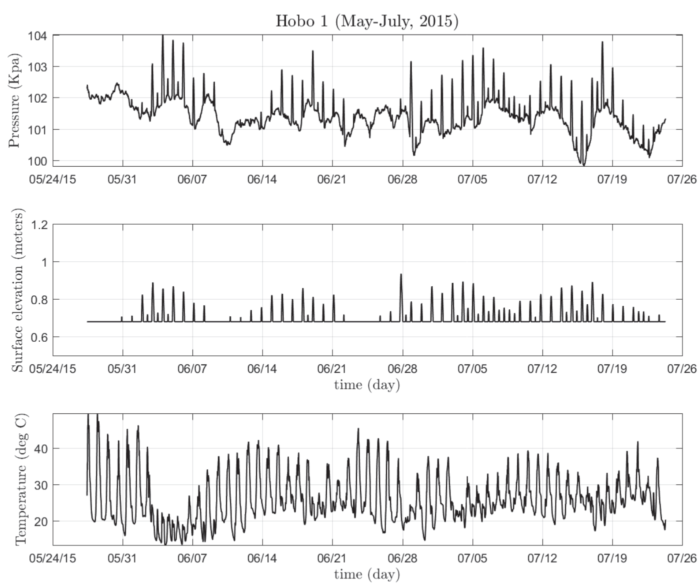

Figure 3: (a) Hobo raw pressure p_m^1 (Kpa), (b) calculated water surface elevation η^1 (m), (c) temperature (°C) at location 1 from May-July 2015.

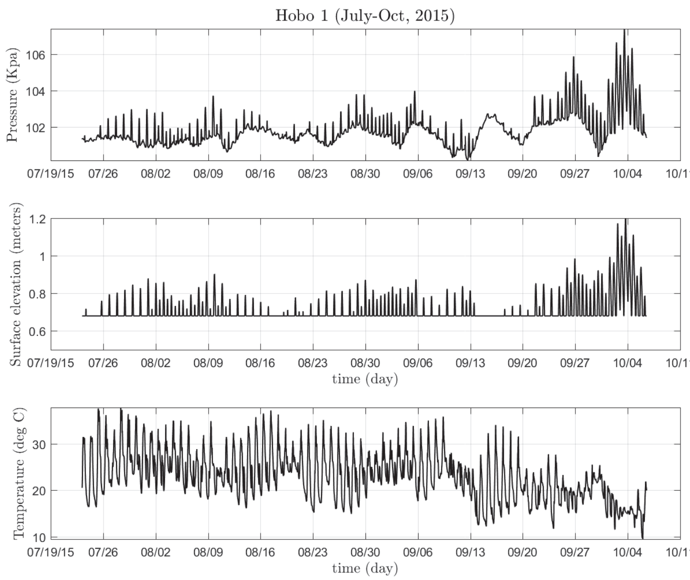

Figure 4: (a) Hobo raw pressure p_m^1 (Kpa), (b) calculated water surface elevation η^1 (m), (c) temperature (°C) at location 1 from July-October 2015.

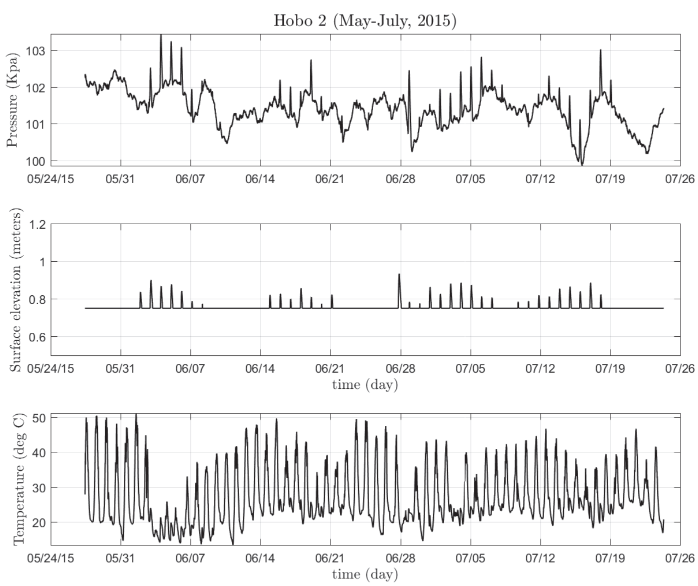

Figure 5: (a) Hobo raw pressure p_m^2 (Kpa), (b) calculated water surface elevation η^2 (m), (c) temperature (°C) at location 2 from May-July 2015.

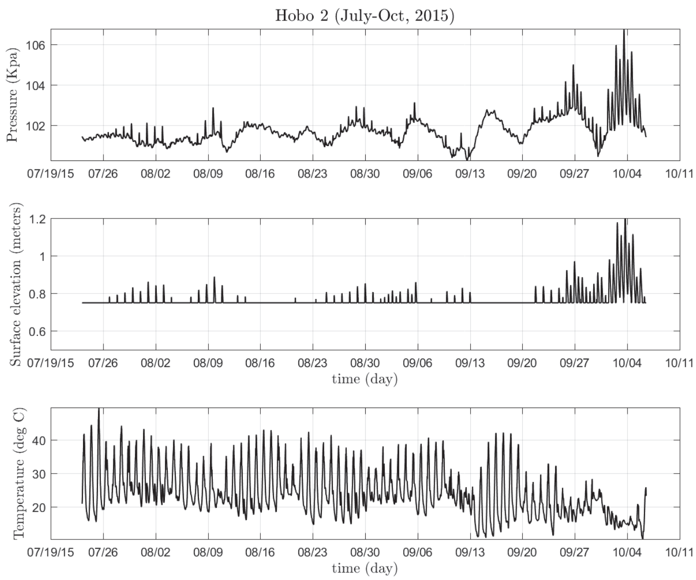

Figure 6: (a) Hobo raw pressure p_m^2 (Kpa), (b) calculated water surface elevation η^2 (m), (c) temperature (°C) at location 2 from July-October 2015.

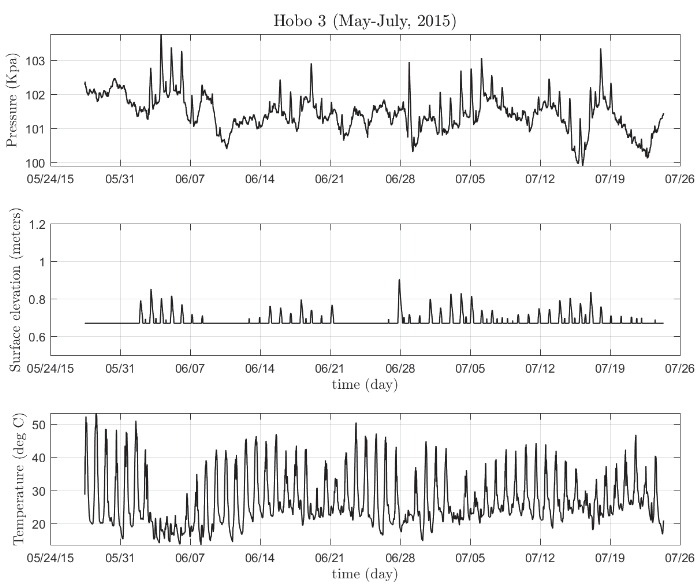

Figure 7: (a) Hobo raw pressure p_m^3 (Kpa), (b) calculated water surface elevation η^3 (m), (c) temperature (°C) at location 3 from May-July 2015.

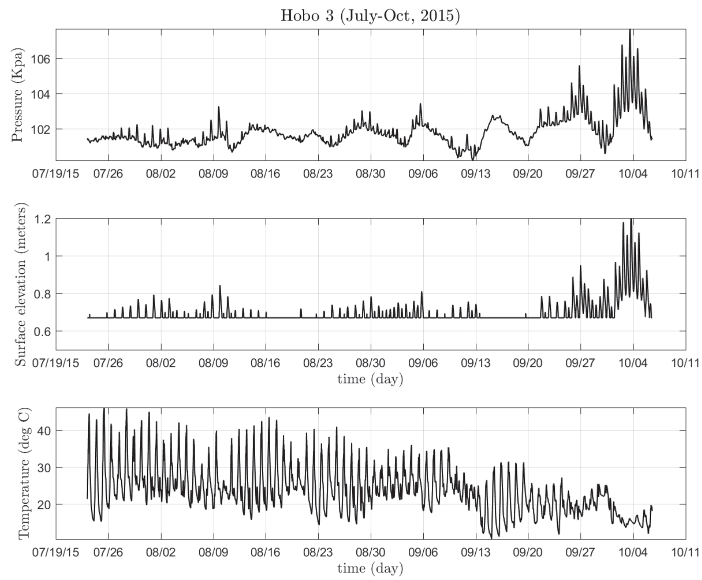

Figure 8: (a) Hobo raw pressure p_m^3 (Kpa), (b) calculated water surface elevation η^3 (m), (c) temperature (°C) at location 3 from July-October 2015.

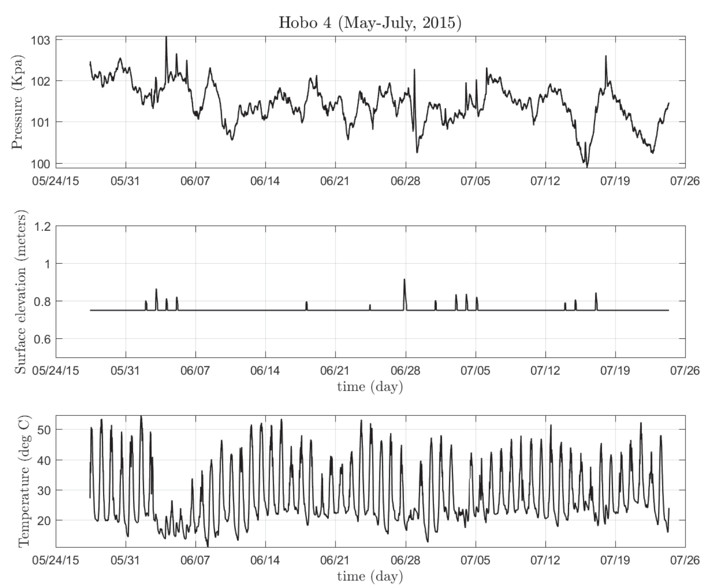

Figure 9: (a) Hobo raw pressure p_m^4 (Kpa), (b) calculated water surface elevationη^4 (m), (c) temperature (°C) at location 4 from May-July 2015.

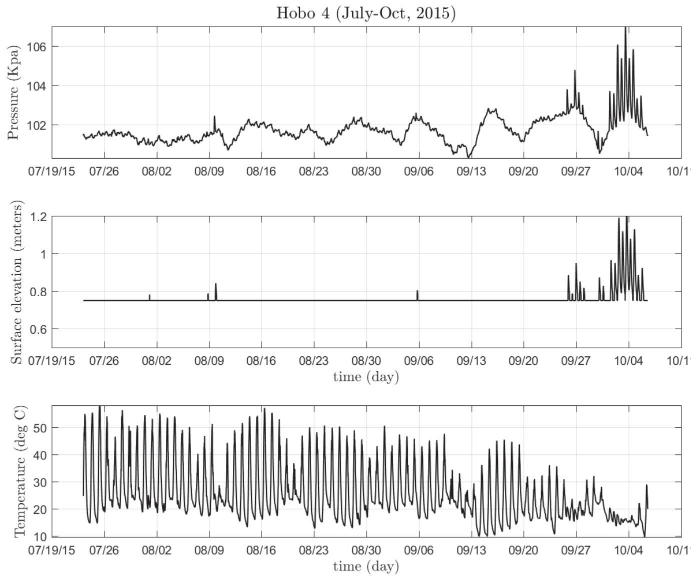

Figure 10: (a) Hobo raw pressure p_m^4 (Kpa), (b) calculated water surface elevation η^4 (m), (c) temperature (°C) at location 4 from July-October 2015.

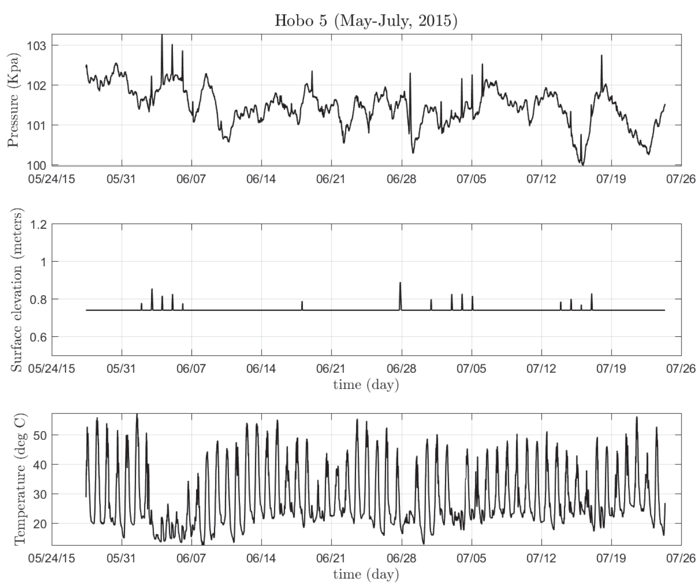

Figure 11: (a) Hobo raw pressure p_m^5 (Kpa), (b) calculated water surface elevation η^5 (m), (c) temperature (°C) at location 5 from May-July 2015.

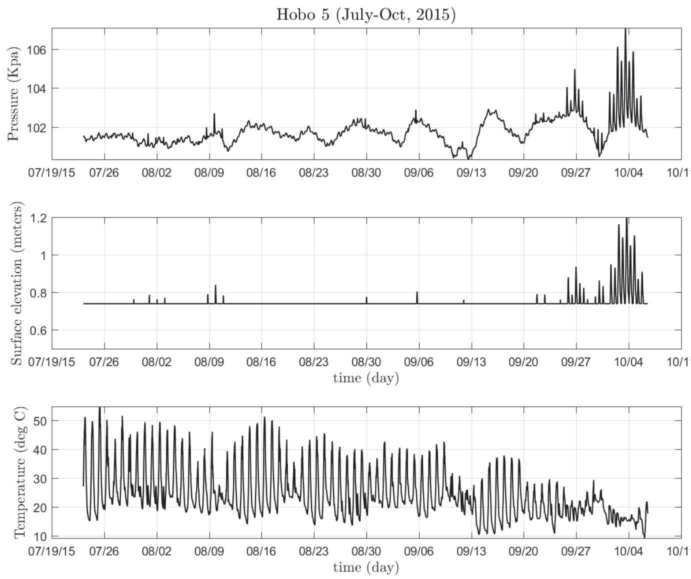

Figure 12: (a) Hobo raw pressure p_m^5 (dKpa), (b) calculated water surface elevation η^5 (m), (c) temperature (°C) at location 5 from July-October 2015.

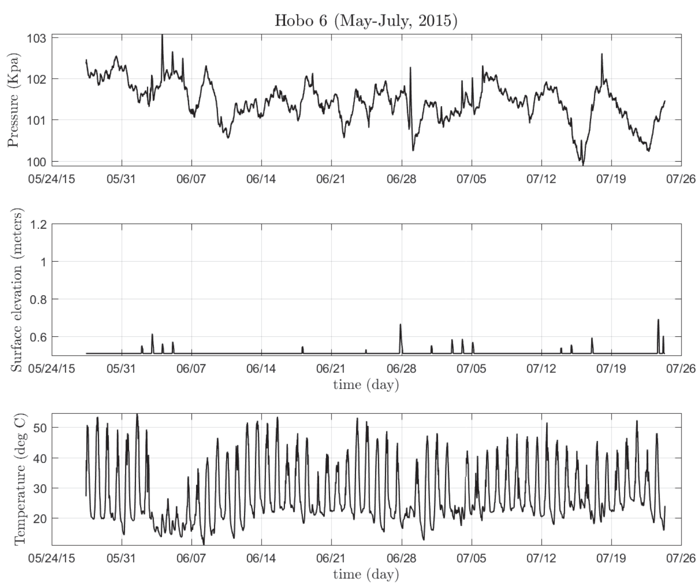

Figure 13: (a) Hobo raw pressure p_m^6 (Kpa), (b) calculated water surface elevation η^6 (m), (c) temperature (°C) at location 6 from May-July, 2015.

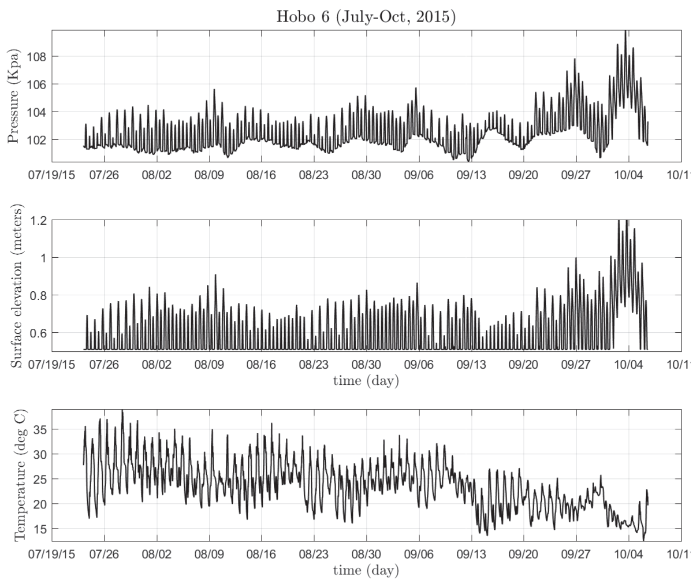

Figure 14: (a) Hobo raw pressure p_m^6 (Kpa), (b) calculated water surface elevation η^6 (m), (c) temperature (°C) at location 6 from July-October 2015.

2 High frequency pressure measurements in Money Marsh

In-situ measurement of pressure fluctuation caused by moving water surface is essential in reconstructing the surface displacement time series in shallow water. There are two parts of the pressure under water, mainly hydrostatic pressure and pressure caused by the waves. In this study, we use two subsurface pressure sensors (RBRsolo D wave) deployed at the bottom of the tidal flat to continuously record tidal elevation and superposed short wind waves at a frequency of 16 Hz. Atmospheric pressure collected at the same time is removed from the raw data to get pressure due to water waves only.

2.1 RBRsolo D pressure gauges

Two RBRsolo high frequency wave gauges were deployed on the Money Marsh mudflat, BHNWR from April, 2015 to January, 2016 to measure the wind wave properties . The RBRsolo D gauge take pressure readings at rates up to 16Hz to provide accurate wave and tidal information. The wave recorder bursts continuously or intermittently to measure high frequency signals such as boat wakes. Technical specification of the instrument along with the file type and structure is briefly described in the Appendix B.

The RBRsolo D wave submersible pressure loggers are capable of sampling continuously at a speed up to 16 Hz and can store 33 million individual readings. The large dataset of burst samples makes it easier to detect low frequency waves, while fast sampling resolves high frequency wind waves. The manufacturer-specified accuracy and resolution are $\pm 0.05\%$ and 0.001% of full scale respectively.

During the deployment, the RBRsolo D sensors were mounted on an expanded metal grating which provided security and additional weight to restrict any lateral movement (Figure 15.

2.2 Instrument deployment and location

Also, we collected data from another tide gauge (HOBO) deployed at Leatherberry mudflat to describe the time varying water level in our non-stationary SWAN model simulations. Geographic

Figure 15: RBR pressure sensor mounted on expanded metal grating.

location of the sensors is shown in Figure 16. The RBR1 sensor is on the shallower side of the tidal flat, where the depth is about 0.2 m only from the NAVD88 vertical reference level and the other one (RBR2) is on the northern side at a slightly higher depth of 0.8 m. Both sensor locations are influenced by the wetting and drying effects from a tidal range of 2.0 m and measures only atmospheric pressure during a low tide.

2.3 Data collection

We have collected the in-situ RBR pressure data from April, 2015 to December, 2015 with a few erratic gaps due to local extreme conditions or instrument errors. At the very outset we fixed the erroneous and irregular values using smooth linear interpolation (or extrapolation). After initial error correction, we removed the barometric pressure from raw data to retain only the pressure contribution from the water column. The additional details on collection and post-processing of the raw data is given in Deb et al (2018).

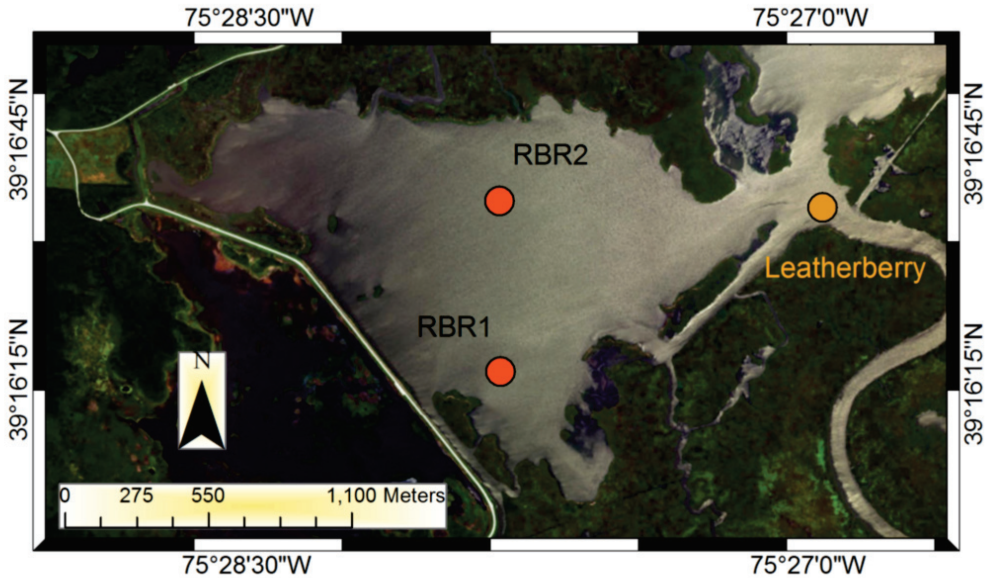

Figure 16: Pressure gauge positions in the Money Marsh tidal flat.

2.4 RBRsolo data

2.4.1 RBRsolo filenames and deployment period

A brief description about the collected wave datasets and their measurement period at location 1 (39.271750, -75.4837) and location 2 (39.277667, -75.463767) is presented below:

2.4.2 Data processing

The sequence of steps followed before the instrument deployment and during post-processing of the wave data follows

1. The wave gauges were deployed at the mudflat bottom.
2. The gauge recorded temperature and pressure data at the rate of 16Hz frequency.
3. After getting the raw data, initially we removed the barometric pressure using a local atmospheric gauge.
4. Then, the mean value or linear trend has been removed for separating the low and high frequency waves.

deployment period	RBR1 data filename	RBR2 data file name
03/31/2015 - 04/23/2015	RBR1_20150423.mat	RBR2_20150423.mat
04/23/2015 - 05/15/2015	RBR1_20150515.mat	RBR2_20150515.mat
05/15/2015 - 06/03/2015	RBR1_20150603.mat	RBR2_20150603.mat
06/03/2015 - 06/24/2015	RBR1_20150714.mat	RBR2_20150714.mat
06/24/2015 - 07/14/2015	RBR1_20150828.mat	RBR2_20150828.mat
07/14/2015 - 08/04/2015	RBR1_20151016.mat	RBR2_20151016.mat
08/04/2015 - 08/28/2015	RBR1_20150624.mat	RBR2_20150624.mat
08/28/2015 - 09/21/2015	RBR1_20150804.mat	RBR2_20150804.mat
09/21/2015 - 10/16/2015	RBR1_20150921.mat	RBR2_20150921.mat
10/16/2015 - 11/17/2015	RBR1_20151117.mat	RBR2_20151117.mat
12/09/2015 - 01/08/2016	RBR1_20160108.mat	RBR2_20160108.mat

Table 3: RBR file names and sampling durations.

5. High frequency pressure signals were then converted to surface by using a pressure response function calculated from linear wave theory.

6. Finally, the statistical properties of the wind waves were estimated using spectral analysis . We used a 15 minutes window for the averaging and the following figures will demonstrate the raw and processed data in a subsequent manner.

Additional details on the estimation of wave statistics (shown in Figure 28) is provided in Deb et al (2018).

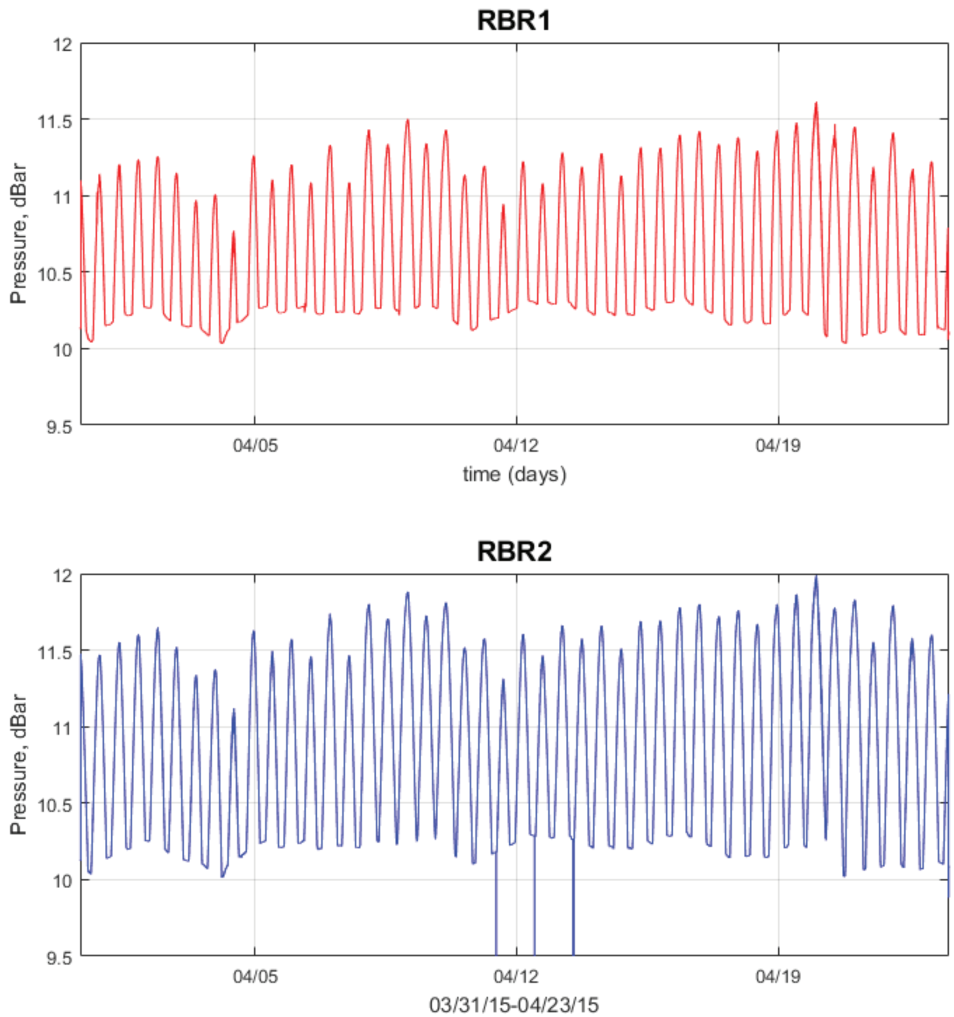

Figure 17: RBRsolo wave gauge raw pressure data at location 1 and 2 from March 31 - April 23, 2015 [filenames: `RBR1_20150423.mat` & `RBR2_20150423.mat`]

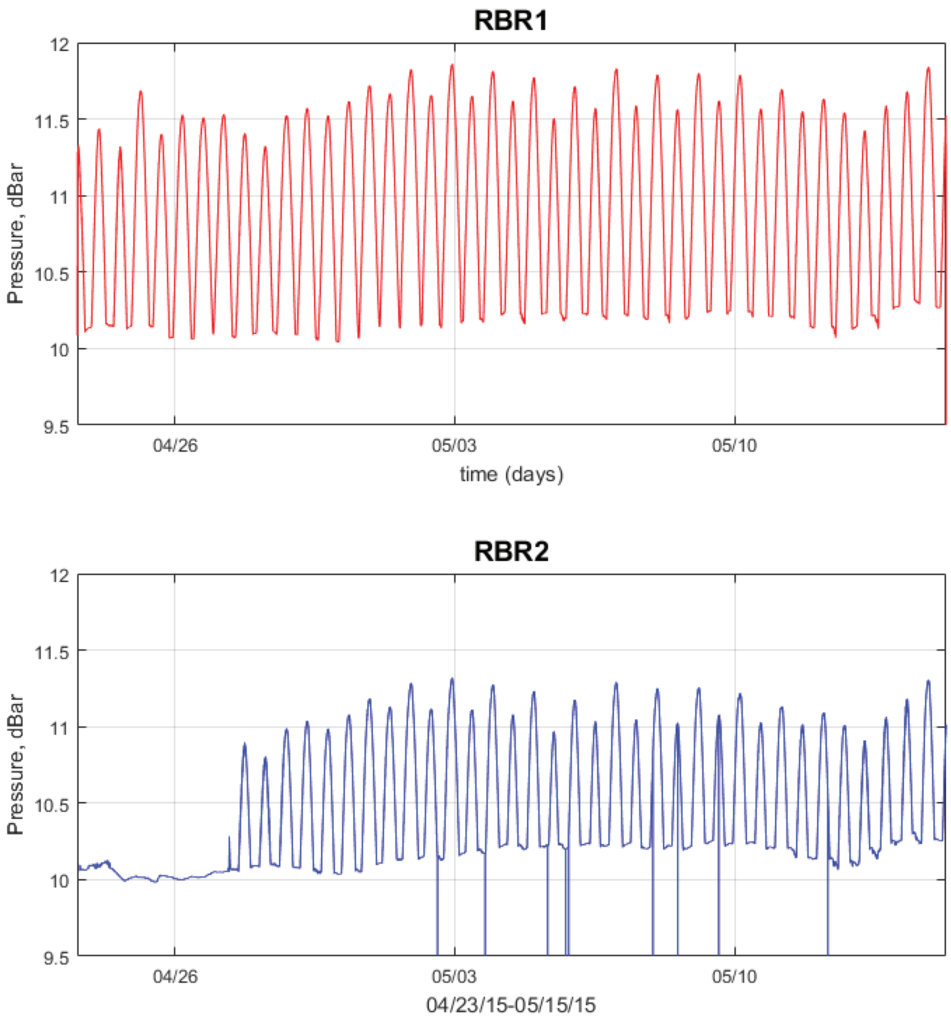

Figure 18: RBRsolo wave gauge raw pressure data at location 1 and 2 from April 23 - May 15, 2015 [filenames: `RBR1_20150515.mat` & `RBR2_20150515.mat`]

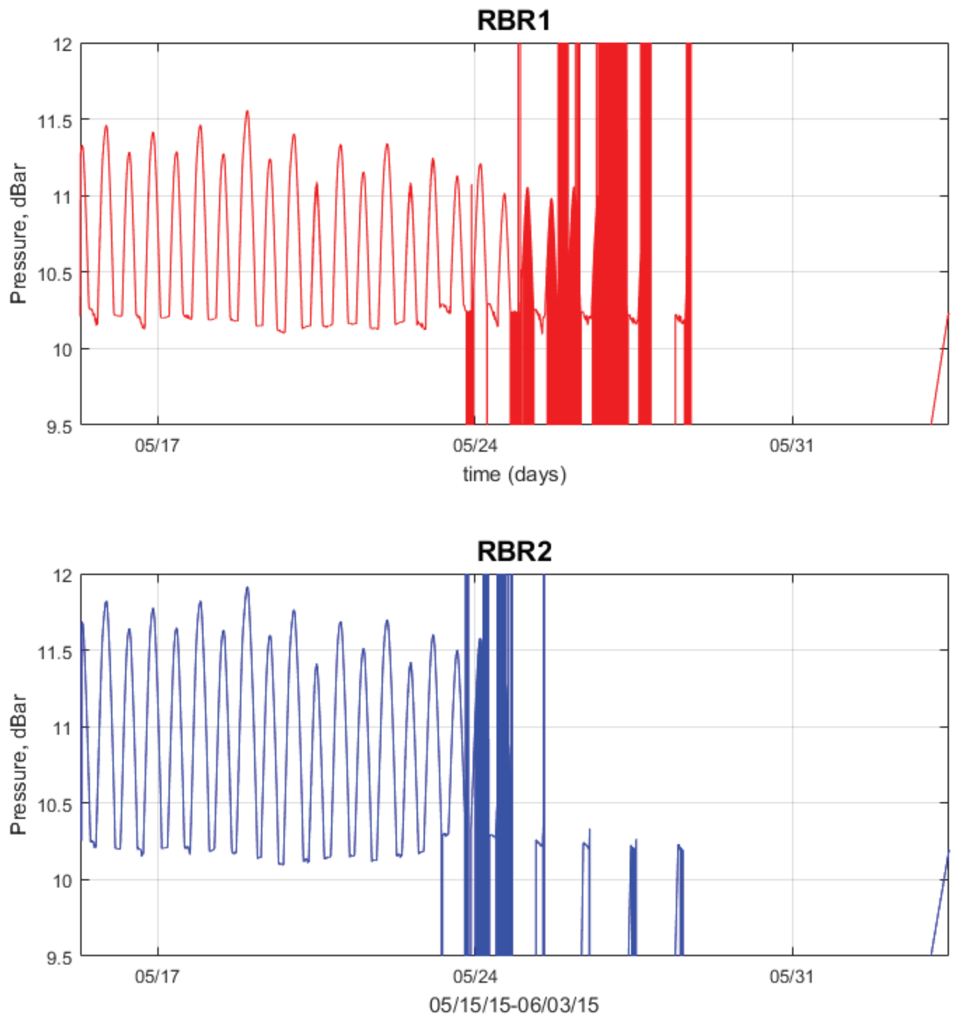

Figure 19: RBRsolo wave gauge raw pressure data at location 1 and 2 from May 15 - June 3, 2015 [filenames: `RBR1_20150603.mat` & `RBR2_20150603.mat`]

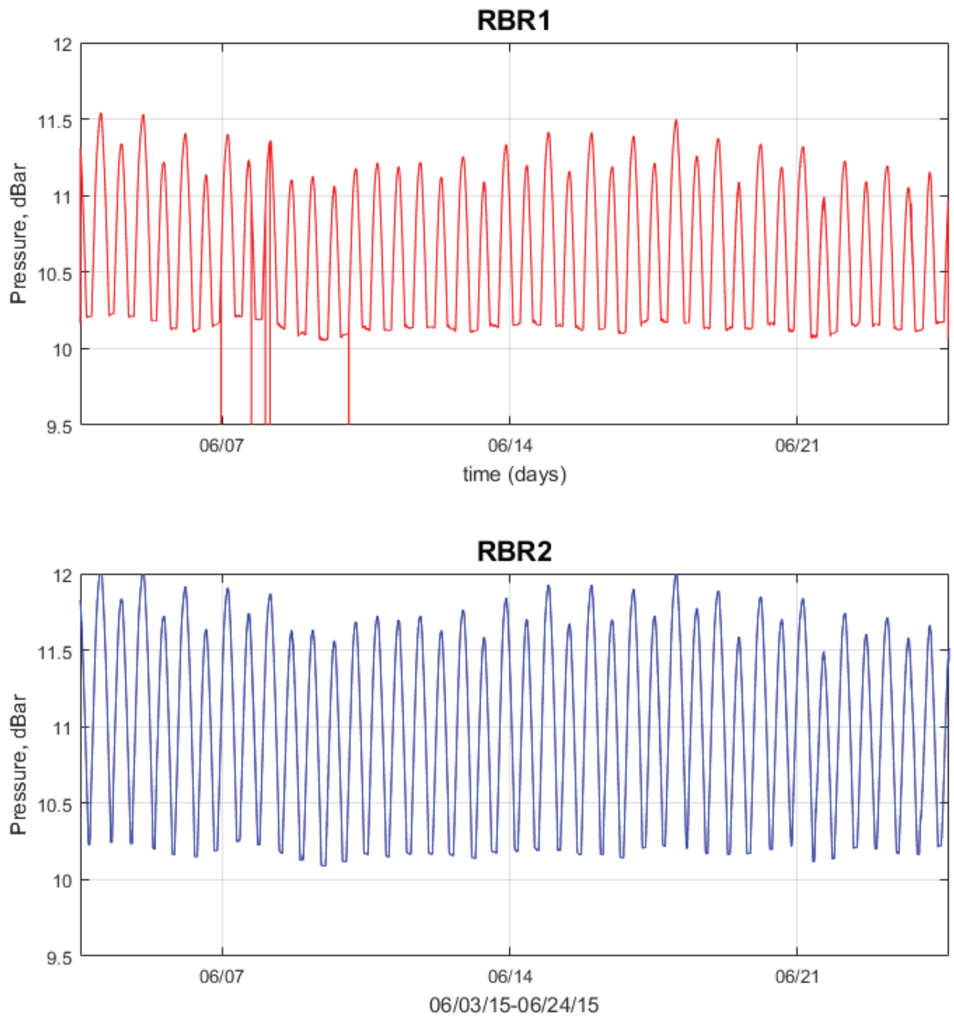

Figure 20: RBRsolo wave gauge raw pressure data at location 1 and 2 from June 3 - June 24, 2015 [filenames: `RBR1_20150624.mat` & `RBR2_20150624.mat`]

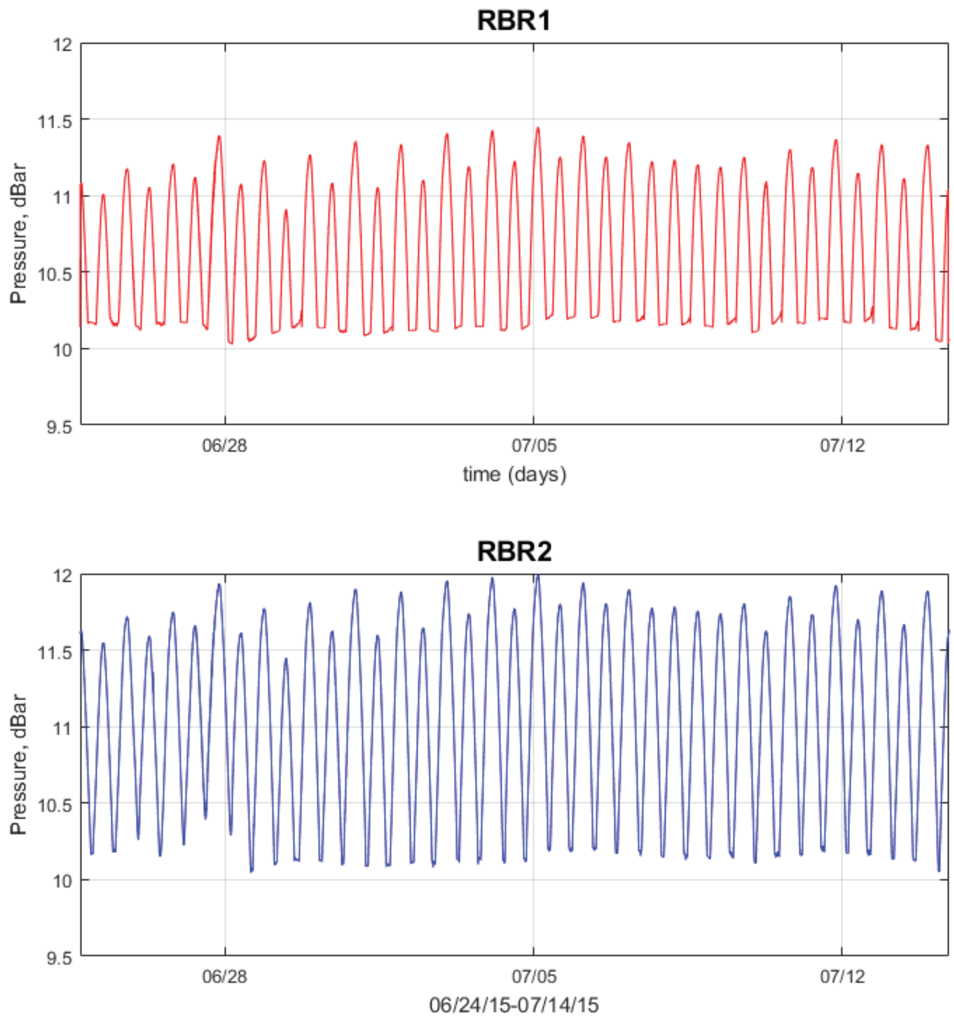

Figure 21: RBRsolo wave gauge raw pressure data at location 1 and 2 from June 24 - July 14, 2015 [filenames: `RBR1_20150714.mat` & `RBR2_20150714.mat`]

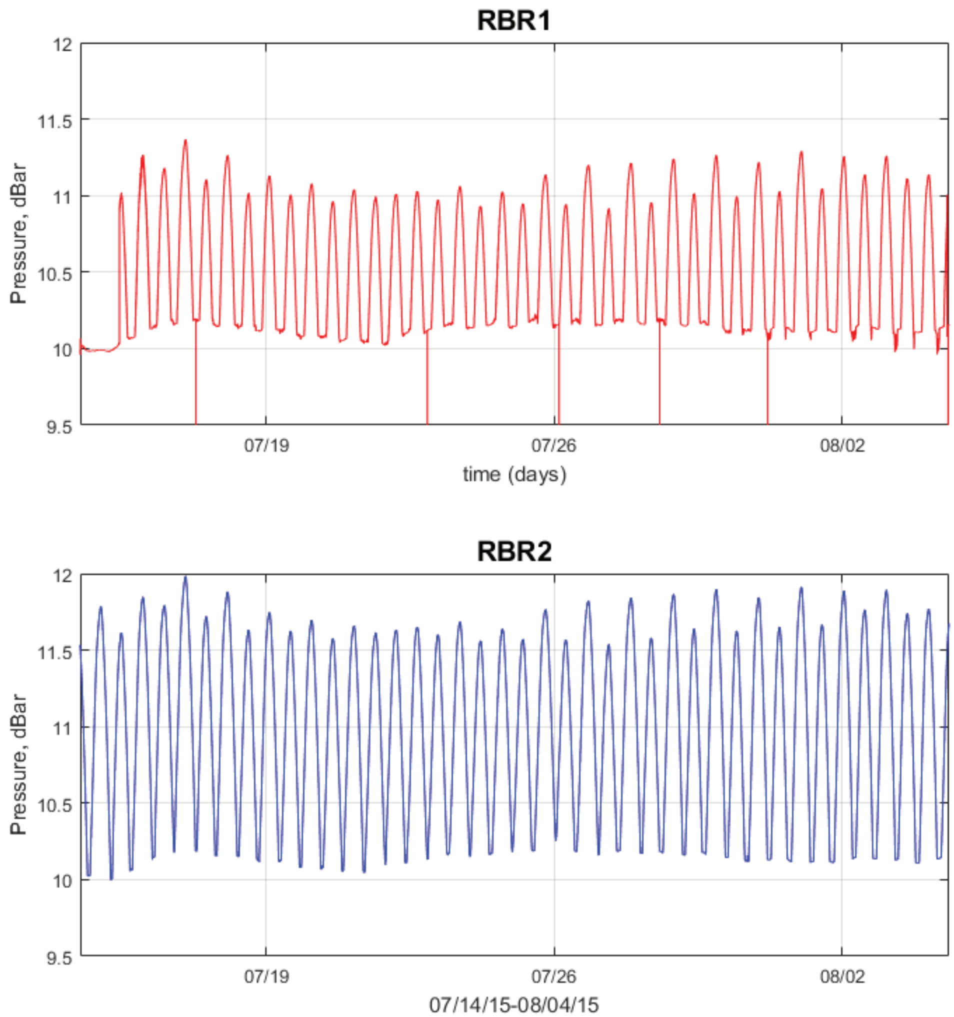

Figure 22: RBRsolo wave gauge raw pressure data at location 1 and 2 from July 14 - August 4, 2015 [filenames: `RBR1_20150804.mat` & `RBR2_20150804.mat`]

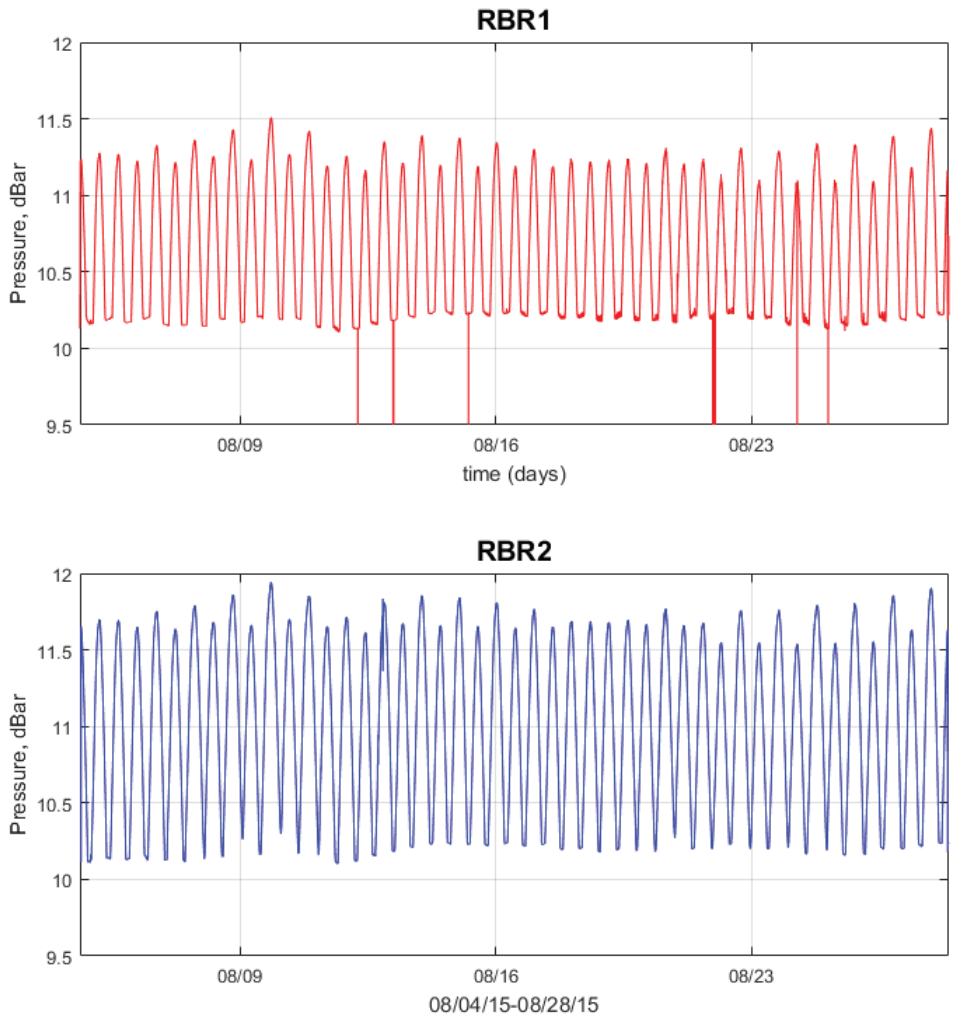

Figure 23: RBRsolo wave gauge raw pressure data at location 1 and 2 from August 4 - August 28, 2015 [filenames: `RBR1_20150828.mat` & `RBR2_20150828.mat`]

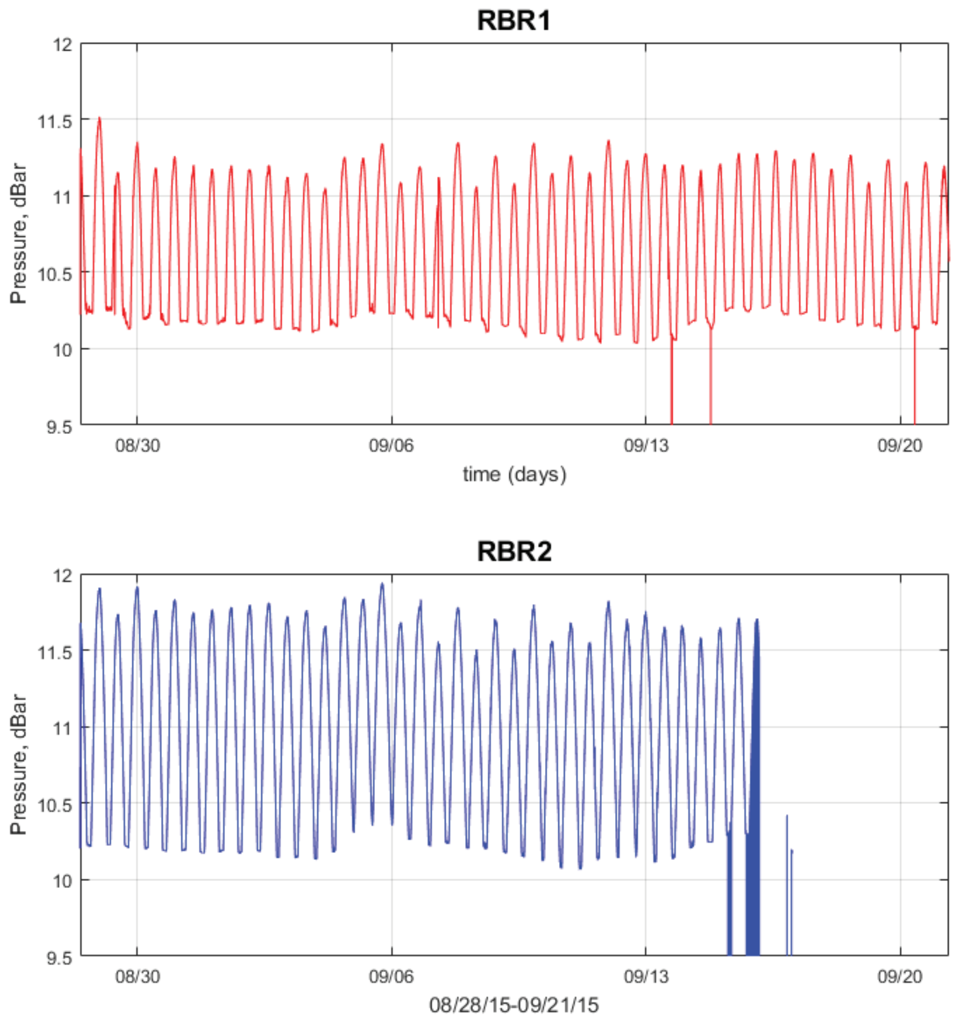

Figure 24: RBRsolo wave gauge raw pressure data at location 1 and 2 from August 28 - September 21, 2015 [filenames: `RBR1_20150921.mat` & `RBR2_20150921.mat`]

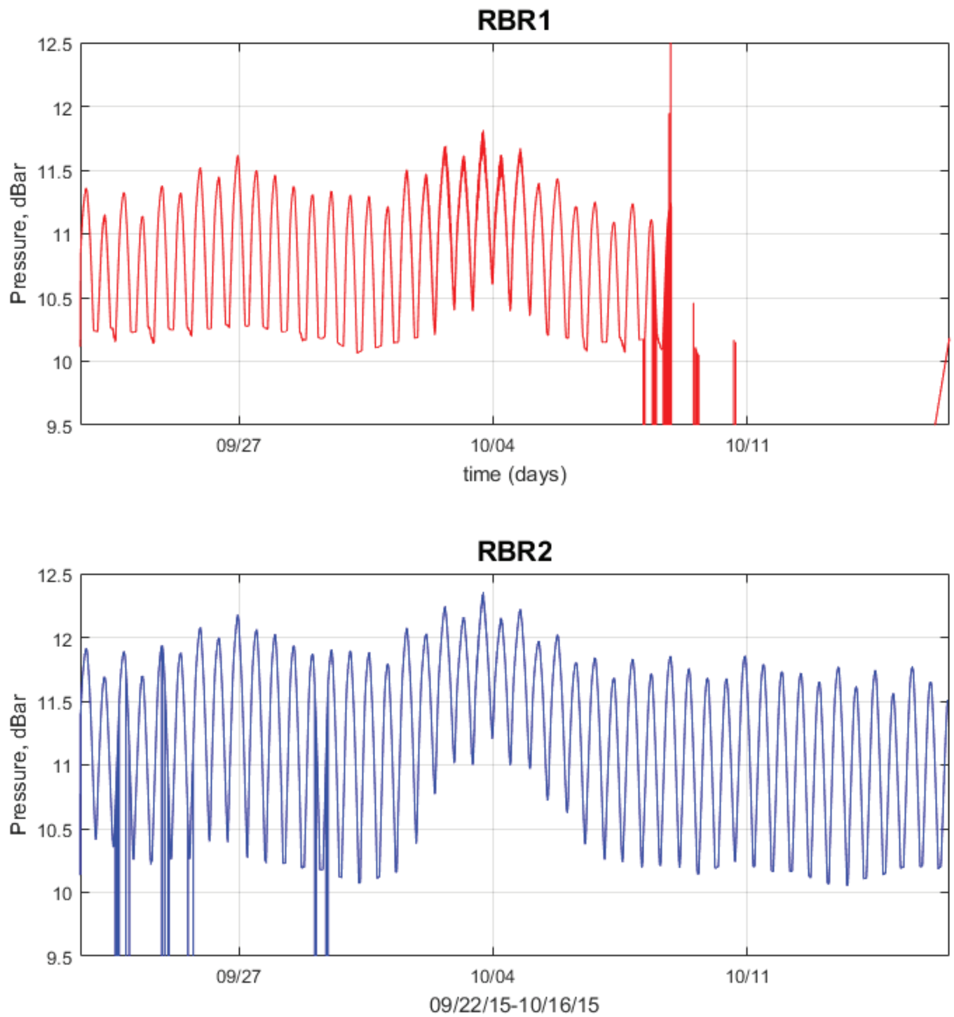

Figure 25: RBRsolo wave gauge raw pressure data at location 1 and 2 from September 21 - October 16, 2015 [filenames: `RBR1_20151016.mat` & `RBR2_20151016.mat`]

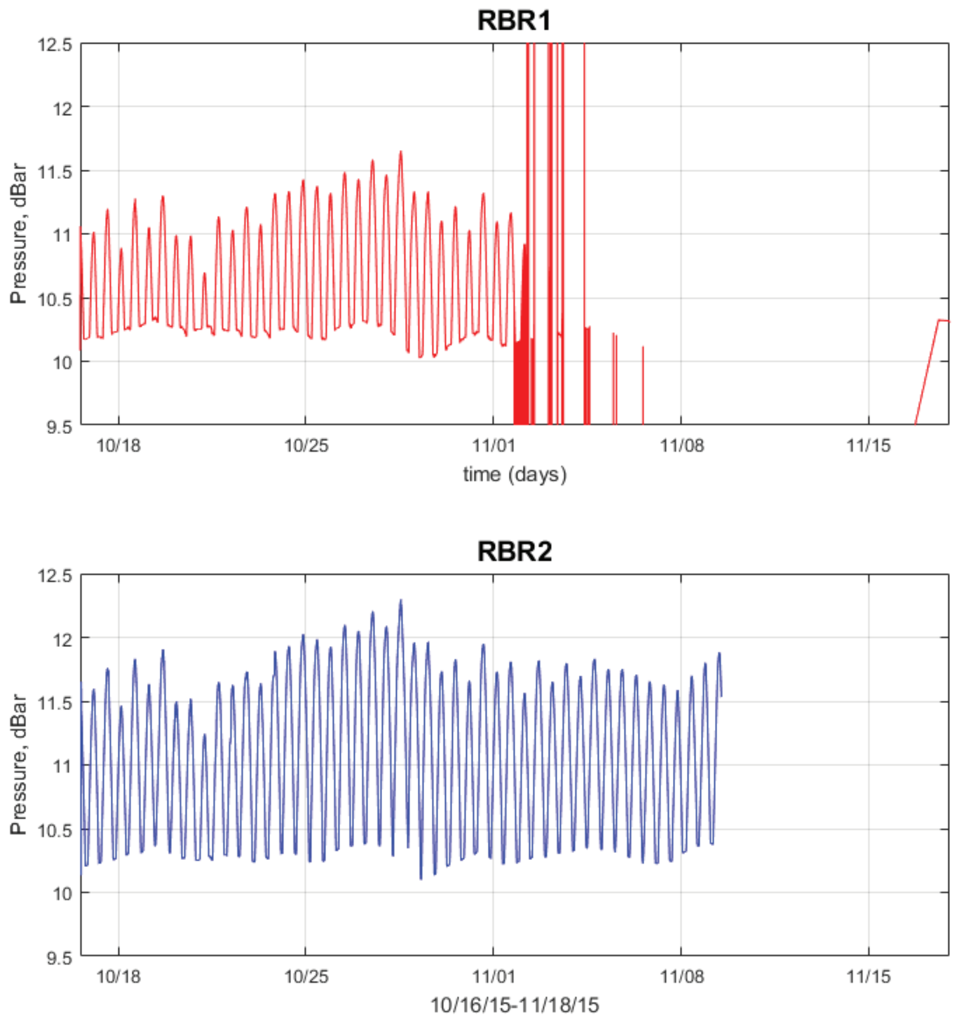

Figure 26: RBRsolo wave gauge raw pressure data at location 1 and 2 from October 16 - November 17, 2015 [filenames: `RBR1_20151117.mat` & `RBR2_20151117.mat`]

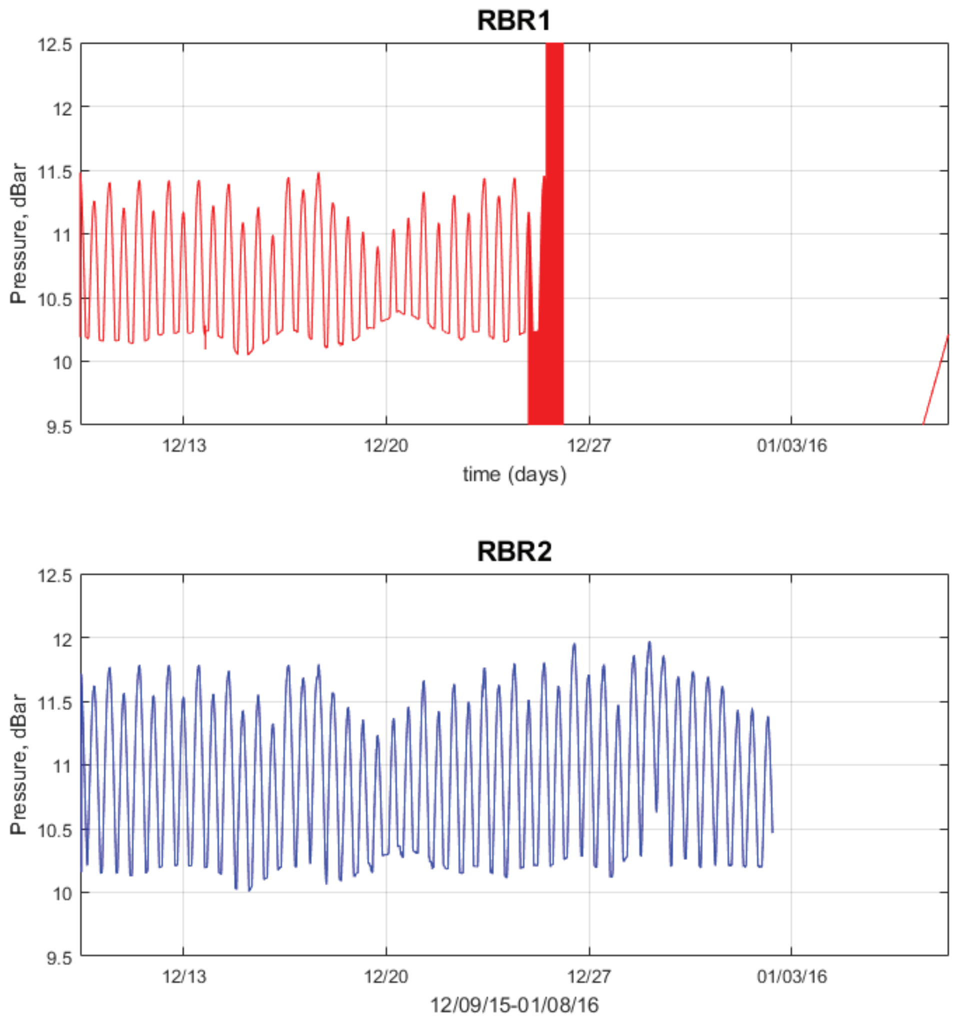

Figure 27: RBRsolo wave gauge raw pressure data at location 1 and 2 from December 9, 2015 - January 8, 2016 [filenames: `RBR1_20160108.mat` & `RBR2_20160108.mat`]

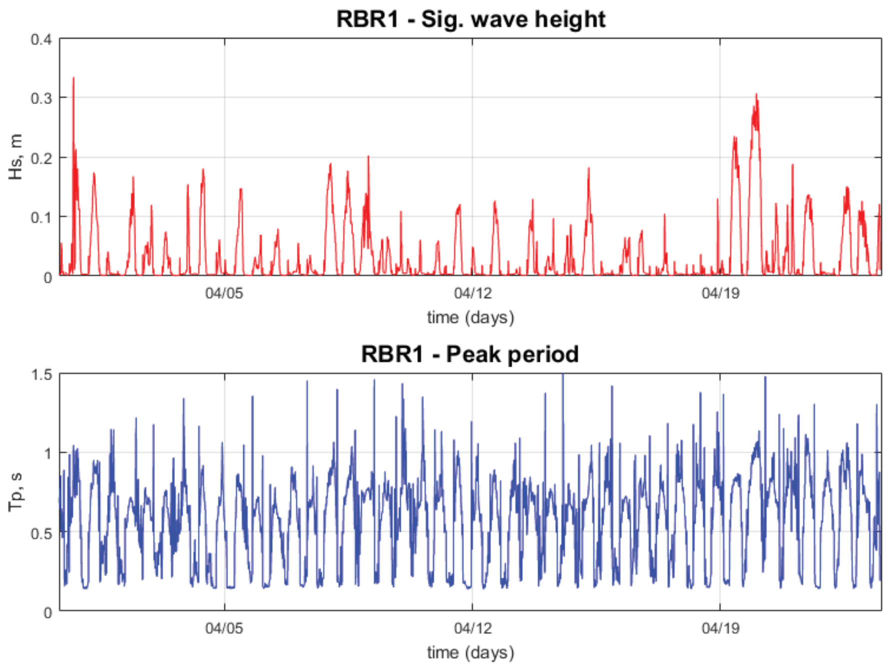

(a)

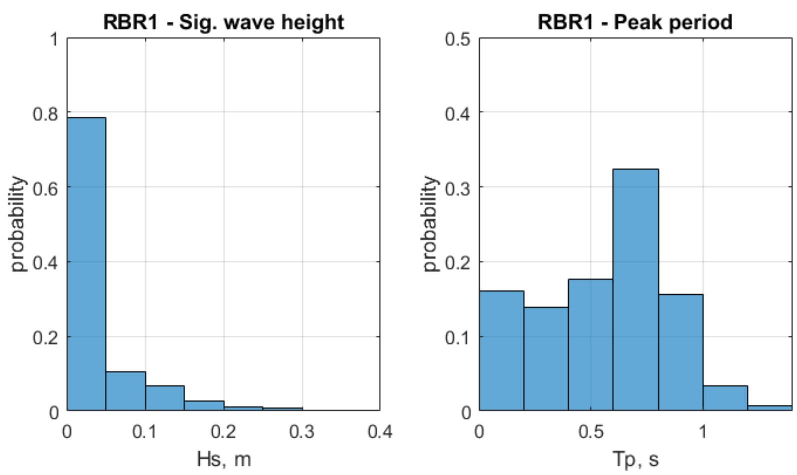

(b)

Figure 28: (a) Significant wave height, Hs (m) and Peak wave period, Tp (s) calculated using the linear wave theory and spectral analysis at location 1 from March 31 - April 23, 2015 (b) Histogram of the wind wave properties. [filename: `RBR1_20150423.mat`]

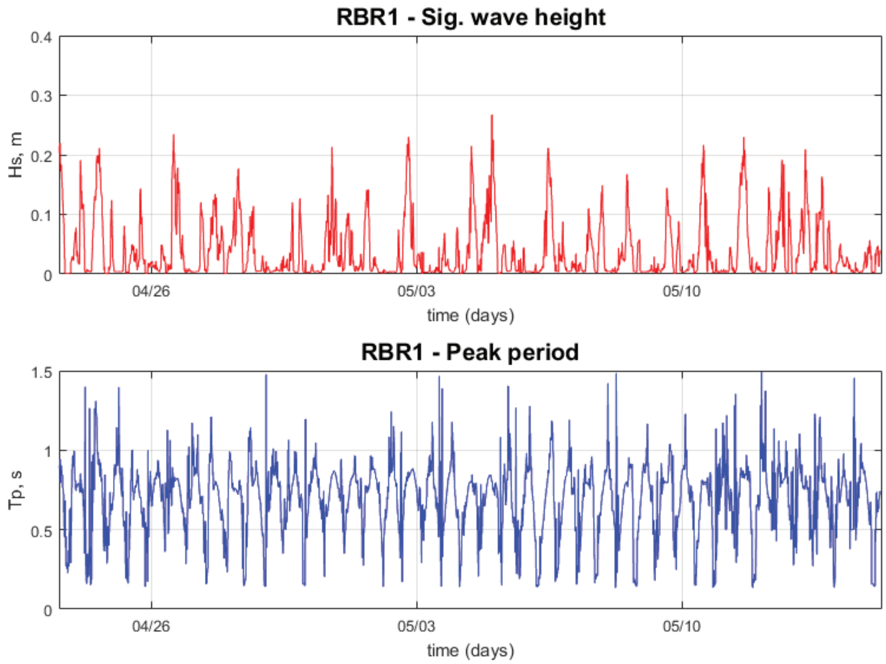

(a)

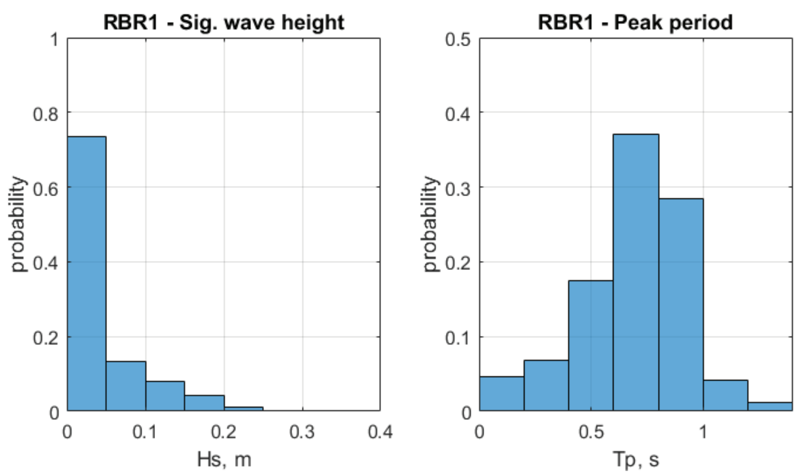

(b)

Figure 29: (a) Significant wave height, Hs (m) and Peak wave period, Tp (s) calculated using the linear wave theory and spectral analysis at location 1 from April 23 - May 15, 2015 (b) Histogram of the wind wave properties. [filename: `RBR1_20150515.mat`]

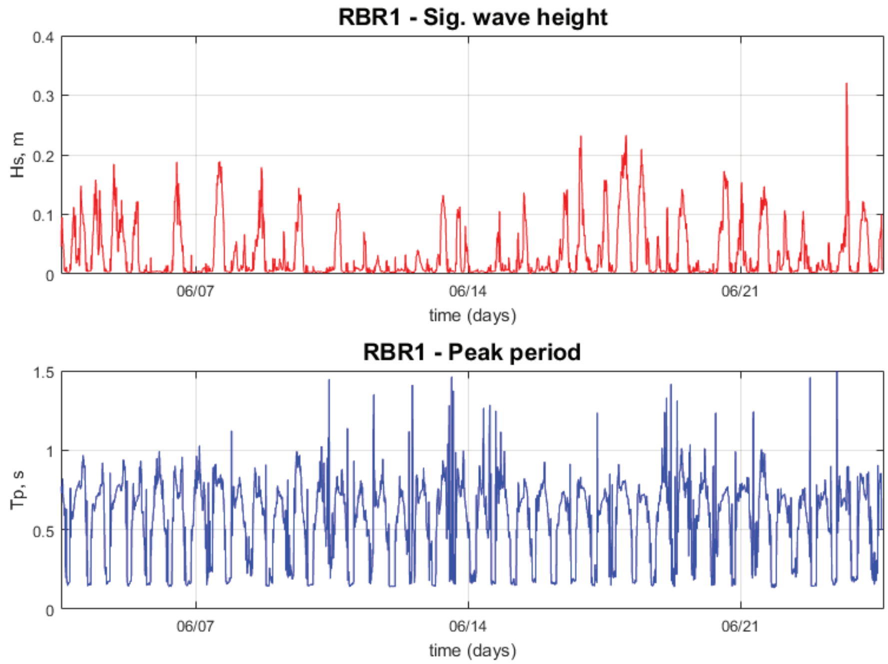

(a)

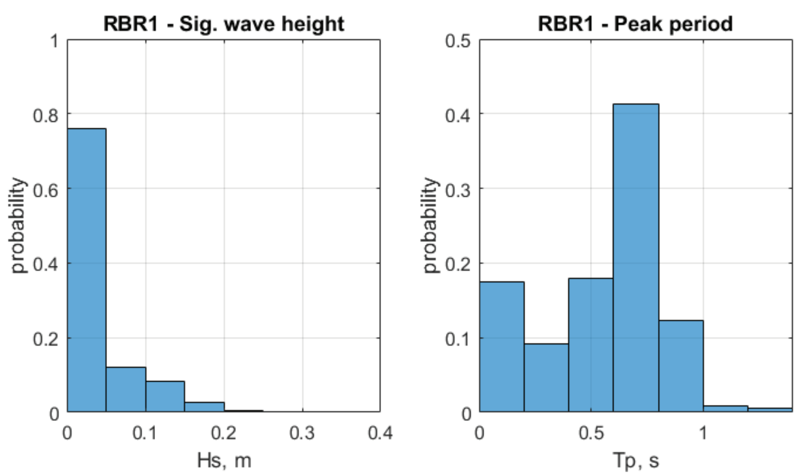

(b)

Figure 30: (a) Significant wave height, Hs (m) and Peak wave period, Tp (s) calculated using the linear wave theory and spectral analysis at location 1 from June 3 - June 24, 2015 (b) Histogram of the wind wave properties. [filename: `RBR1_20150624.mat`]

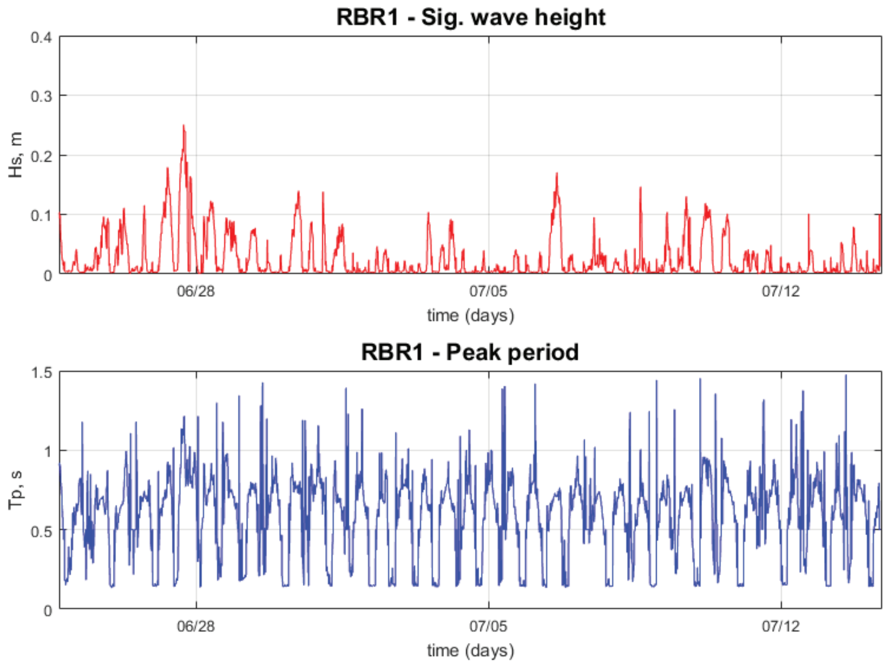

(a)

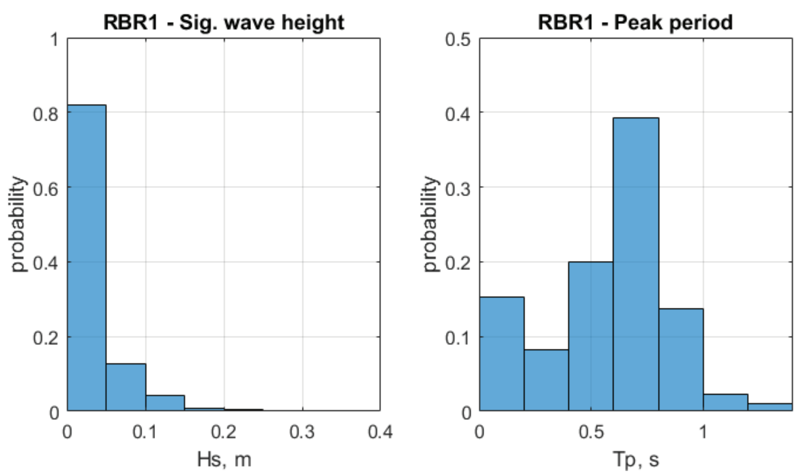

(b)

Figure 31: (a) Significant wave height, Hs (m) and Peak wave period, Tp (s) calculated using the linear wave theory and spectral analysis at location 1 from June 24 - July 14, 2015 (b) Histogram of the wind wave properties. [filename: `RBR1_20150714.mat`]

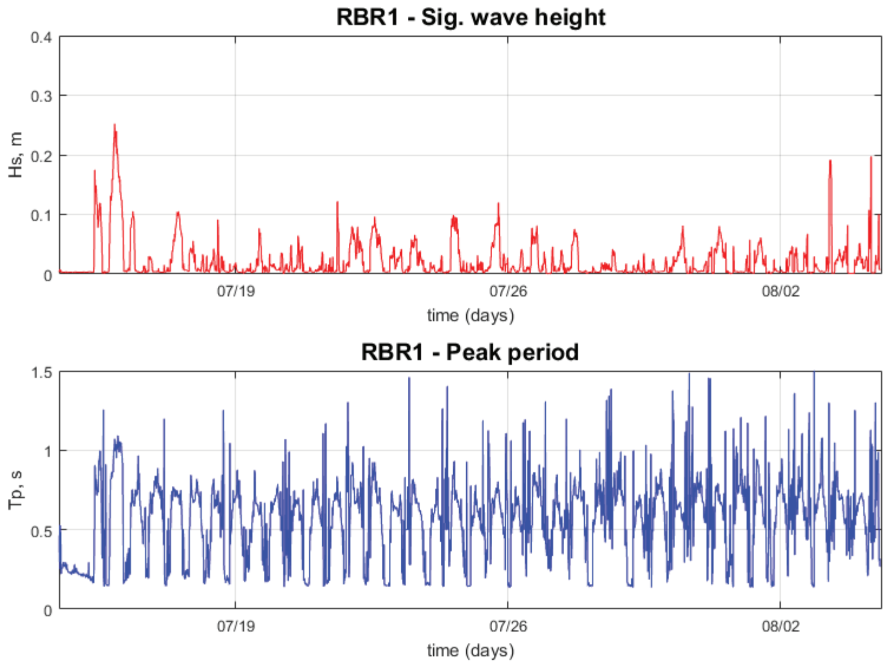

(a)

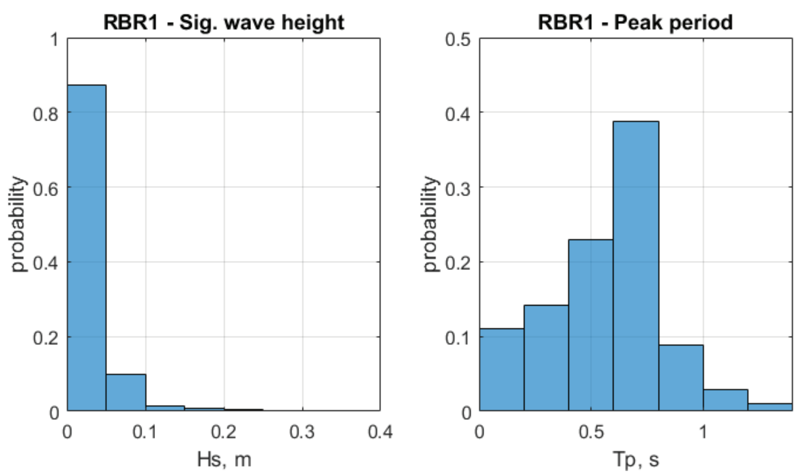

(b)

Figure 32: (a) Significant wave height, Hs (m) and Peak wave period, Tp (s) calculated using the linear wave theory and spectral analysis at location 1 from July 14 - August 4, 2015 (b) Histogram of the wind wave properties. [filename: `RBR1_20150804.mat`]

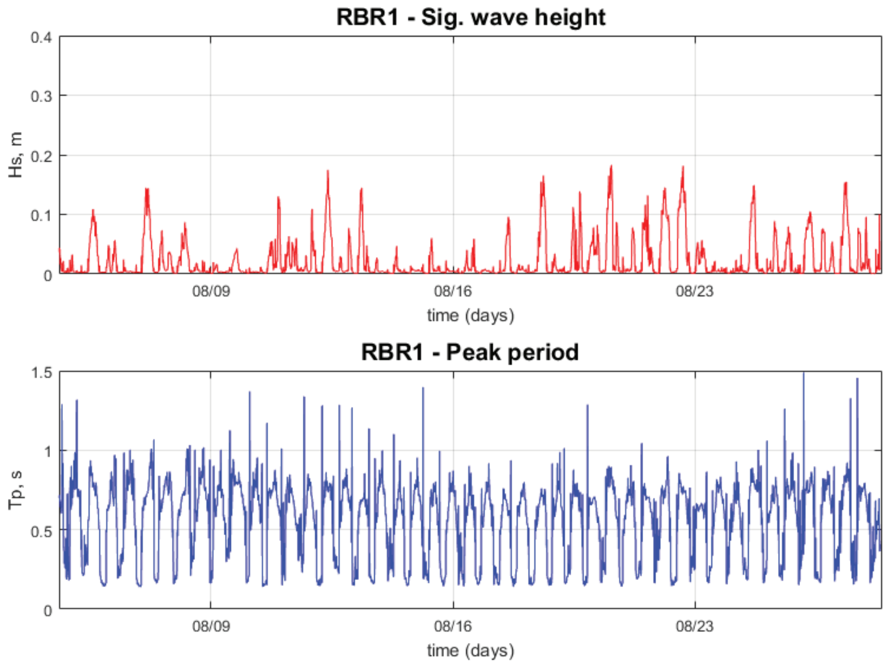

(a)

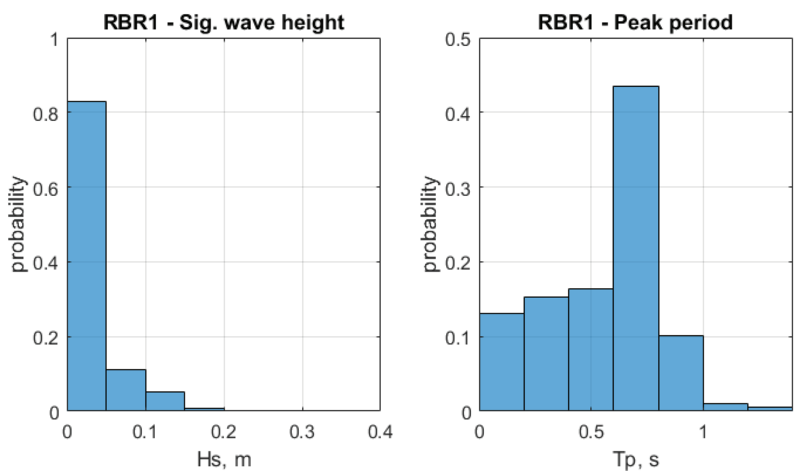

(b)

Figure 33: (a) Significant wave height, Hs (m) and Peak wave period, Tp (s) calculated using the linear wave theory and spectral analysis at location 1 from August 4 - August 28, 2015 (b) Histogram of the wind wave properties. [filename: `RBR1_20150828.mat`]

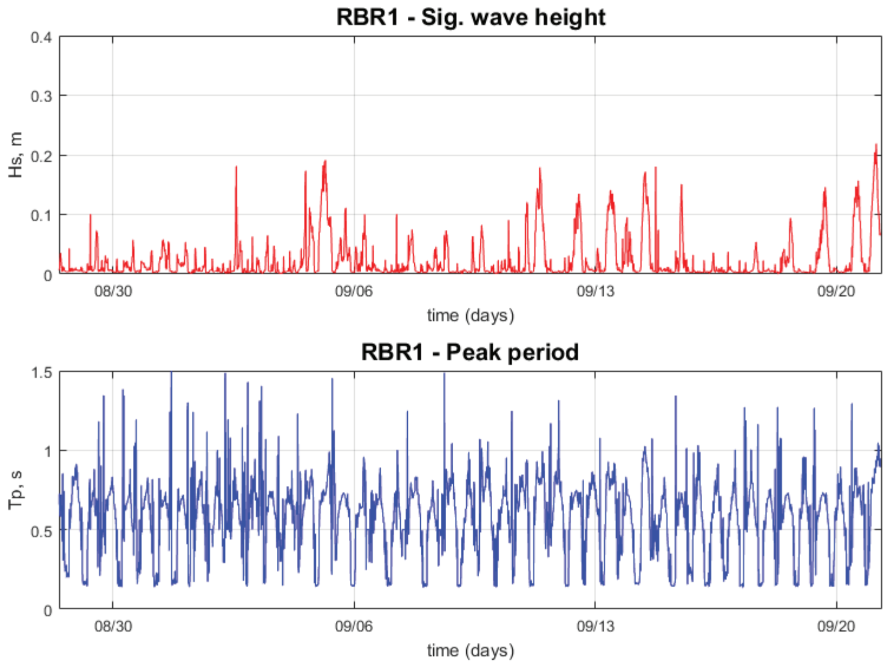

(a)

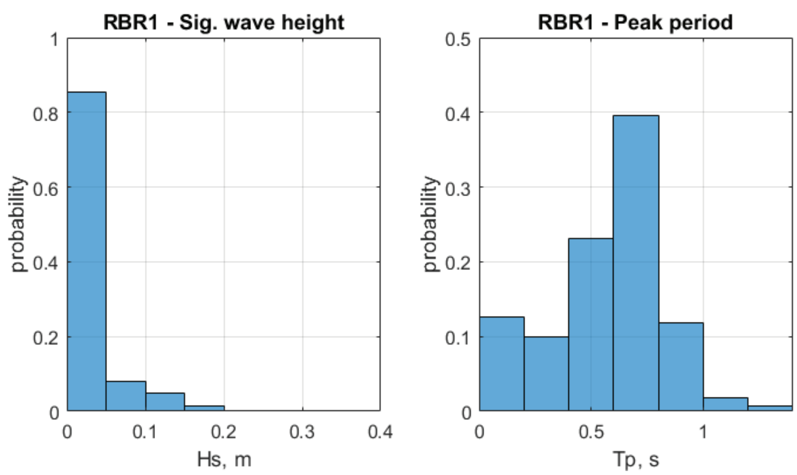

(b)

Figure 34: (a) Significant wave height, Hs (m) and Peak wave period, Tp (s) calculated using the linear wave theory and spectral analysis at location 1 from August 28 - September 21, 2015 (b) Histogram of the wind wave properties. [filename: `RBR1_20150921.mat`]

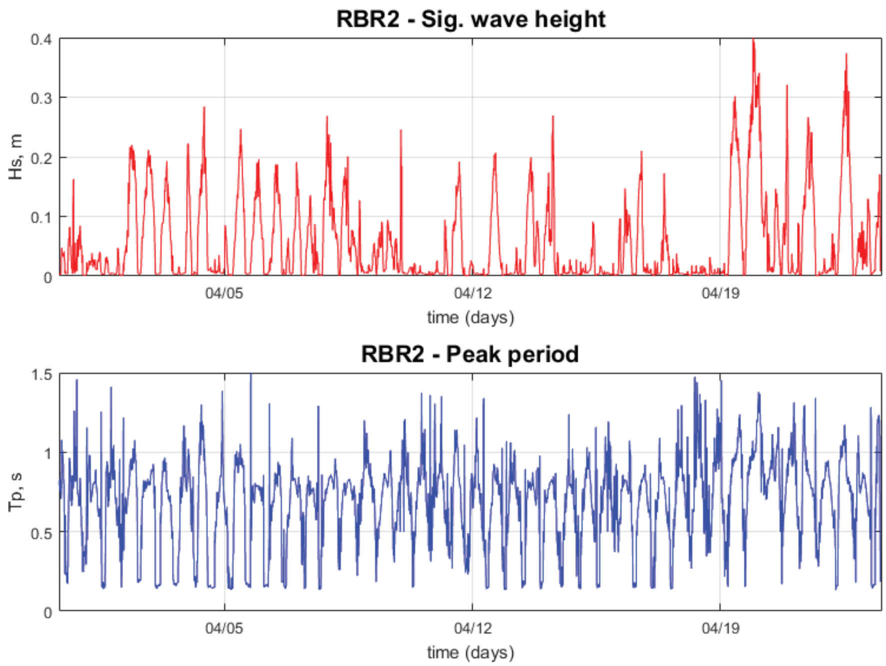

(a)

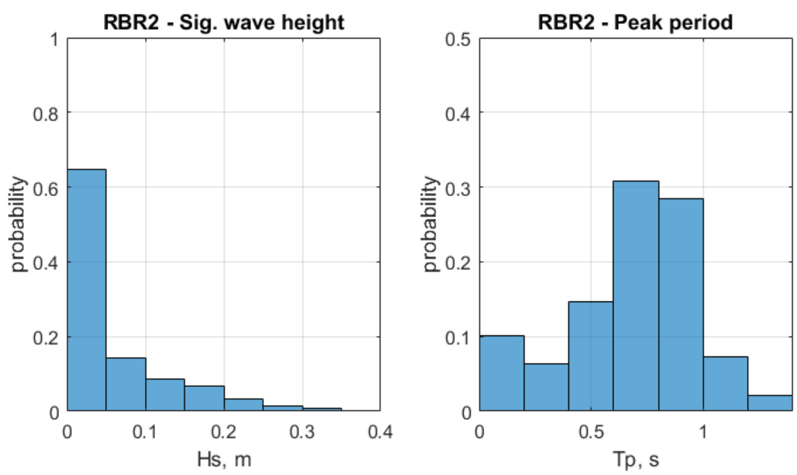

(b)

Figure 35: (a) Significant wave height, Hs (m) and Peak wave period, Tp (s) calculated using the linear wave theory and spectral analysis at location 2 from March 31 - April 23, 2015 (b) Histogram of the wind wave properties. [filename: `RBR2_20150423.mat`]

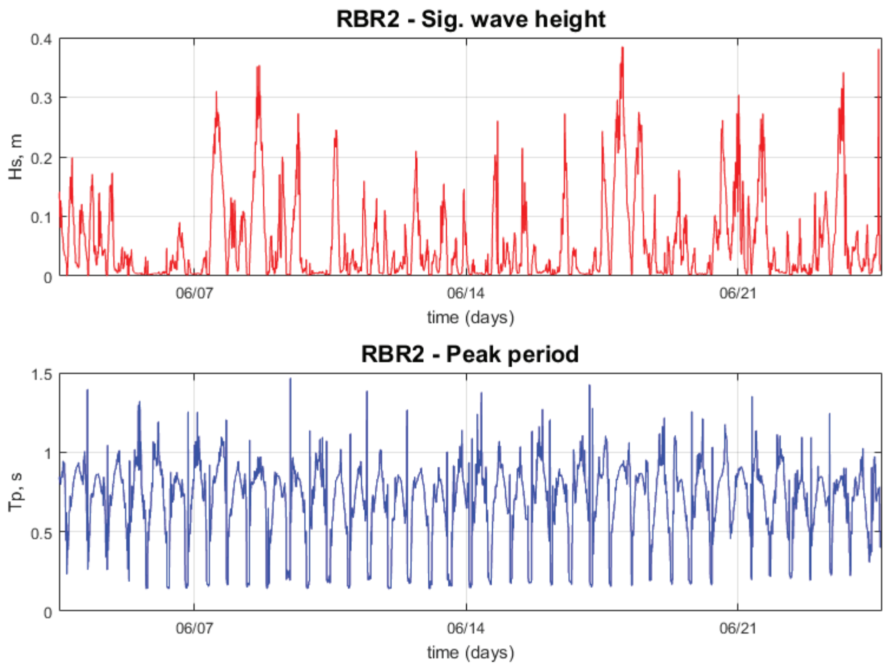

(a)

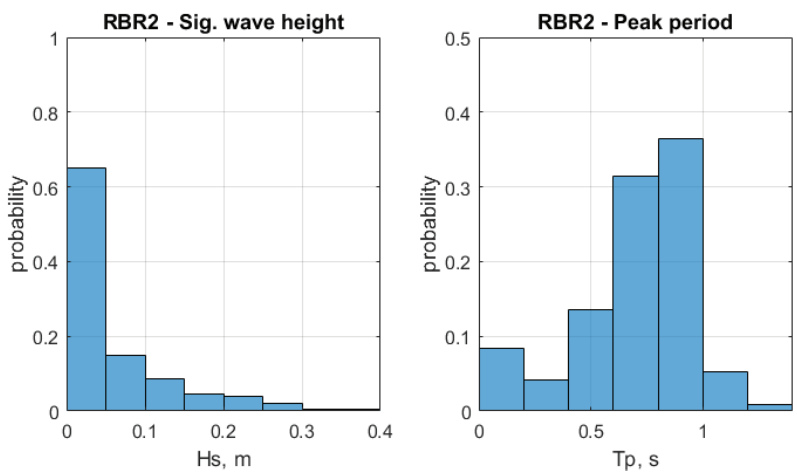

(b)

Figure 36: (a) Significant wave height, Hs (m) and Peak wave period, Tp (s) calculated using the linear wave theory and spectral analysis at location 2 from June 3 - June 24, 2015 (b) Histogram of the wind wave properties. [filename: `RBR2_20150624.mat`]

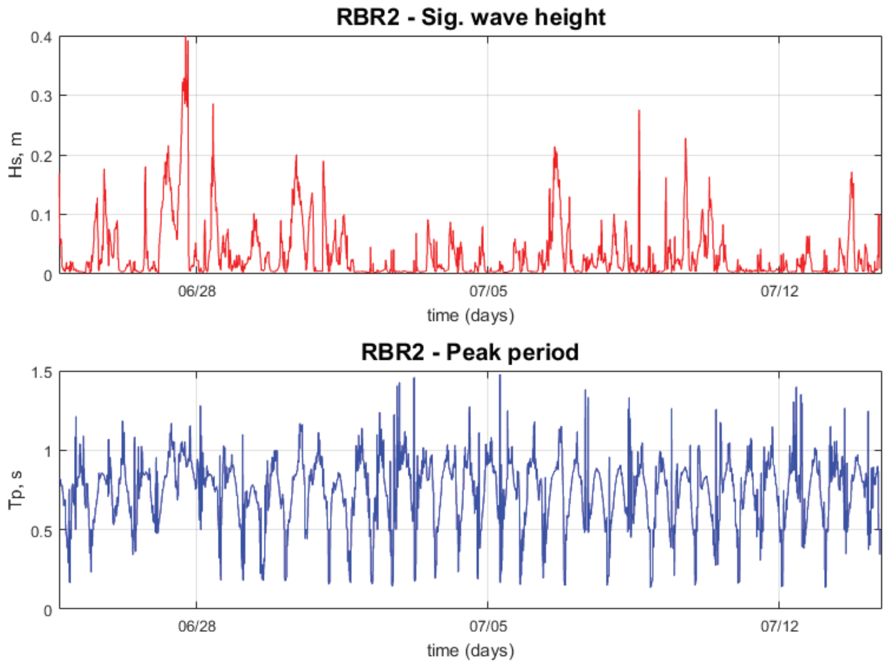

(a)

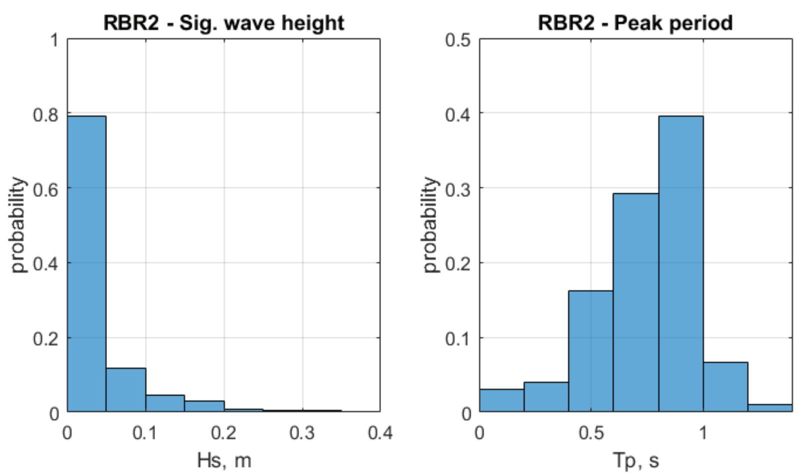

(b)

Figure 37: (a) Significant wave height, Hs (m) and Peak wave period, Tp (s) calculated using the linear wave theory and spectral analysis at location 2 from June 24 - July 14, 2015 (b) Histogram of the wind wave properties. [filename: `RBR2_20150714.mat`]

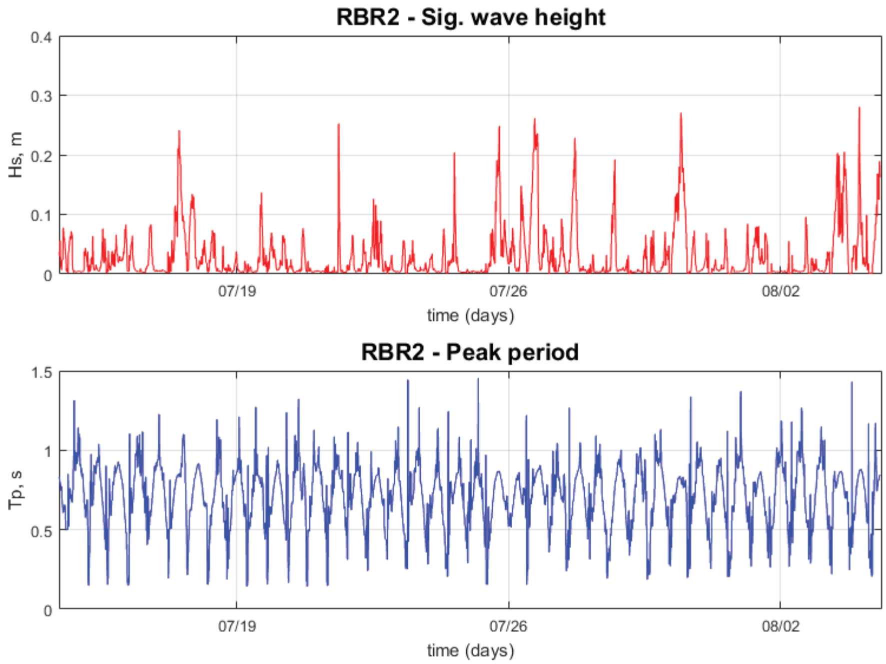

(a)

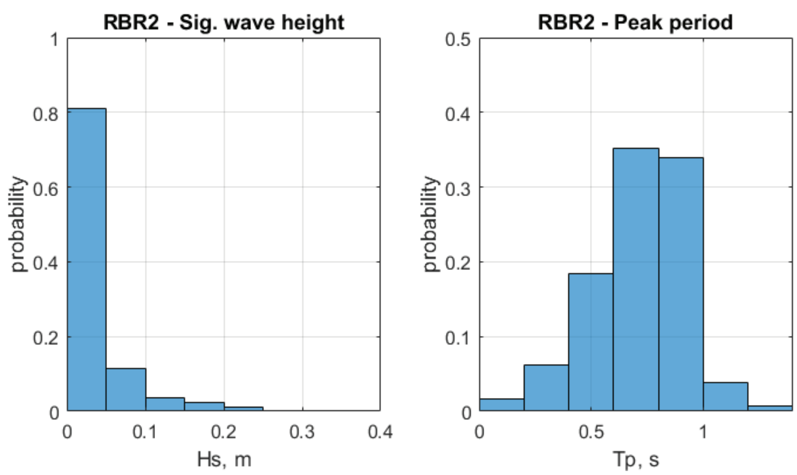

(b)

Figure 38: (a) Significant wave height, Hs (m) and Peak wave period, Tp (s) calculated using the linear wave theory and spectral analysis at location 2 from July 14 - August 4, 2015 (b) Histogram of the wind wave properties. [filename: `RBR2_20150804.mat`]

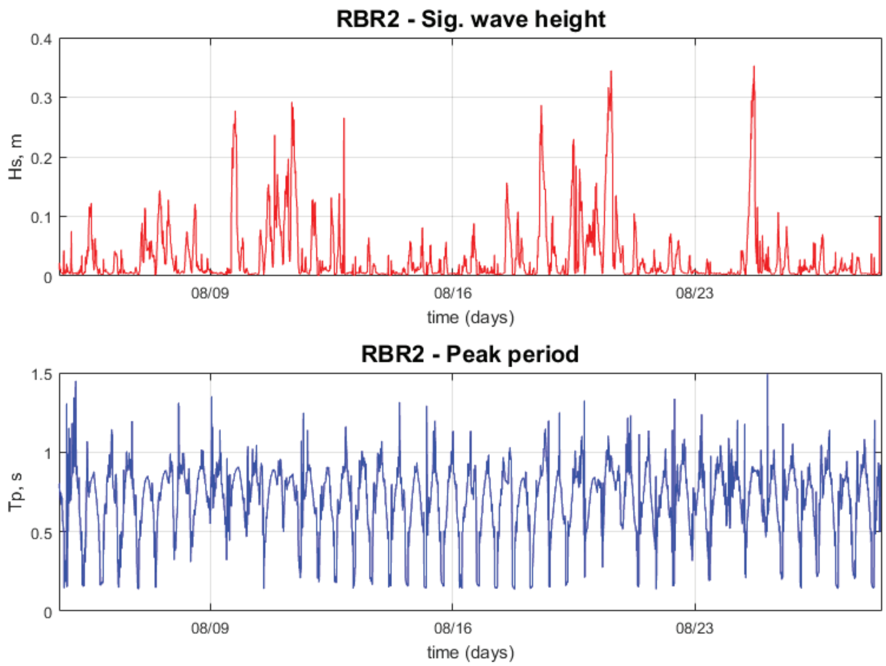

(a)

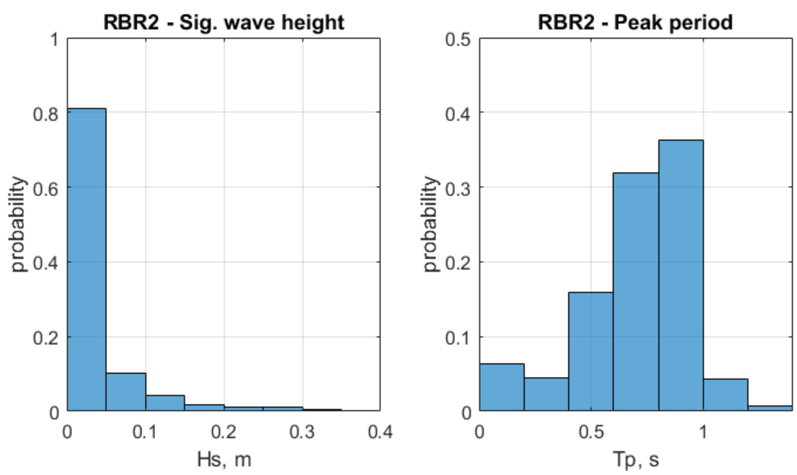

(b)

Figure 39: (a) Significant wave height, Hs (m) and Peak wave period, Tp (s) calculated using the linear wave theory and spectral analysis at location 2 from August 4 - August 28, 2015 (b) Histogram of the wind wave properties. [filename: `RBR2_20150828.mat`]

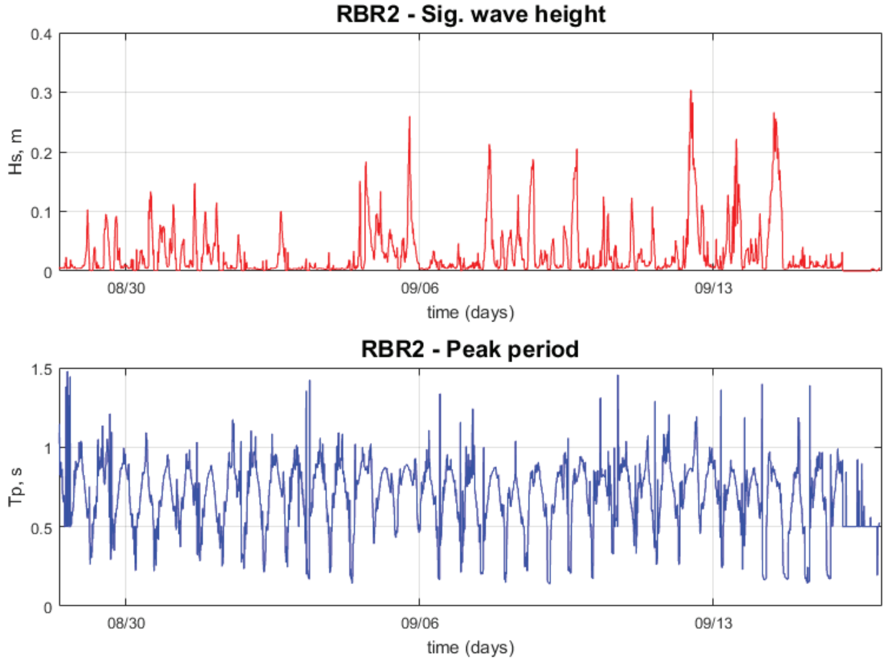

(a)

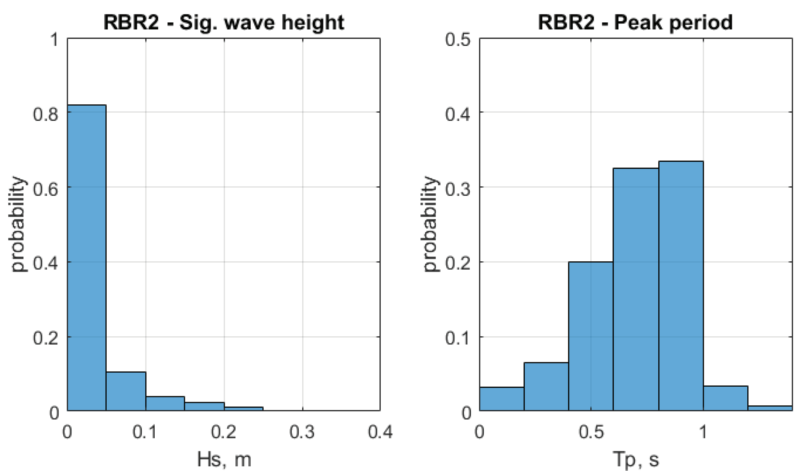

(b)

Figure 40: (a) Significant wave height, Hs (m) and Peak wave period, Tp (s) calculated using the linear wave theory and spectral analysis at location 2 from August 28 - September 17, 2015 (b) Histogram of the wind wave properties. [filename: `RBR2_20150921.mat`]

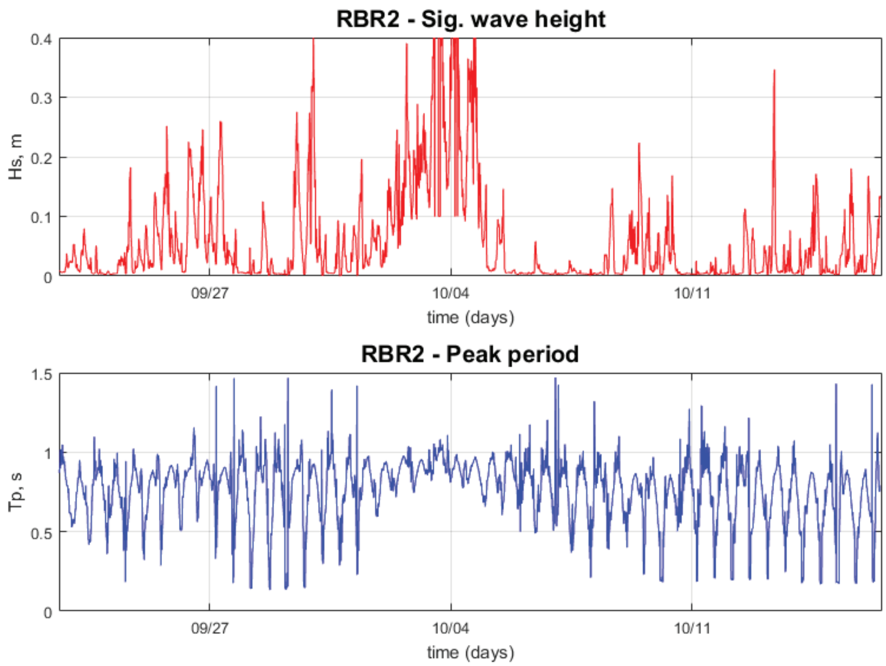

(a)

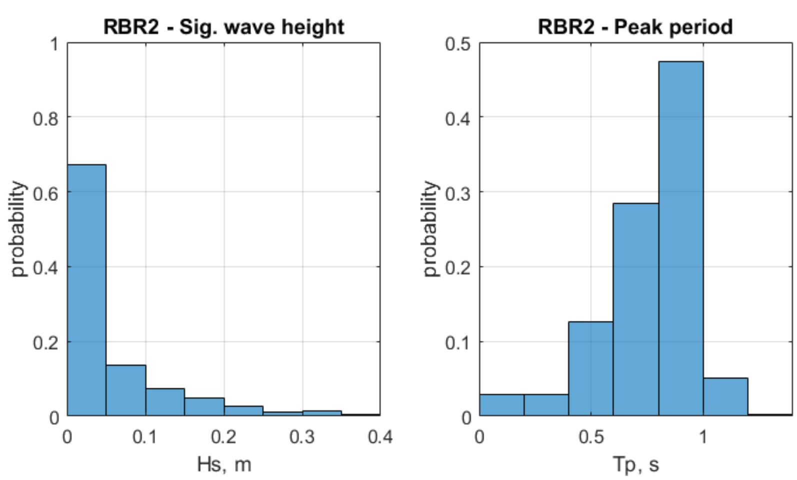

(b)

Figure 41: (a) Significant wave height, Hs (m) and Peak wave period, Tp (s) calculated using the linear wave theory and spectral analysis at location 2 from September 21 - October 16, 2015 (b) Histogram of the wind wave properties. [filename: `RBR2_20151016.mat`]

3 Current data

3.1 Aquadopp profiler

To measure 3D water flow velocity we deployed five Nortek AS Aquadopp HR-Profilers at different channel locations in the BHNWR. The Aquadopp HR is an upgraded version of the standard 1 or 2 MHz Nortek Aquadopp profiler, and the new pulse-coherent processing technique can measure velocity profiles with vertical resolution as fine as 0.7 cm or as fast as 8 Hz. The locations, deployment period and filenames are provided in the Table 4. Technical specification of the instrument along with the file type and structure is briefly described in the Appendix C.

Location	Deployment period	Depth (meters)	Filenames
Sluice Ditch (39°17.740'N 75°26.587'W)	04/16/2015 - 06/12/2015	7.5	AquaA_20150612
Leipsic River (39°14.280'N 75°24.900'W)	04/16/2015 - 06/12/2015	4.0	AquaB_20150612
North Duck (39°17.809'N 75°27.313'W)	04/16/2015 - 06/12/2015	5.0	AquaC_20150612
South Duck (39°16.069'N 75°26.913'W)	04/16/2015 - 06/12/2015	6.0	AquaD_20150612
Sheerness (39°16.003'N 75°27.820'W)	04/16/2015 - 06/12/2015	2.5	AquaE_20150612

Table 4: Aquadopp file names and sampling durations.

3.1.1 Data processing

Some necessary steps are briefly described here which we followed before the instrument deployment and during post-processing of the current data:

1. Before the deployment, we performed the compass calibration of all gauges.

2. The time interval, the blank distance, and the number of levels where at each level the gauge measures the velocity were defined in the gauge settings.

3. Once the gauge is mounted in the channel bottom, the water level was measured, and the pressure data then converted to water elevation based on the known vertical datum (i.e. NAVD88). We measured the water surface with RTK unit from NAVD88 datum.

4. The gauge starts recording the data, and at each time step, it records the pressure, orientation

(roll, heading, and pitch) and the velocity components at each level.

5. After gauge retrieval, the barometric pressure was removed from pressure time series and then the signal was shifted to the proper vertical reference.

Figure 42: Position and orientation of the Aquadopp HR-profiler at location A during deployment and retrieval [filename: AquaA_20150612.csv]

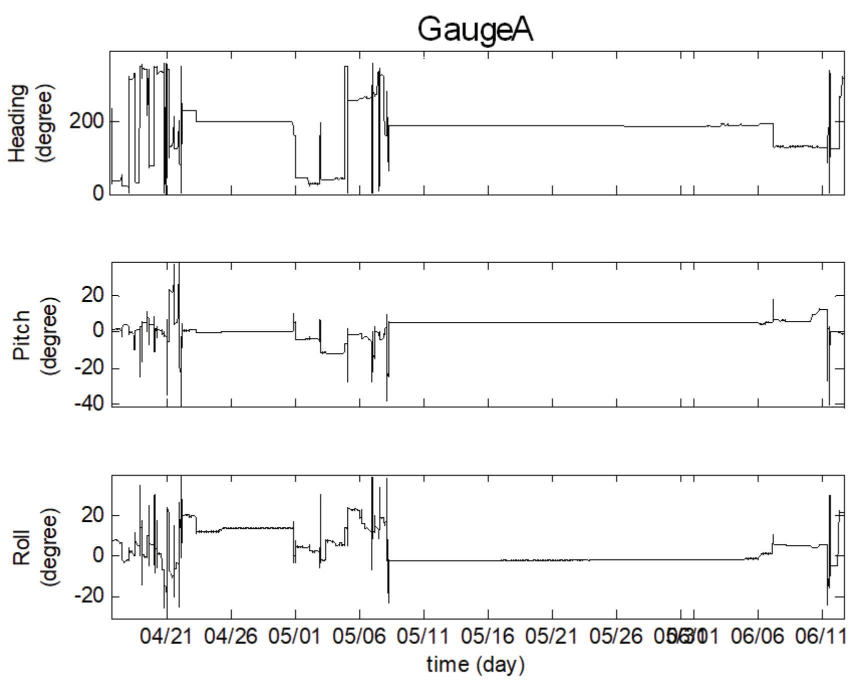

Figure 43: Aquadopp HR-profiler Heading, Pitch and Roll at location A during April 16 - June 12, 2015

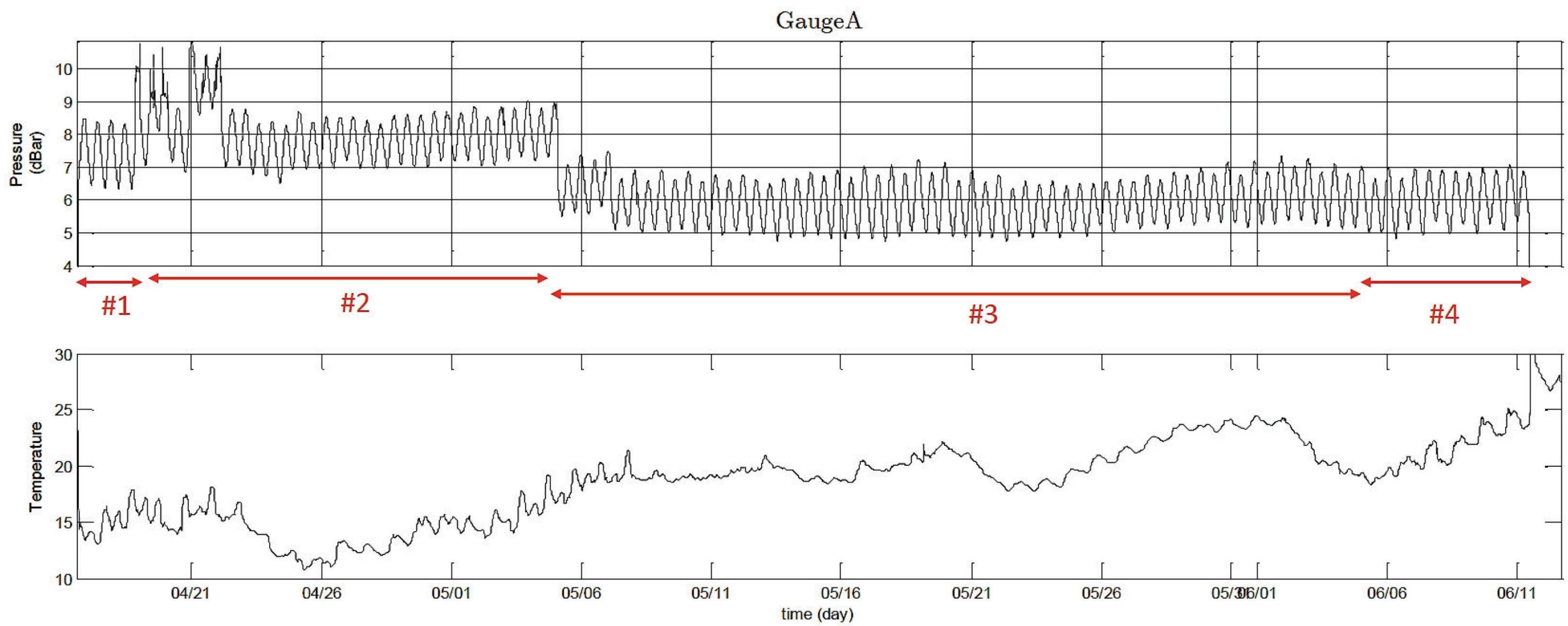

Figure 44: Pressure and temperature variation at location A. We can notice that the instrument shifted several times from its origin. Hence, the recorded data is separated into four segments in the following figures.

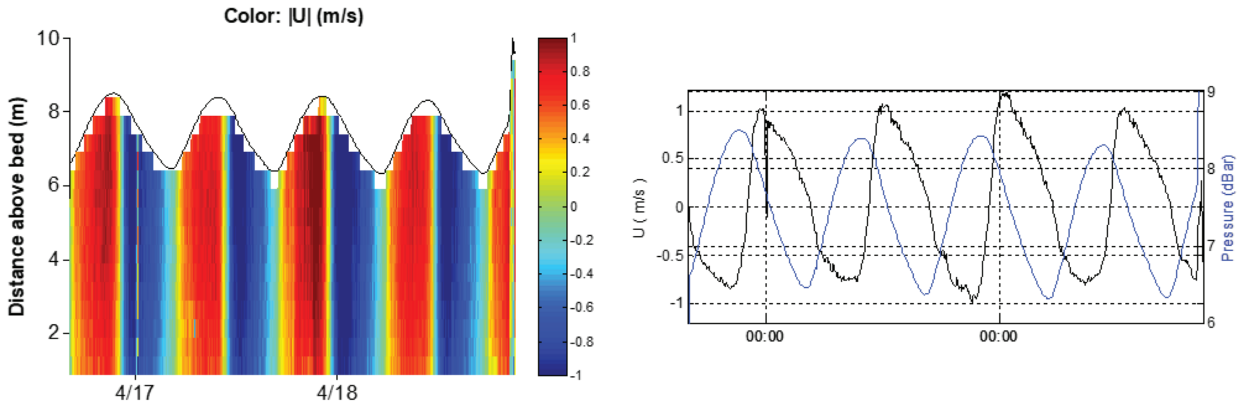

Figure 45: Depth varying velocity (in m/s) [on the left], and depth averaged velocity and pressure (in dBar, blue line) [on the right] for segment 1 (location A)

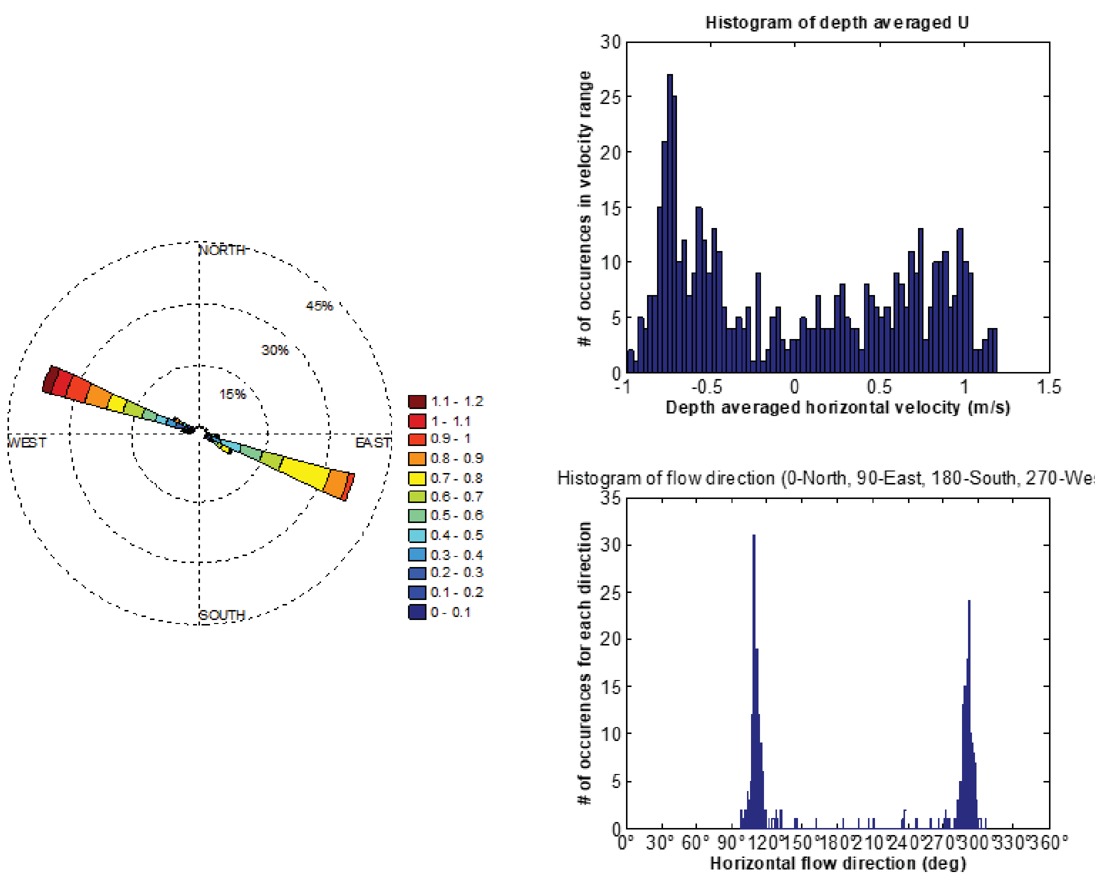

Figure 46: Direction and magnitude of depth averaged velocity (in m/s) [on the left], Histogram of the flow velocity and direction [on the right] for segment 1 (location A).

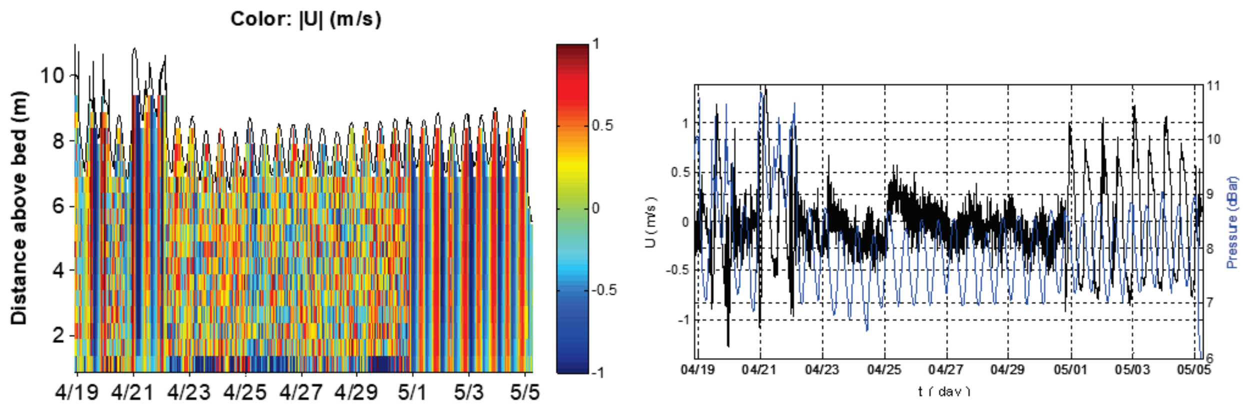

Figure 47: Depth varying velocity (in m/s) [on the left], and depth averaged velocity and pressure (in dBar, blue line) [on the right] for segment 2 (location A).

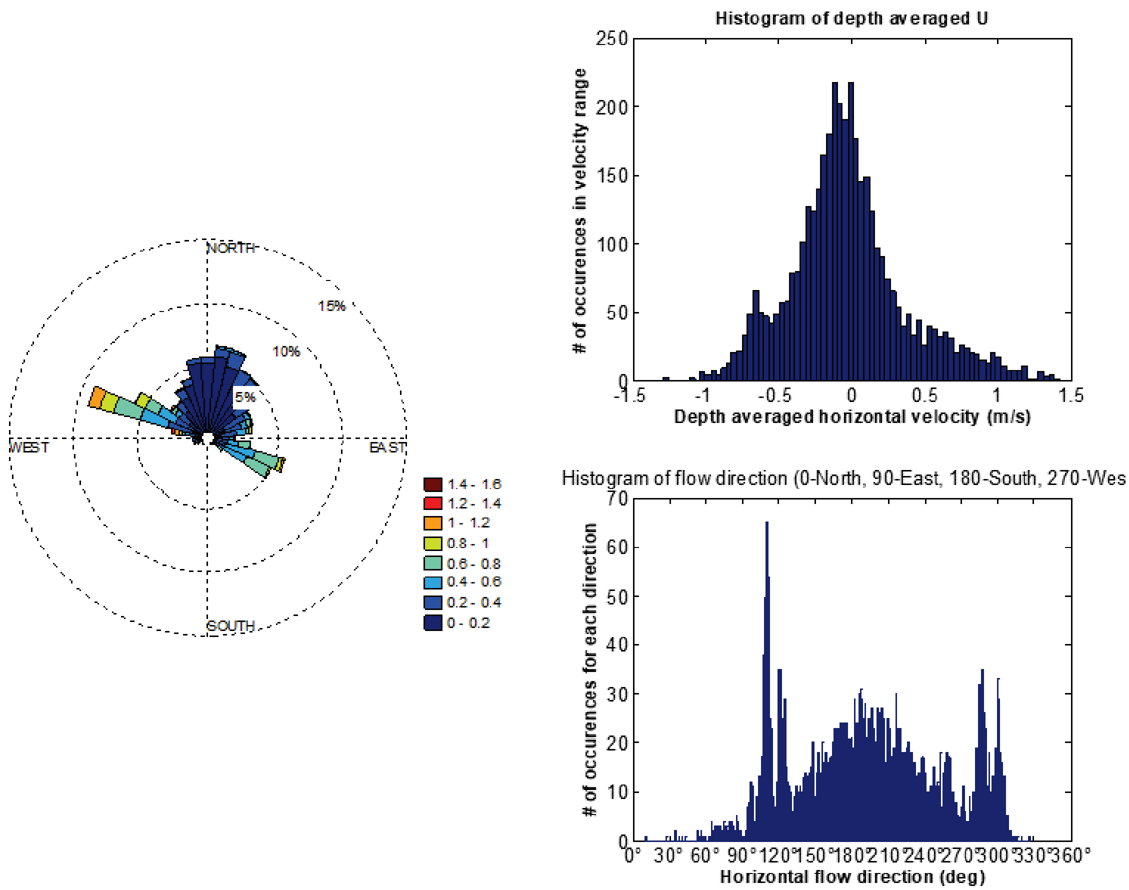

Figure 48: Direction and magnitude of depth averaged velocity (in m/s) [on the left], Histogram of the flow velocity and direction [on the right] for segment 2 (location A)

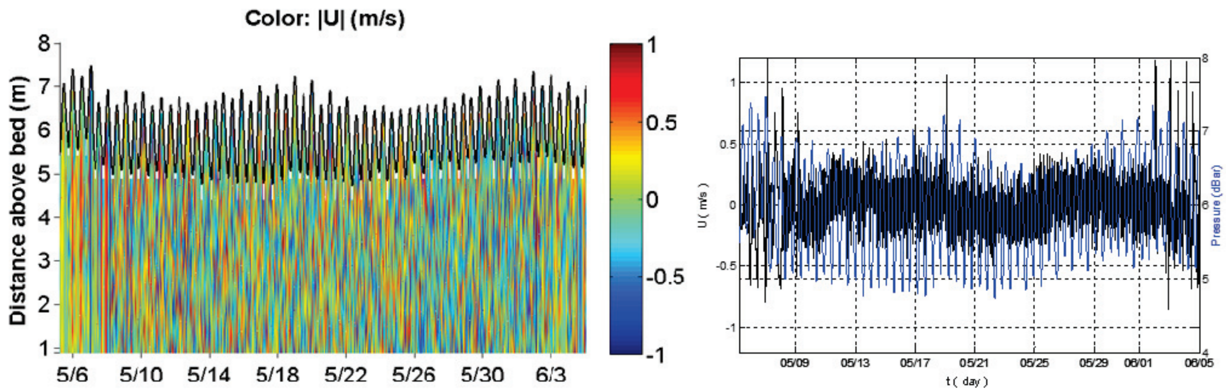

Figure 49: Depth varying velocity (in m/s) [on the left], and depth averaged velocity and pressure (in dBar, blue line) [on the right] for segment 3 (location A)

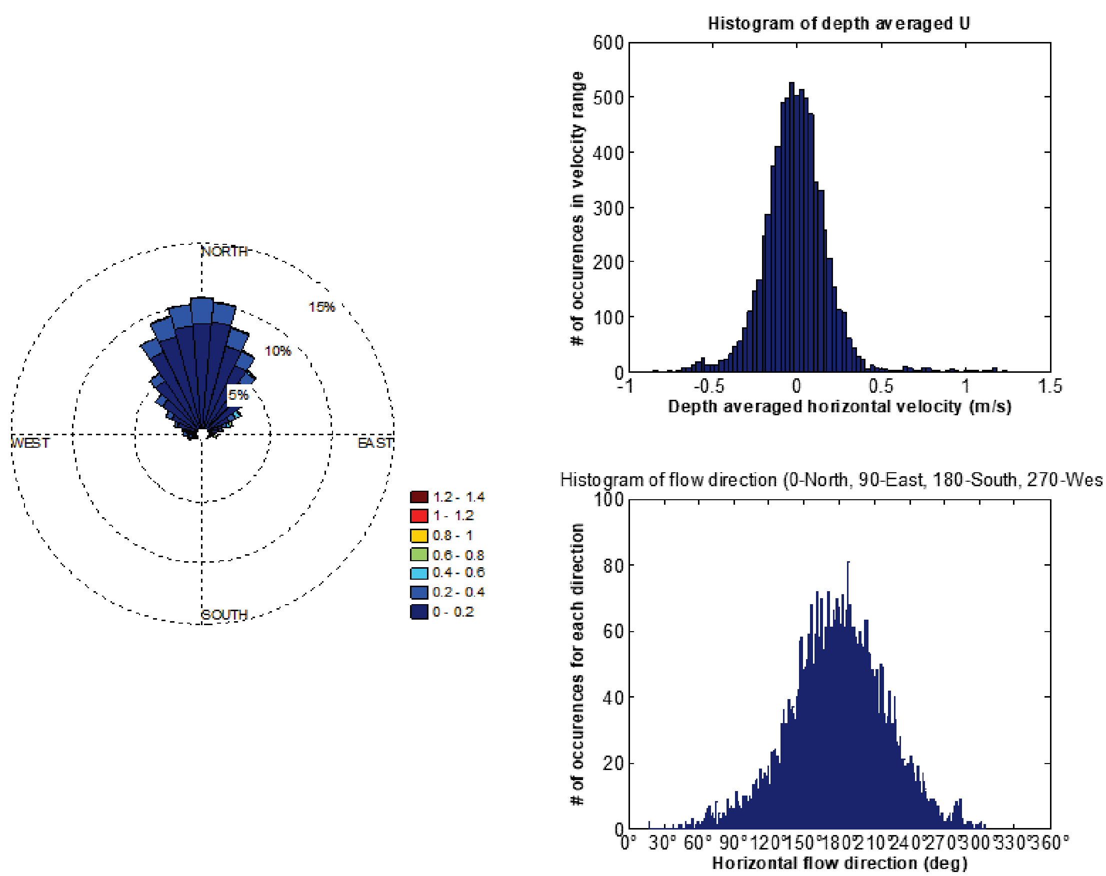

Figure 50: Direction and magnitude of depth averaged velocity (in m/s) [on the left], Histogram of the flow velocity and direction [on the right] for segment 3 (location A)

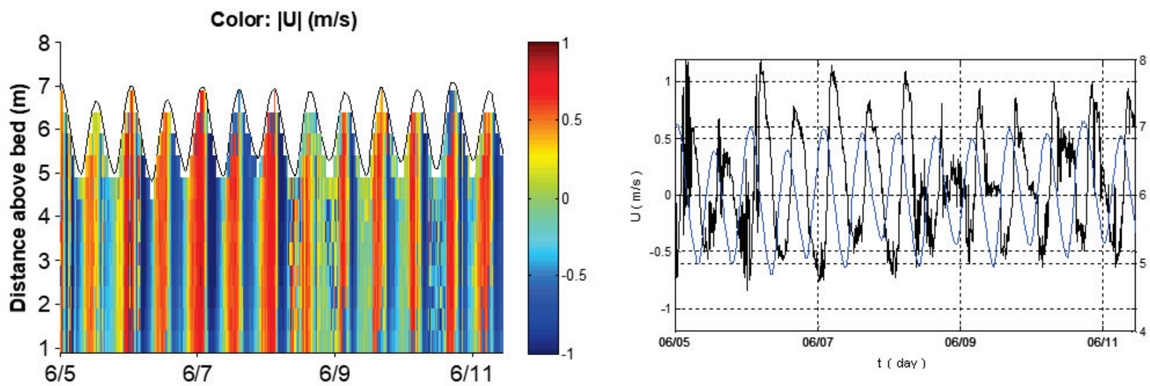

Figure 51: Depth varying velocity (in m/s) [on the left], and depth averaged velocity and pressure (in dBar, blue line) [on the right] for segment 4 (location A)

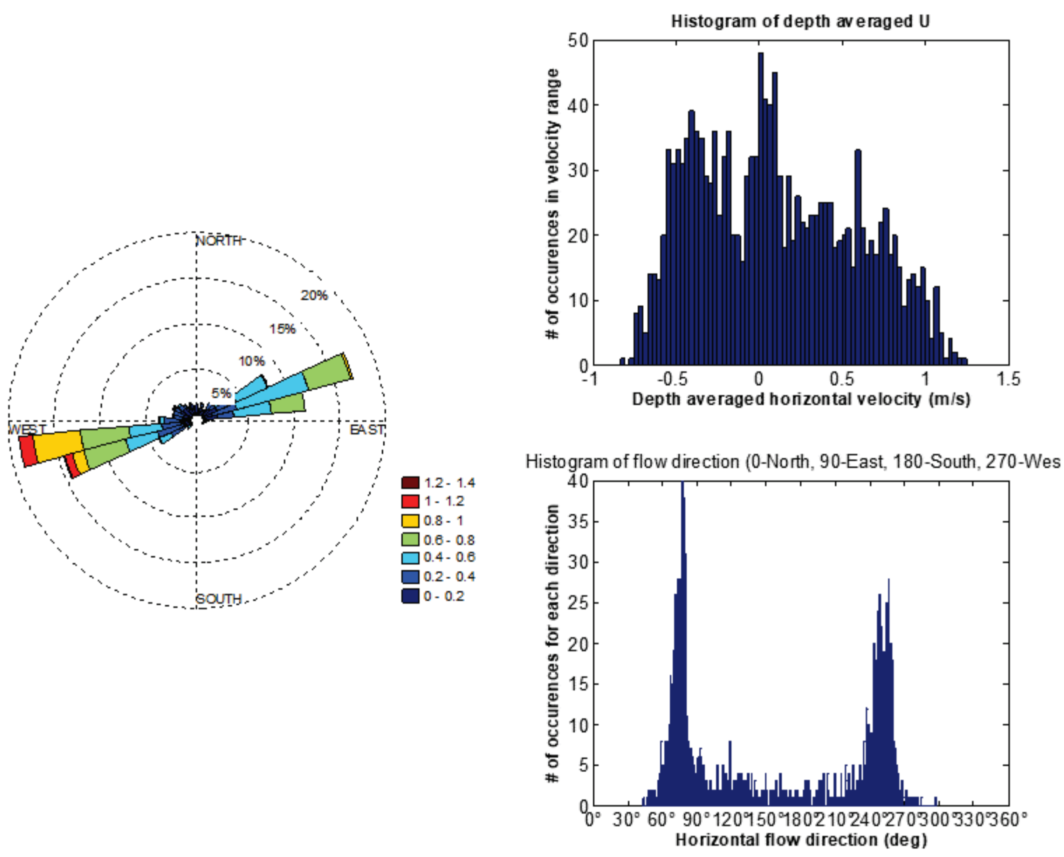

Figure 52: Direction and magnitude of depth averaged velocity (in m/s) [on the left], Histogram of the flow velocity and direction [on the right] for segment 4 (location A)

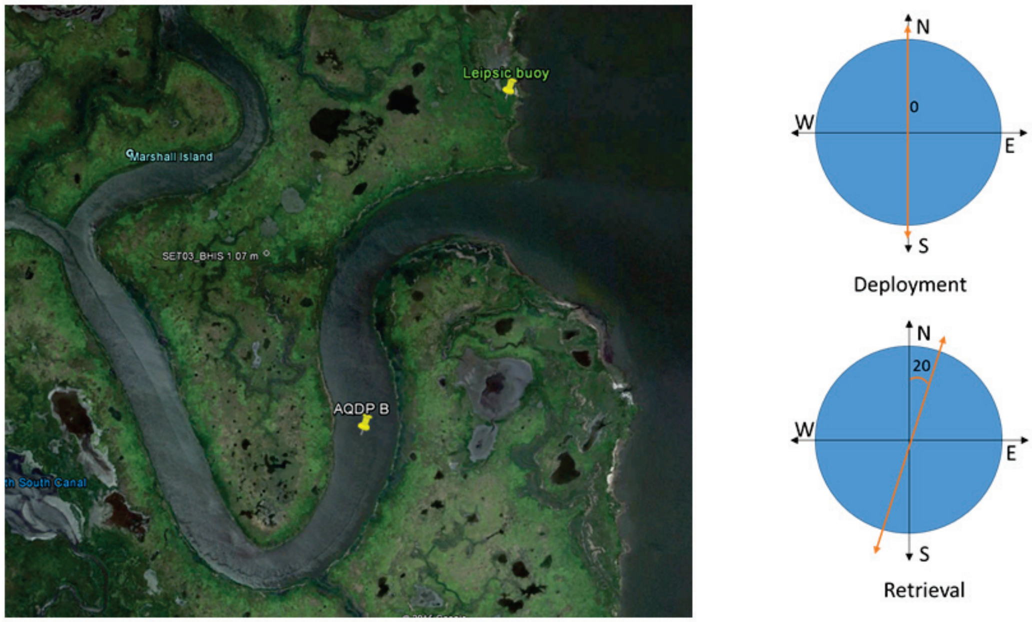

Figure 53: Position and orientation of the Aquadopp HR-profiler at location B during deployment and retrieval [filename: `AquaB_20150612.csv`]

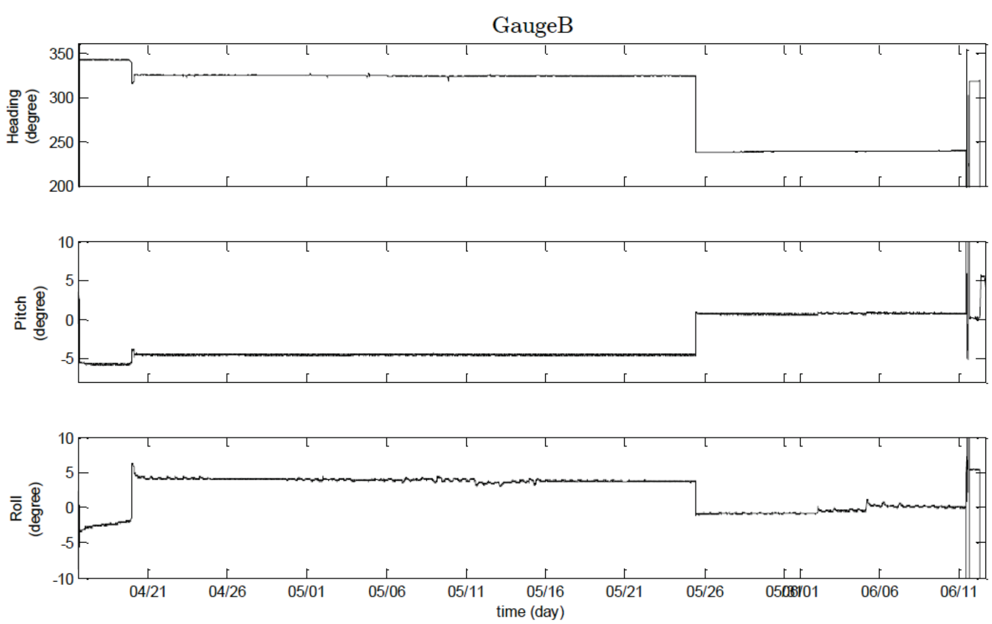

Figure 54: Aquadopp HR-profiler Heading, Pitch and Roll at location B during April 16 - June 12, 2015

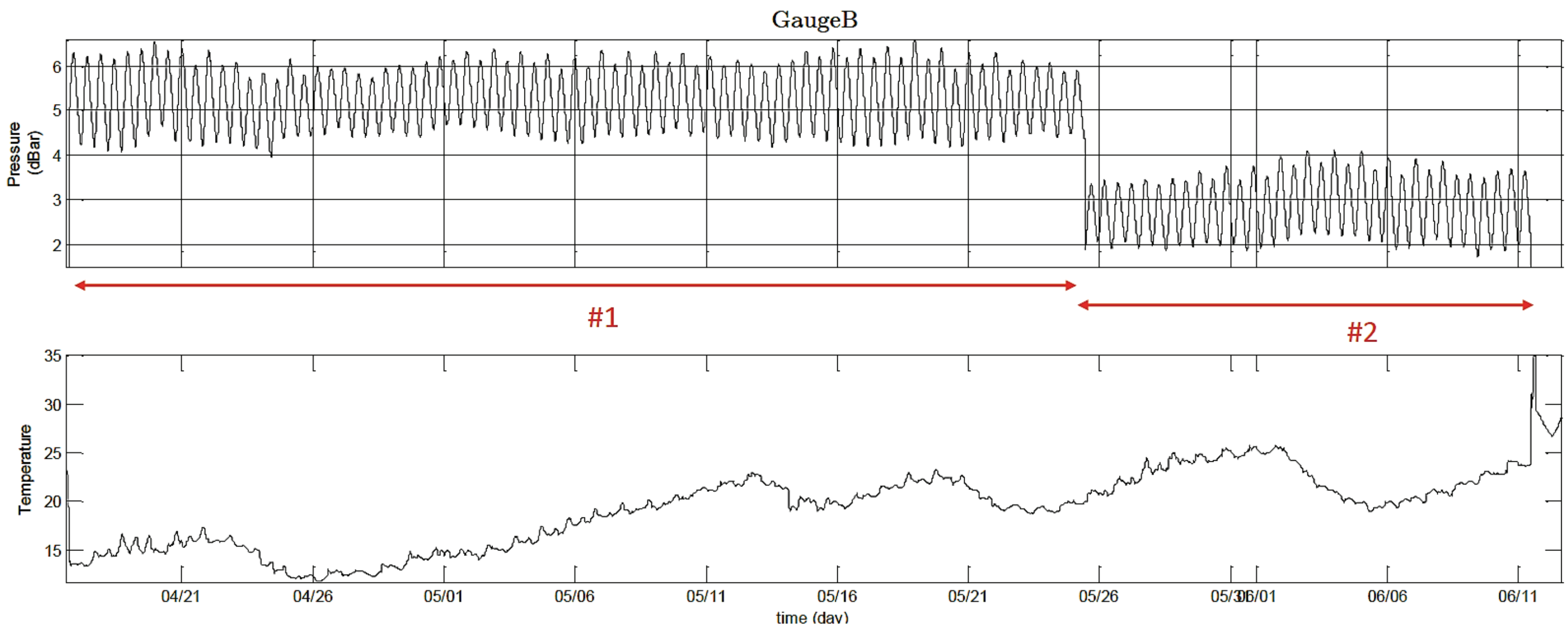

Figure 55: Pressure and temperature variation at location B. We can notice that the instrument shifted several times from its origin. Hence, the recorded data is separated into two segments in the following figures.

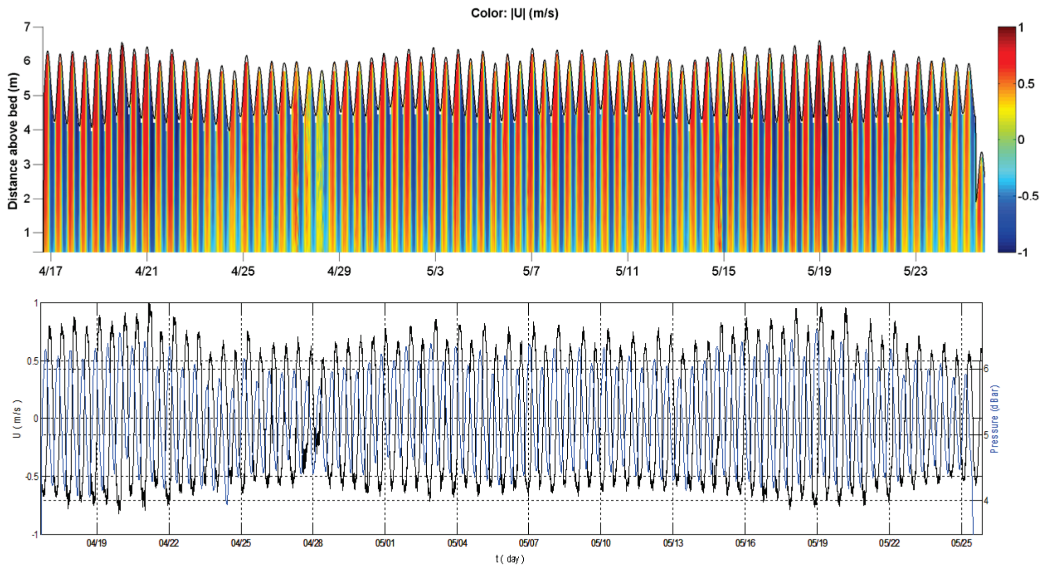

Figure 56: Depth varying velocity (in m/s) [upper subplot], and depth averaged velocity and pressure (in dBar, blue line) [lower subplot] for segment 1 (location B)

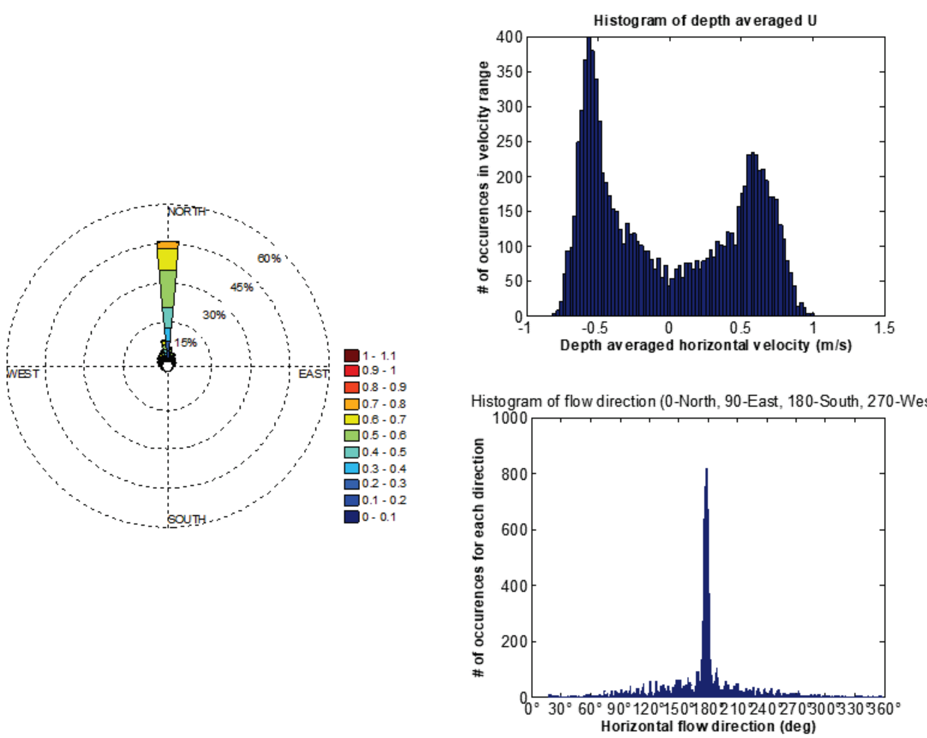

Figure 57: Direction and magnitude of depth averaged velocity (in m/s) [on the left], Histogram of the flow velocity and direction [on the right] for segment 1 (location B)

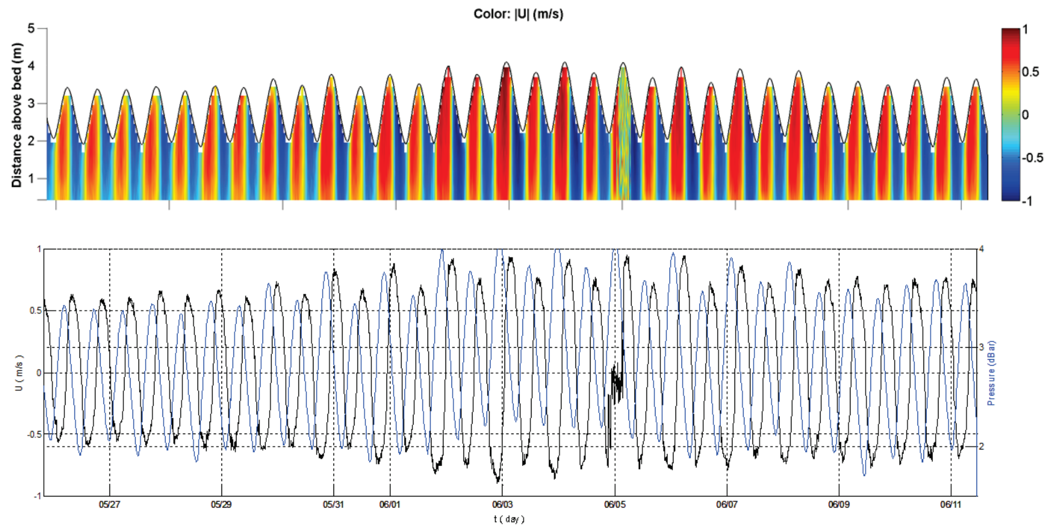

Figure 58: Depth varying velocity (in m/s) [upper subplot], and depth averaged velocity and pressure (in dBar, blue line) [lower subplot] for segment 2 (location B)

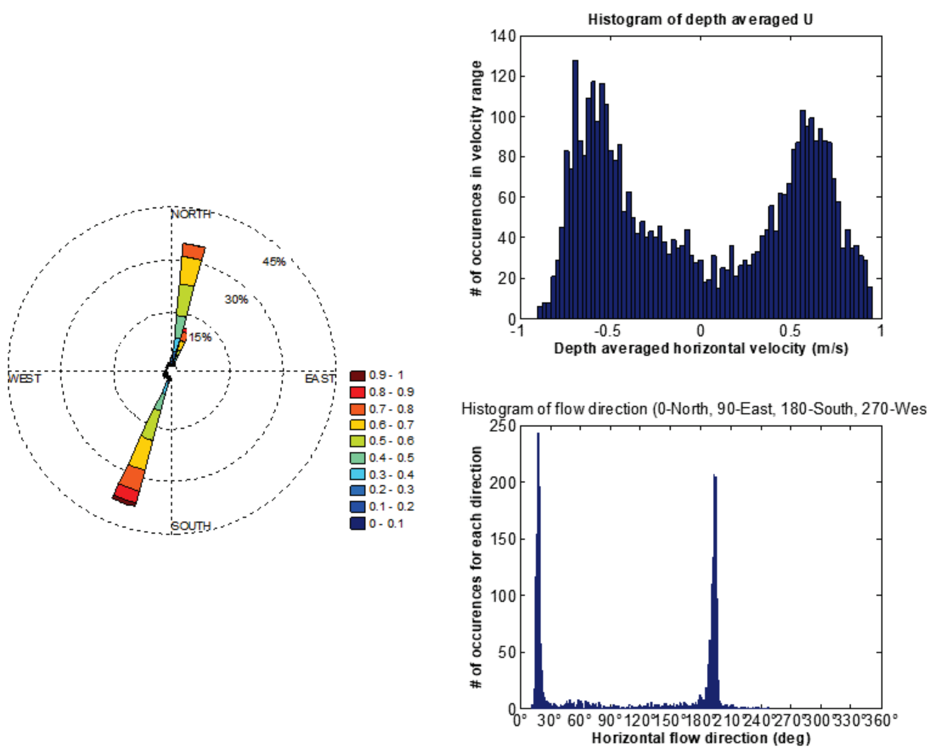

Figure 59: Direction and magnitude of depth averaged velocity (in m/s) [on the left], Histogram of the flow velocity and direction [on the right] for segment 2 (location B)

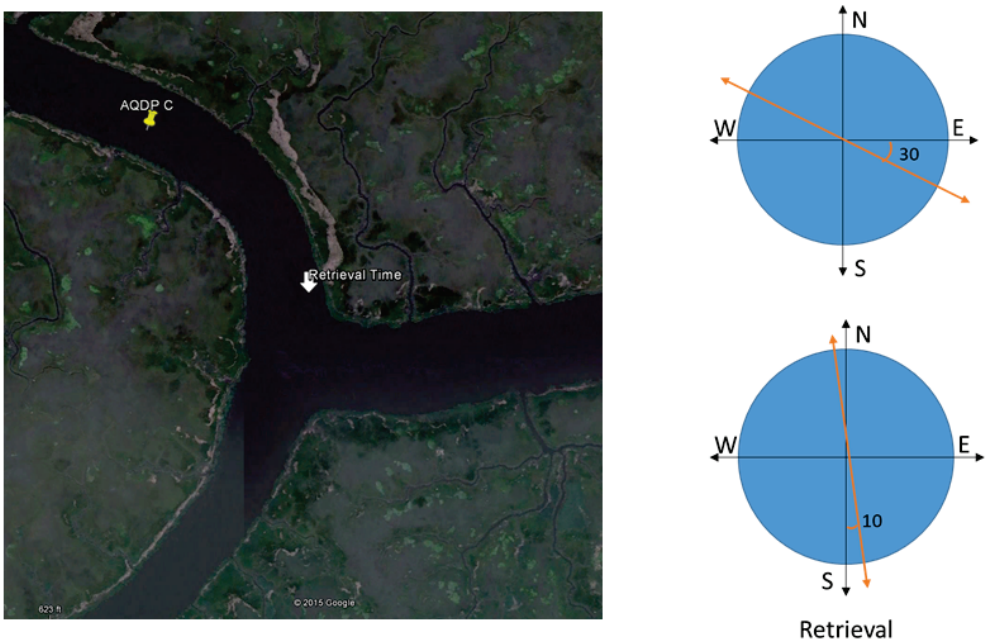

Figure 60: Position and orientation of the Aquadopp HR-profiler at location C during deployment and retrieval [filename: `AquaC_20150612.csv`]

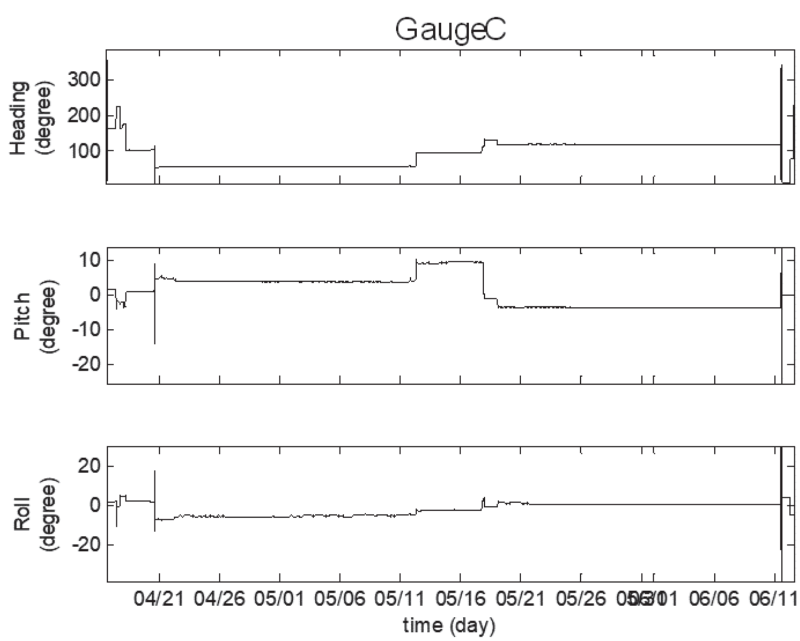

Figure 61: Aquadopp HR-profiler Heading, Pitch and Roll at location C during April 16 - June 12, 2015

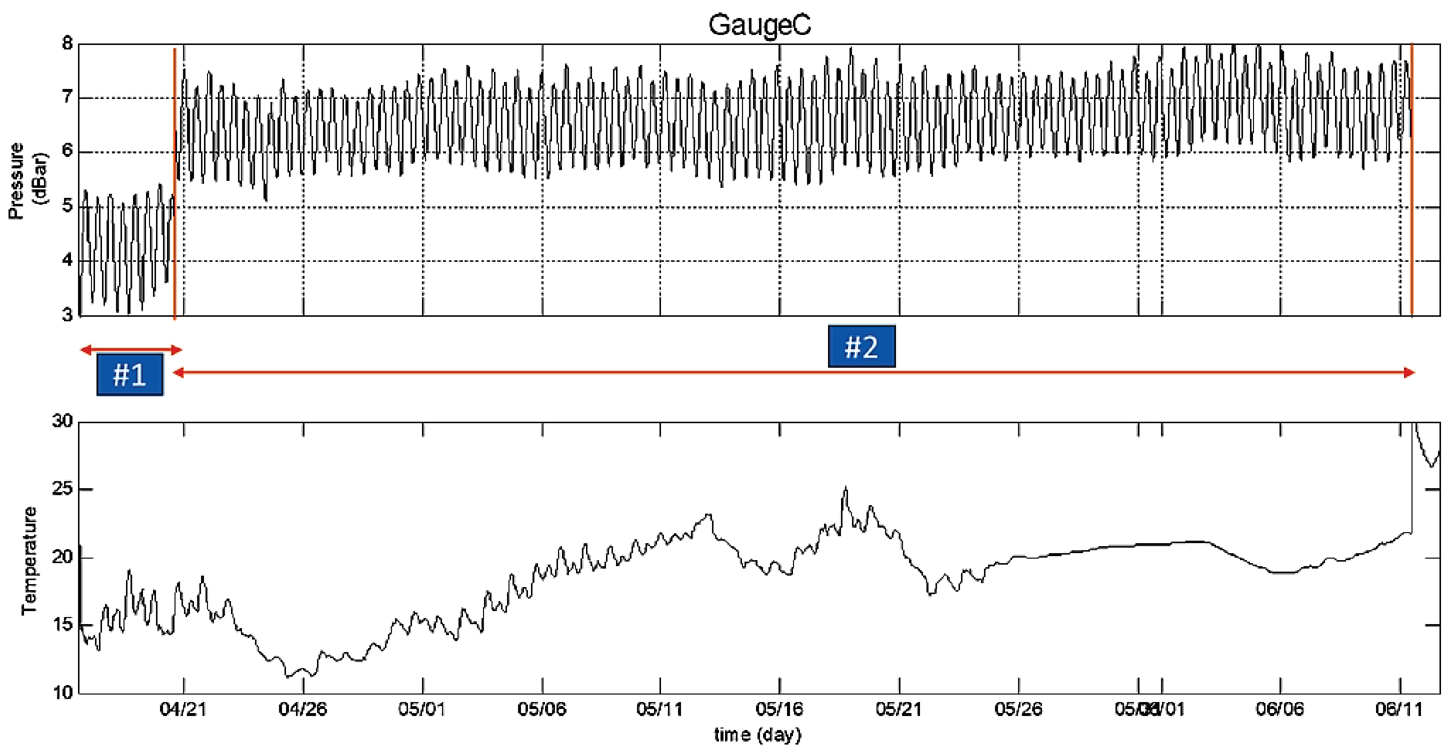

Figure 62: Pressure and temperature variation at location C. We can notice that the instrument shifted several times from its origin. Hence, the recorded data is separated into two segments in the following figures.

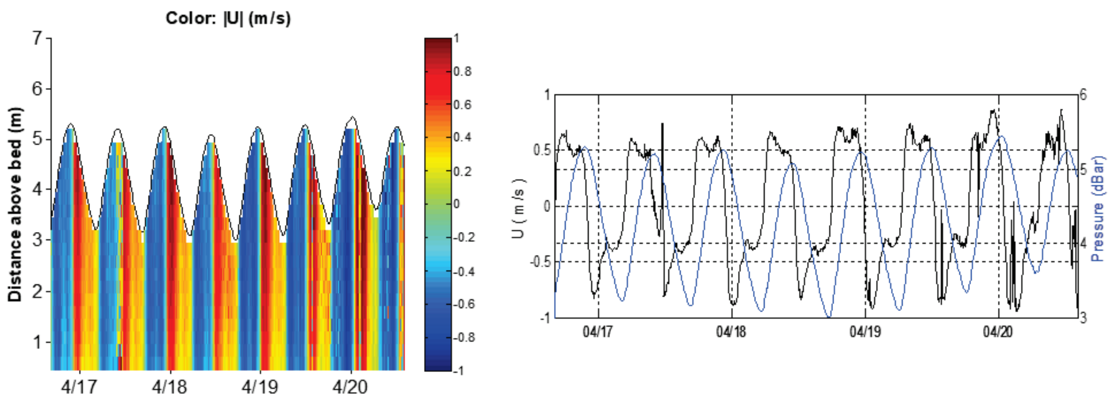

Figure 63: Depth varying velocity (in m/s) [on the left], and depth averaged velocity and pressure (in dBar, blue line) [on the right] for segment 1 (location C)

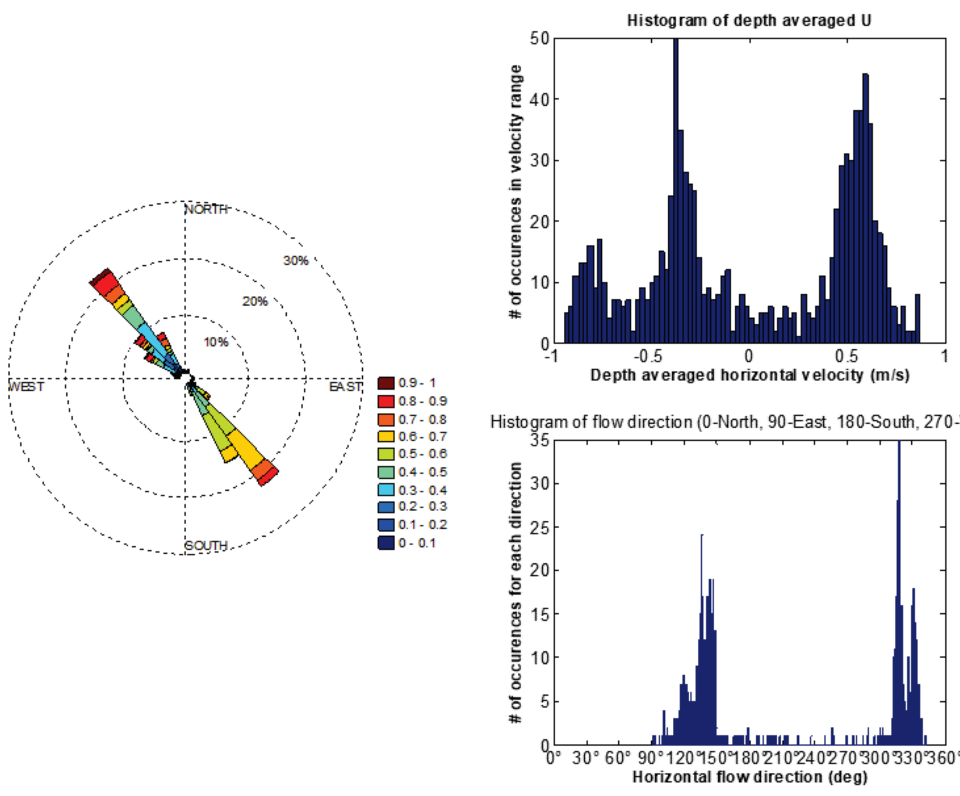

Figure 64: Direction and magnitude of depth averaged velocity (in m/s) [on the left], Histogram of the flow velocity and direction [on the right] for segment 1 (location C)

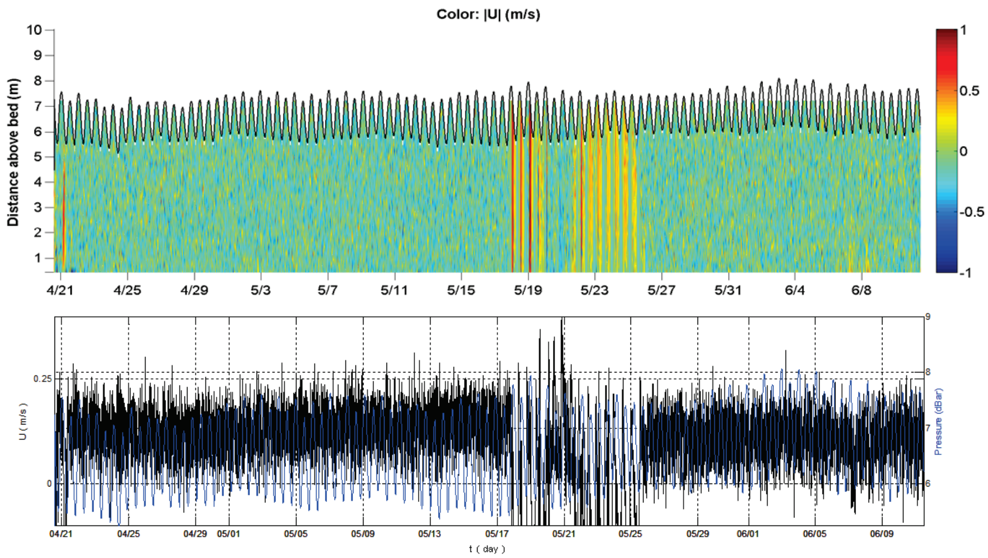

Figure 65: Depth varying velocity (in m/s) [upper subplot], and depth averaged velocity and pressure (in dBar, blue line) [lower subplot] for segment 2 (location C)

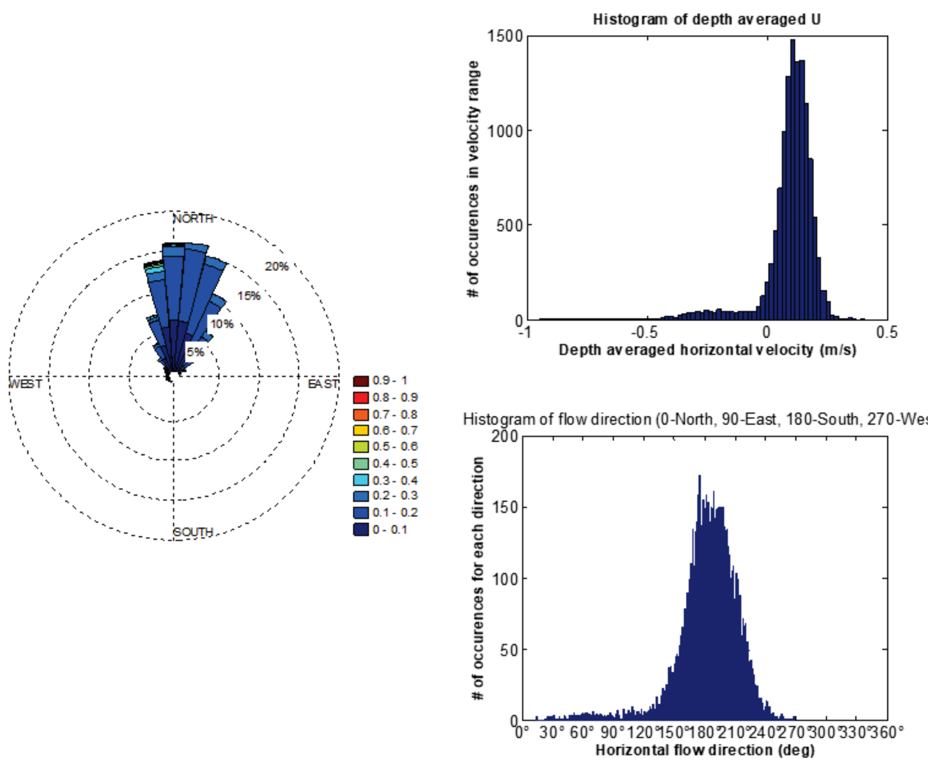

Figure 66: Direction and magnitude of depth averaged velocity (in m/s) [on the left], Histogram of the flow velocity and direction [on the right] for segment 2 (location C)

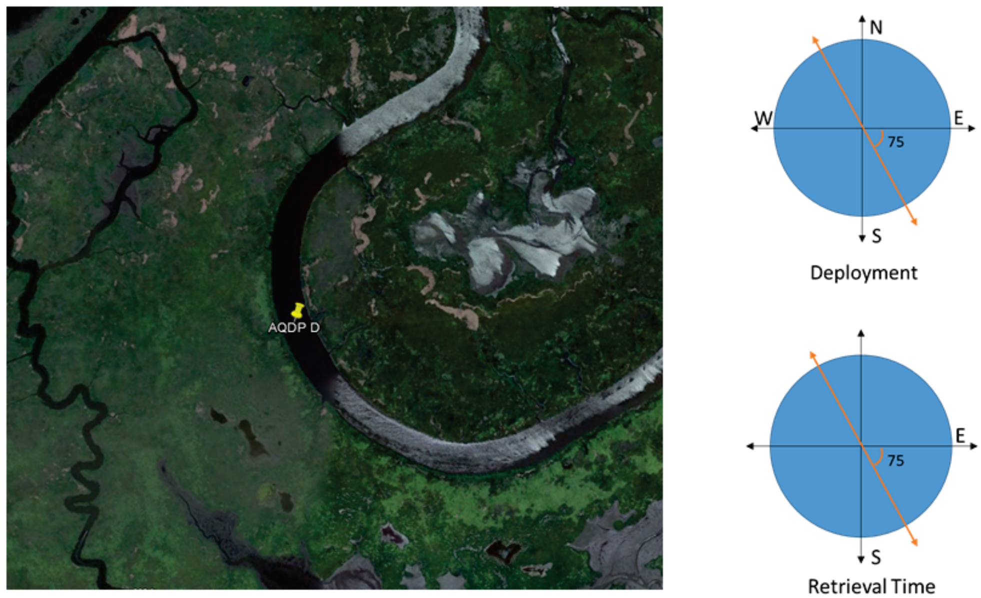

Figure 67: Position and orientation of the Aquadopp HR-profiler at location D during deployment and retrieval [filename: `AquaD_20150612.csv`]

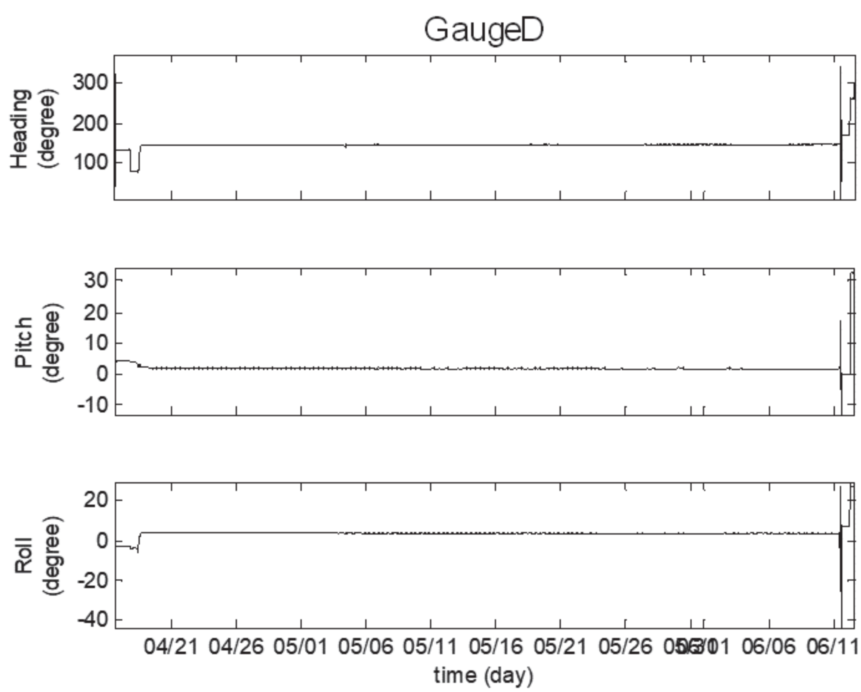

Figure 68: Aquadopp HR-profiler Heading, Pitch and Roll at location D during April 16 - June 12, 2015

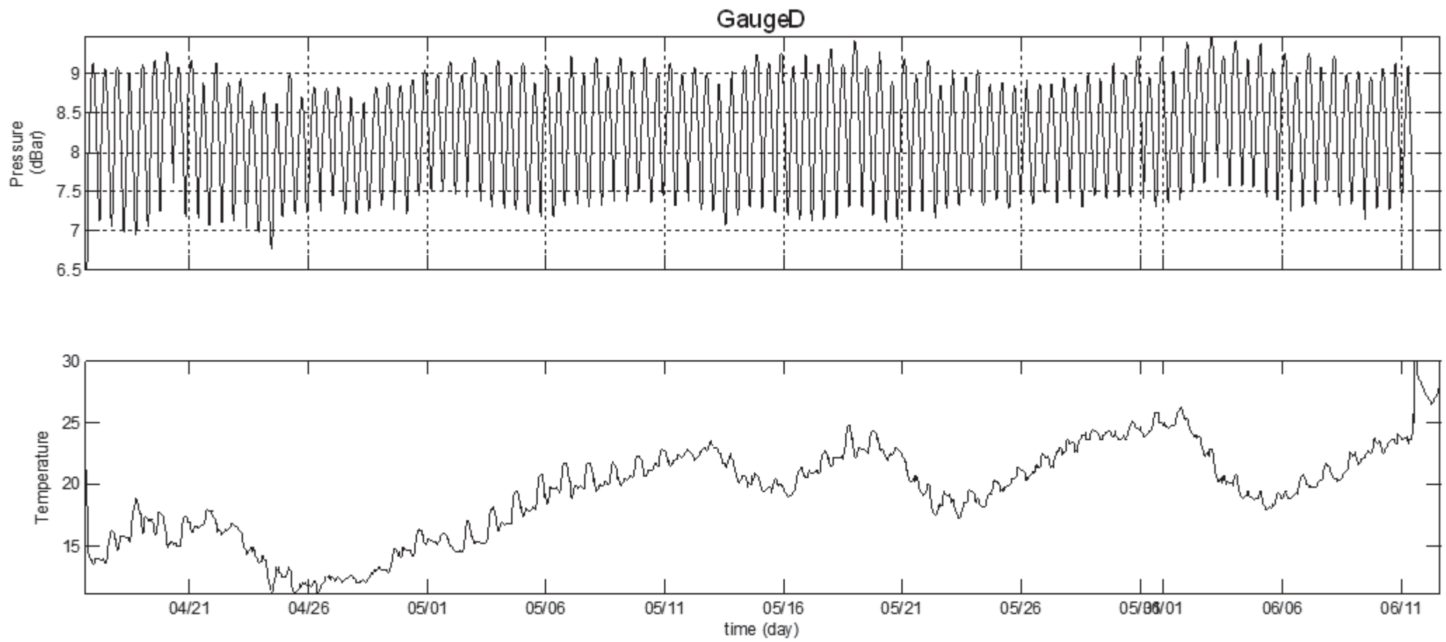

Figure 69: Pressure and temperature variation at location D. The recorded data is separated into multiple segments in the following figures.

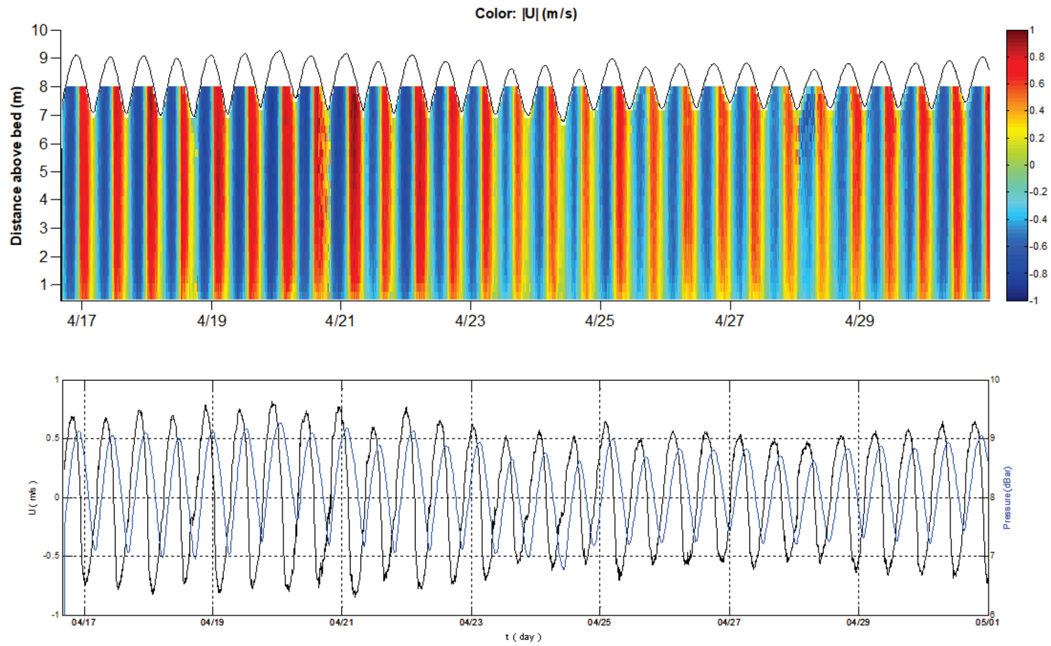

Figure 70: Depth varying velocity (in m/s) [upper subplot], and depth averaged velocity and pressure (in dBar, blue line) [lower subplot] from April 16 - May 1, 2015 (location D)

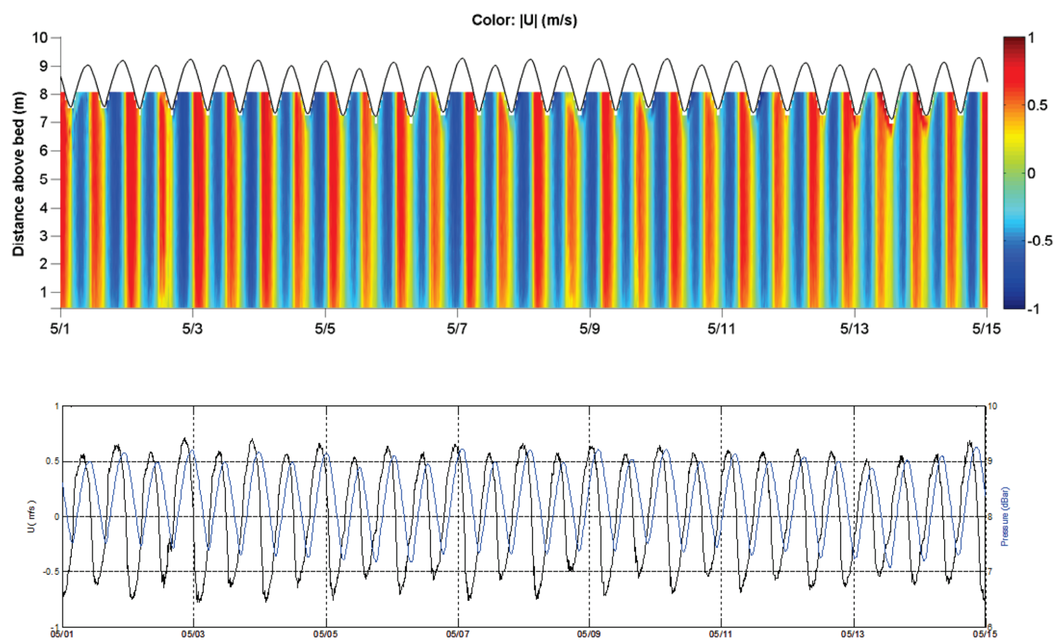

Figure 71: Depth varying velocity (in m/s) [upper subplot], and depth averaged velocity and pressure (in dBar, blue line) [lower subplot] from May 1 - May 15, 2015 (location D)

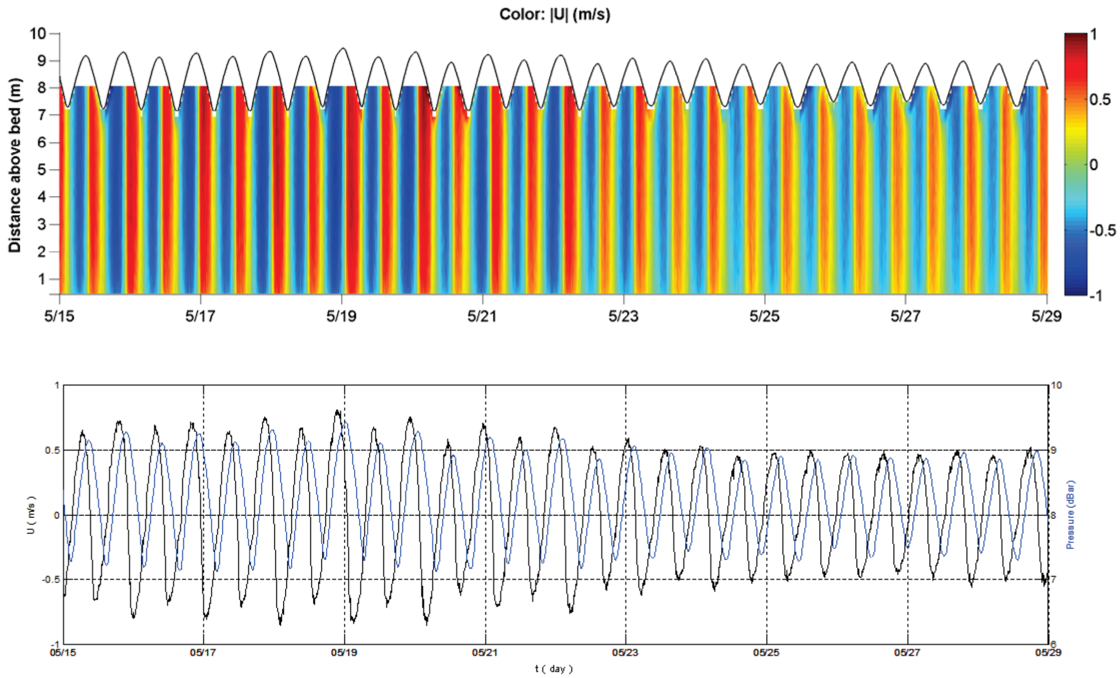

Figure 72: Depth varying velocity (in m/s) [upper subplot], and depth averaged velocity and pressure (in dBar, blue line) [lower subplot] from May 15 - May 29, 2015 (location D)

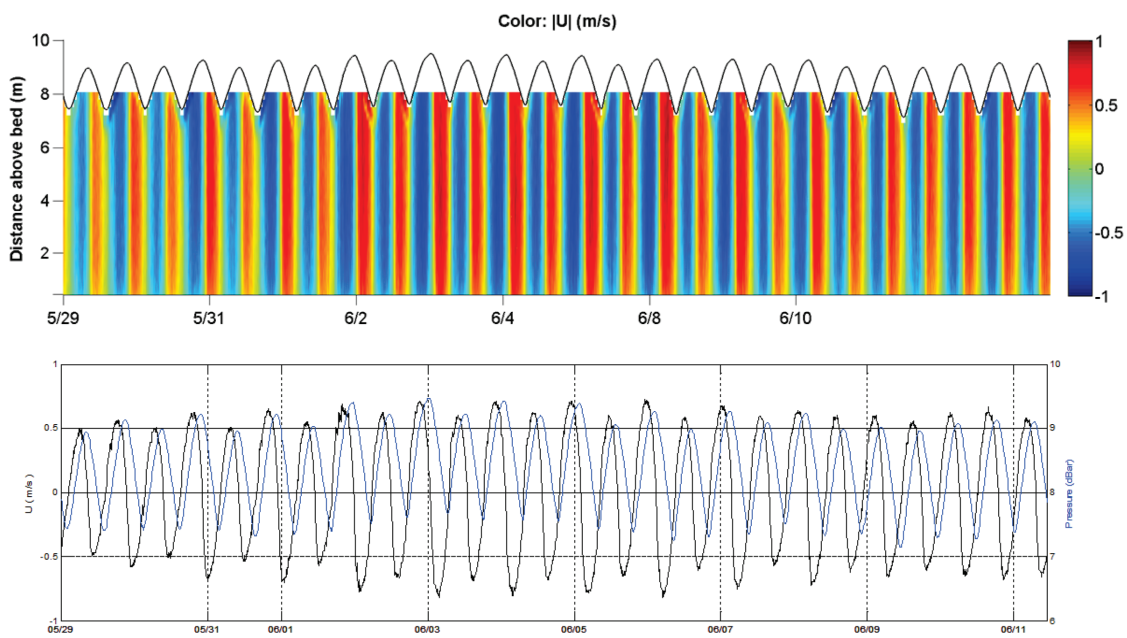

Figure 73: Depth varying velocity (in m/s) [upper subplot], and depth averaged velocity and pressure (in dBar, blue line) [lower subplot] from May 29 - June 12, 2015 (location D)

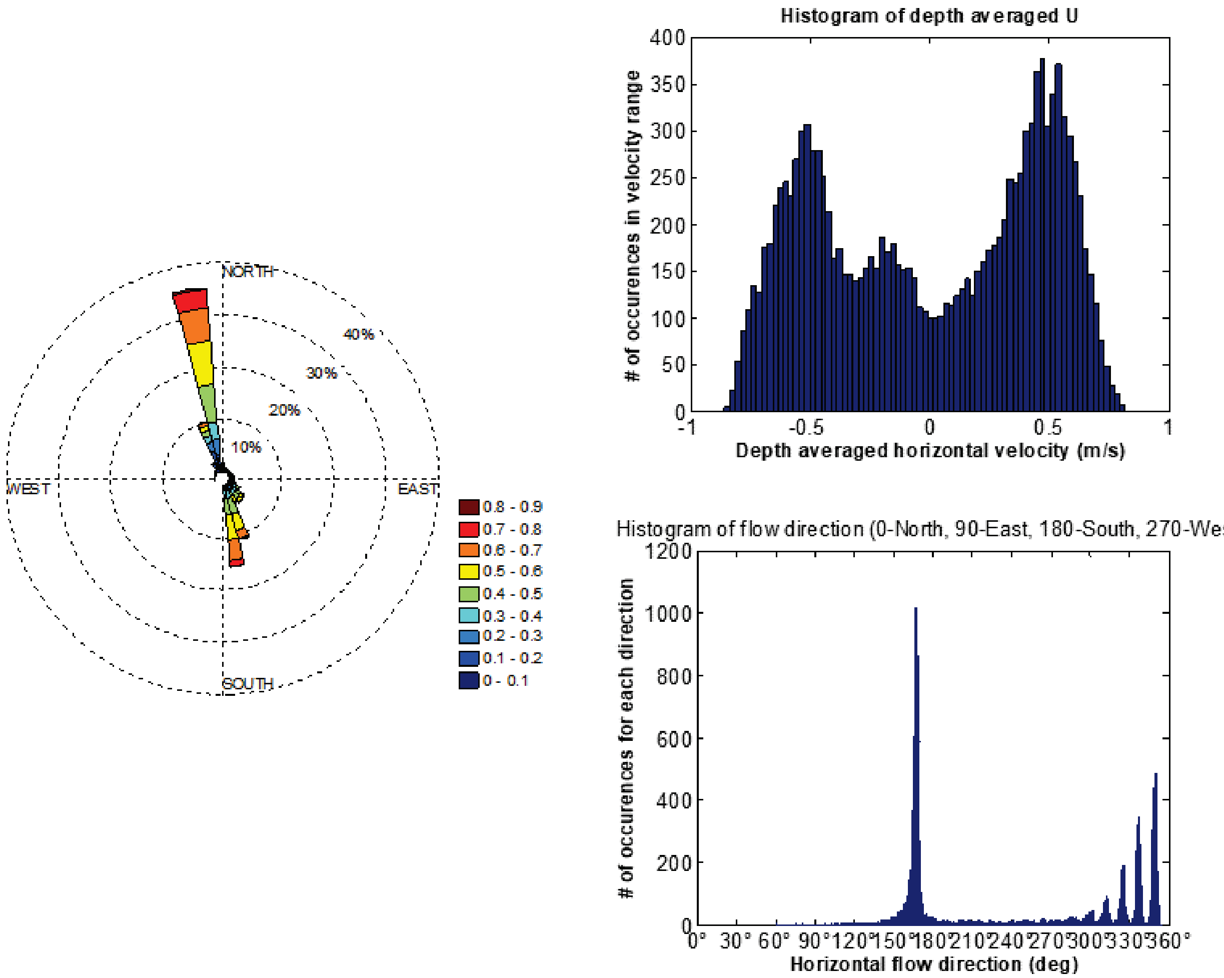

Figure 74: Direction and magnitude of depth averaged velocity (in m/s) [on the left], Histogram of the flow velocity and direction [on the right] (location D)

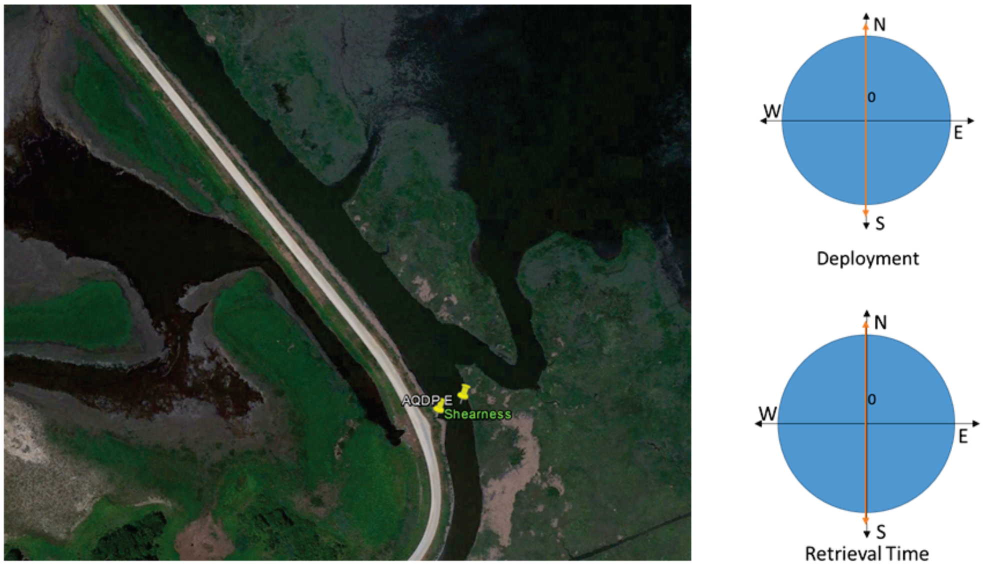

Figure 75: Position and orientation of the Aquadopp HR-profiler at location E during deployment and retrieval [filename: AquaE_20150612.csv]

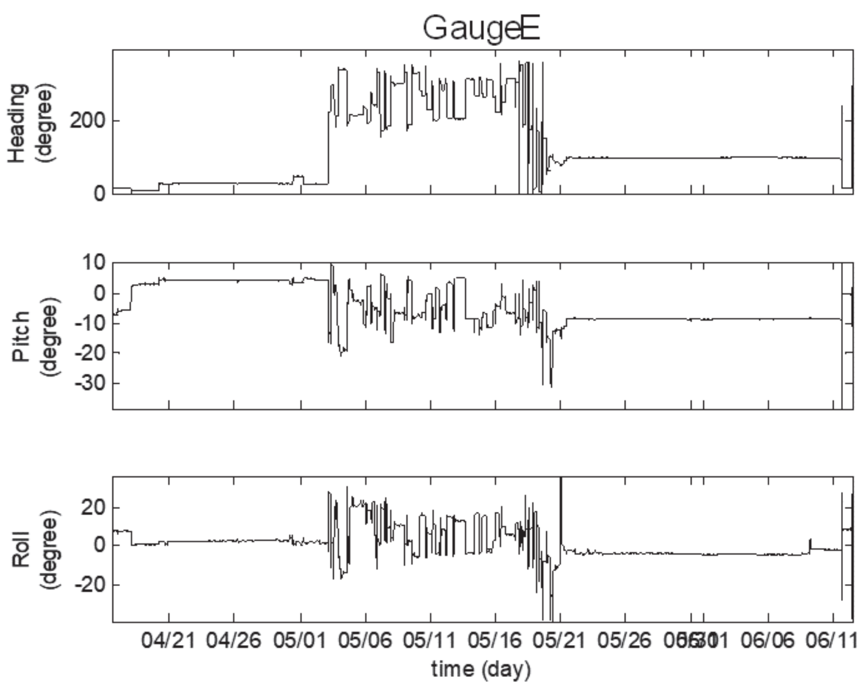

Figure 76: Aquadopp HR-profiler Heading, Pitch and Roll at location E during April 16 - June 12, 2015

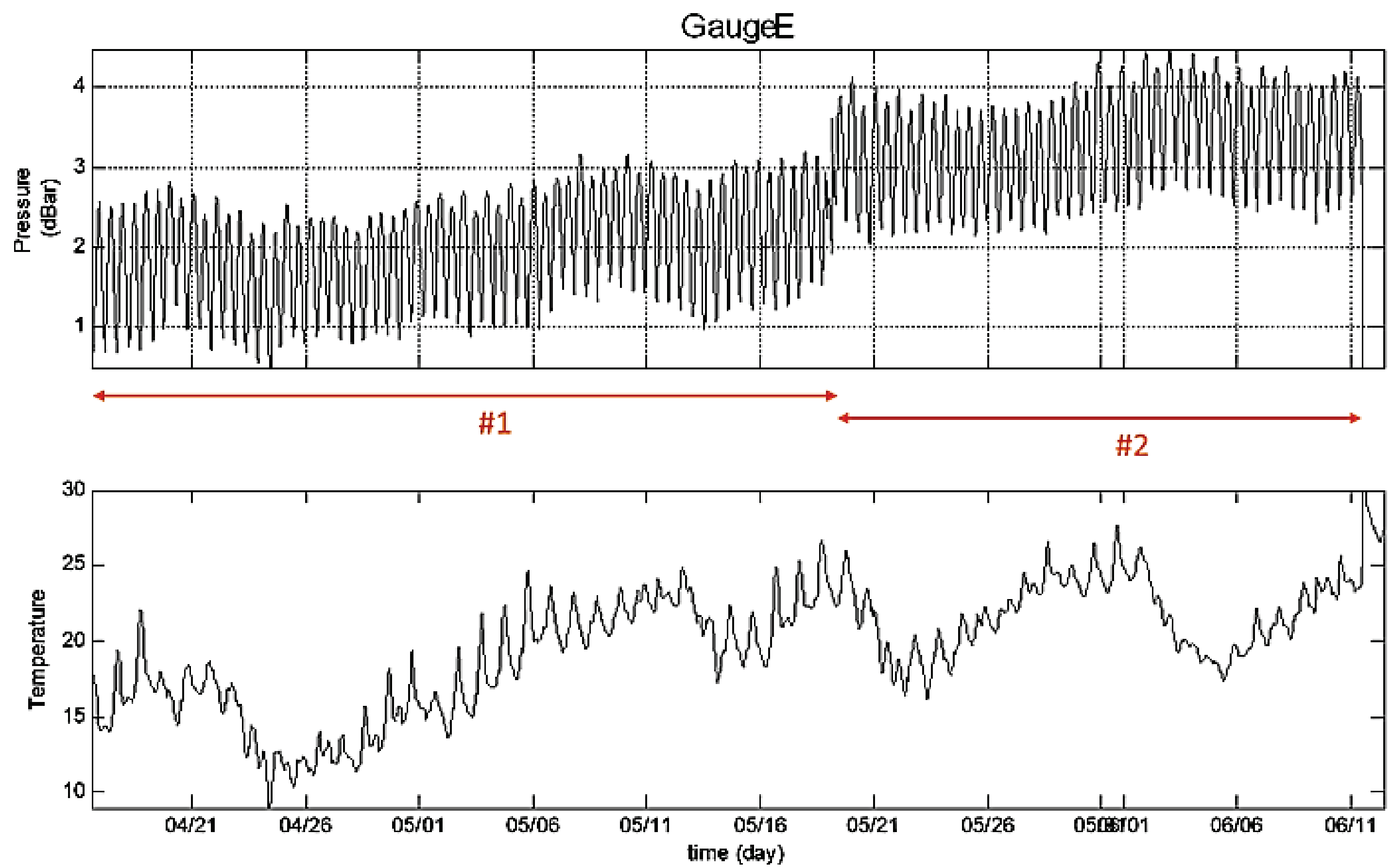

Figure 77: Pressure and temperature variation at location E. We can notice that the instrument shifted several times from its origin. Hence, the recorded data is separated into two segments in the following figures.

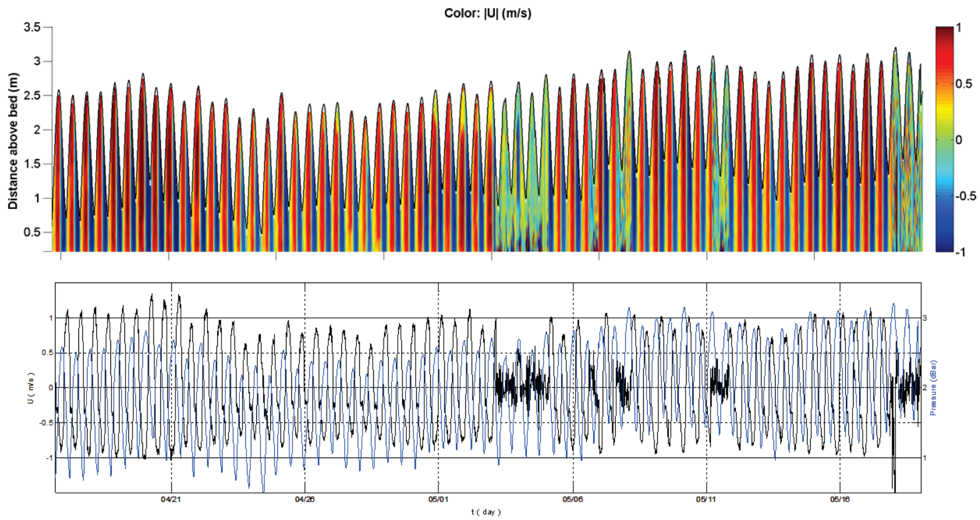

Figure 78: Depth varying velocity (in m/s) [upper subplot], and depth averaged velocity and pressure (in dBar, blue line) [lower subplot] for segment 1 (location E)

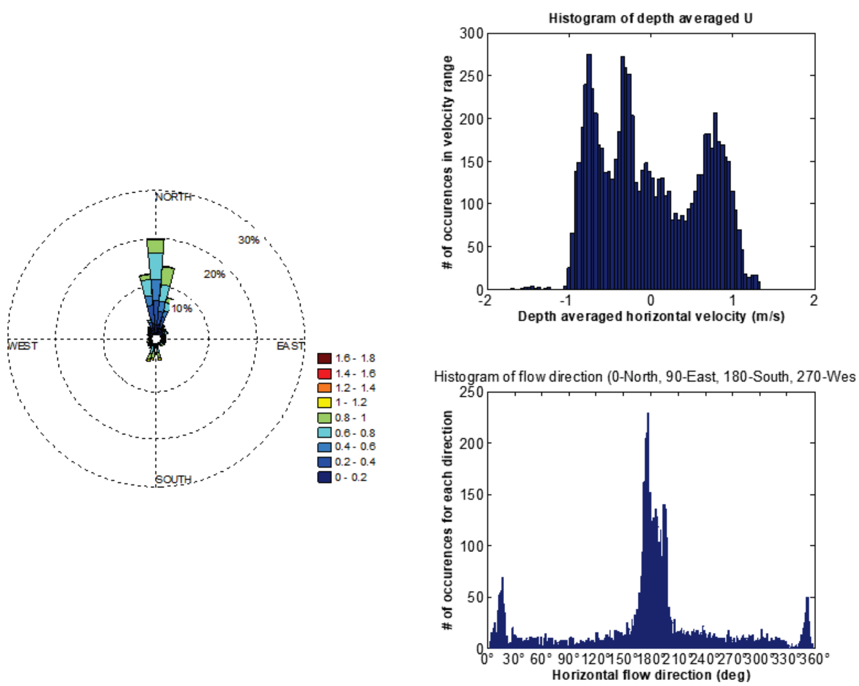

Figure 79: Direction and magnitude of depth averaged velocity (in m/s) [on the left], Histogram of the flow velocity and direction [on the right] for segment 1 (location E)

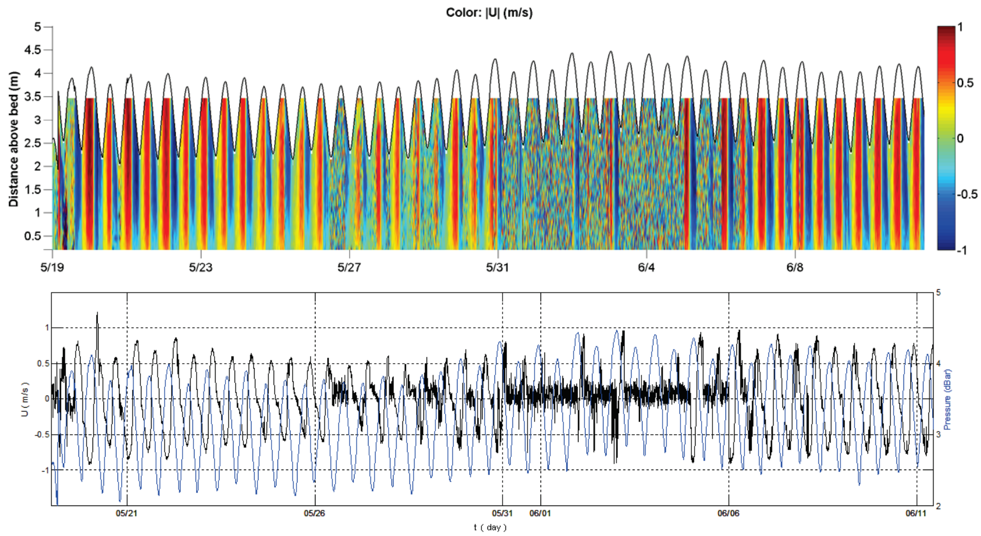

Figure 80: Depth varying velocity (in m/s) [upper subplot], and depth averaged velocity and pressure (in dBar, blue line) [lower subplot] for segment 2 (location E)

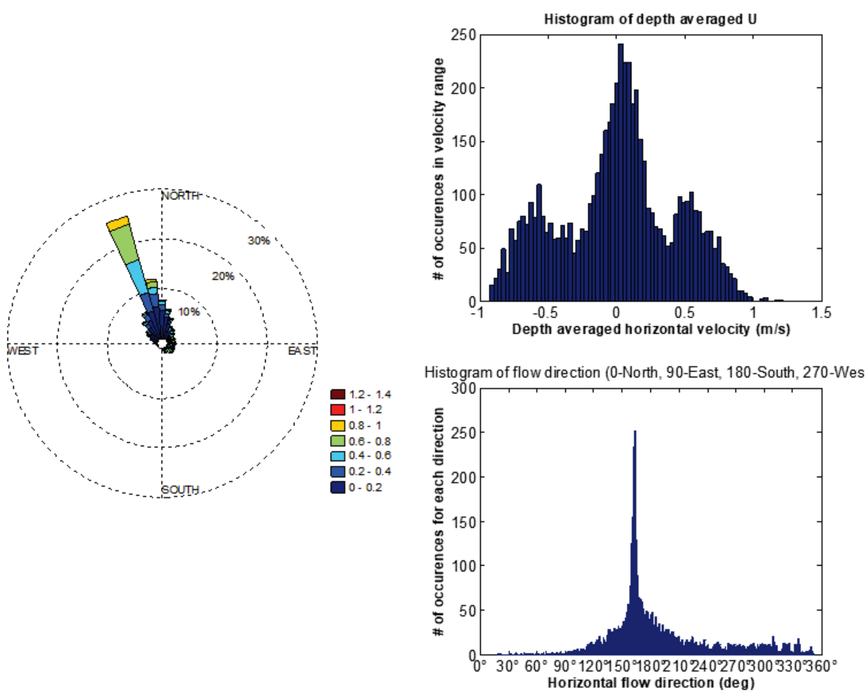

Figure 81: Direction and magnitude of depth averaged velocity (in m/s) [on the left], Histogram of the flow velocity and direction [on the right] for segment 2 (location E)

4 Bathymetric/topographic data

Bathy/topo data used in the project was taken from existing gridded LiDAR data sets. The sources for the data sets are described in Section 2 of Deb et al (2018) in conjunction with the development of the model DEM.

5 Survey data

Two types of surveys were carried out specifically to support the project. The first, described in section 5.1, consisted of point surveys on the marsh platform to aid in assessing the magnitude of vegetation bias in available LiDAR data. The second, described in section 5.2, consisted of single-point hydrographic surveying of the principle channels within the marsh complex, which are not subject to airborne LiDAR measurement due to water turbidity.

5.1 Marsh platform surveys

During the field campaign, 2432 scatter points along irregular transects were taken to have adequate number of points at different locations and vegetation species. The surveys were carried out using a GPS base station and rover station operating in RTK mode. The GPS system used was a Trimble R8 GNSS system. The elevation of channel berms determines the threshold for inundation during high water, and wet and drying pattern of the salt marsh. As a result, these points are of interest for the modeling work. Therefore, we extended the transects down the creek banks to the water. For that reason, the so called bare category for these points located at channel berms would have a wide range of elevations. Depends on the time of LiDAR acquisition, the break-lines associated with the hydro data could be problematic because the system is dynamic and the data would be missing in LiDAR dataset. Moreover, the method of minimum bin gridding needs adequate scatter points in LiDAR dataset , within 10 meter radius, that were influenced by the water body. Our study is to investigate the bias present in the LiDAR datasets due to vegetation density in the coastal salt marsh, and not the overall quality of the DEMs, which takes into account decisions on where water bodies are digitized, methodology on hydro-flattening, inland lakes/ponds vs coastaly-connected water bodies, etc. After removing the points close to the water bodies, we arrive to a total of 1484 scatter points. A map of the points is shown in Figure 82.

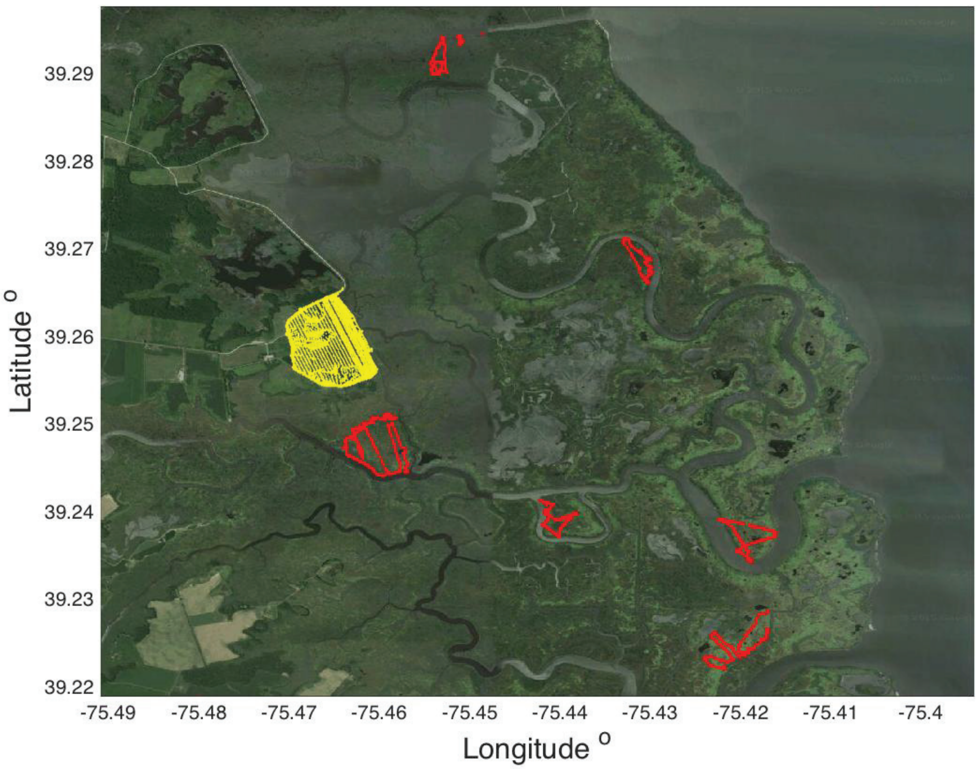

Figure 82: Marsh elevation survey track lines. Here, red represents survey points on the open marsh platform and yellow represents on marsh enclosed by impoundments. Data set filename: marsh_survey.csv and column header in the .csv file:
Longitude (dec deg) | Latitude (dec deg) | Depth (m) | Longitude (UTM) | Latitude (UTM) | Zone

The RTK base station location must be known to sub-meter accuracy. In this study, the accuracy of ground truth survey at the beginning and end of each mission are validated at two benchmarks. The GPS receivers use timing signals from at least four satellites to establish a position with acceptable PDOP to obtain a GPS position (PDOP is Position Dilution of Precision). The satellites are so far out in space that the little distances we travel here on earth are insignificant. So if two receivers are fairly close to each other, say within a few hundred kilometres, the signals that reach both of them will have travelled through virtually the same slice of atmosphere, and so will have virtually the same errors. In general, all recording intervals should be set to 10 seconds, PDOP = 6, and choose a WGS-84 datum. Each of those timing signals is going to have some error or delay depending on what sort of perils have befallen it on its trip down to us. The differential

GPS have one receiver, measure the timing errors and then provide correction information to the other receivers that are roving around. The receiver transmits this encoded error information to the roving receiver so it can use it to correct its measurements. Error transmissions not only include the timing error for each satellite, they also include the rate of change of that error as well. The reference station receives the same GPS signals as the roving receiver but instead of working like a normal GPS receiver it attacks the equations backwards. Instead of using timing signals to calculate its position, it uses its known position to calculate timing. It figures out what the travel time of the GPS signals should be, and compares it with what they actually are. The difference is an "error correction" factor.

The RTK equipment depends on radio broadcasts from the base station to the rover backpack. These radio signals do not travel well through thick vegetation or around steep hills. In our study area and at remote distances, an independent radio repeater was set up in the field to pick up the base station radio signal and re-broadcast the signal to the rover receiver. Set up the repeater radio assures that we have a direct line of sight to the base station, and also to the field area where we do a survey on marsh platform in connection with the rover receiver. Before each mission, we conducted a survey to make sure all you have all the required equipment, verify that all equipment is functioning and that all batteries are fully charged.

In order to cover a wide range of vertical elevation and also to make the missions possible, we did the survey during low tide. The channel side points can be used for checking the overlapped points with the bathymetric survey. We surveyed predefined spots in Bombay Hook area and measured the elevation and horizontal coordinates along transects which covers the channels side, bars and berms and marsh platform. One reason for having surveyed points in different areas was to have a better representation of vegetation types and also checking the LiDAR bias dependency on geographical location. All the surveys were done by at least 2 surveyors. One should calibrate the pole and the other one should operate the Trimble Data Collector and do averaging. At each point, we averaged the vertical elevation and horizontal coordinates for 10 s. An accompanying biologist defined the vegetation type for each point. At the end of each mission, we downloaded the data from Trimble Data Collector 1 (TDC1) and the rover file from the receiver to a laptop computer with the TRIMMAP software and saved in a .csv file.

5.2 Survey of marsh channels

Bathymetric surveys of the main waterways in BHNWR were conducted to obtain continuous depth soundings of the bottom below tide level, to be combined with existing LiDAR topography to create a seamless digital elevation model (DEM) for use with the hydrodynamic model described in Deb et al (2018).

A dual-frequency (200kHz/28kHz), single-beam echosounder (Knudsen 320 B/P) interfaced with a Leica MX 400 GPS system and a Trimble R8 GPS receiver was used to collect the soundings. The echosounder and GPS were set up on the boat at the refuge at the beginning of the surveying campaign, and tested in the water at the beginning of each day of work. The survey was designed to maximize coverage of the bottom, while minimizing the amount of boat time (and costs) required to map the survey area. The survey consisted of along- and cross-channel vessel tracklines spaced more-or-less equidistantly. A map of the executed tracklines is shown in Figure 83.

Upon completion of the survey, the raw bathymetric soundings were processed using Caris HIPS/SIPSTM hydrographic software. The soundings were evaluated for outliers and then referenced to horizontal and vertical datums. Initially, the controlling horizontal datum was Universal Transverse Mercator (UTM) Zone 18 North projection. Because the soundings were made by boat on a tidally fluctuating surface, they were tide-corrected after the work in Caris to a uniform tidal datum using tide-gauge data available for BHNWR. Later, after the dataset as a whole is inspected, the soundings were converted to the NAVD 88 datum for gridding with LiDAR data.

Based on prior survey work using this instrumentation and vessel set up, the estimated horizontal accuracy of the soundings is less than 50 cm, whereas the vertical accuracy is about 40-56 cm. The vertical uncertainty of bathymetric soundings is a combination of vertical datum errors, tidal measurement errors, vertical positioning system errors, instrumental errors, sound velocity errors, vessel motion errors, vessel settlement and squat, ellipsoidal/vertical datum separation model errors, and time synchronization (IHO, 2008). To account for these errors, the vertical uncertainty of the soundings was evaluated empirically using the cross-line check method described in the USACE Hydrographic Surveying Manual (USACE, 2002). To accomplish this, cross-line points (at the intersections of the along- and cross-channel tracklines) were extracted from the soundings dataset using the Caris HIPS/SIPSTM subset editor, and the mean of the differences and standard deviation of the cross-line check points will be used to calculate the error limits for depth accuracy (95% confidence level). An uncertainty of ±40 cm falls below the allowable level stipulated by USACE and the National Ocean Service (0.5-1.0 m for water depths less than 100 m), and is considered acceptable for coastal waterways.

Here, we have shown a hierarchy of the files collected from channel survey and shared on the project drive. Please read the **Bathymetry_readme.docx** file for the detailed description.

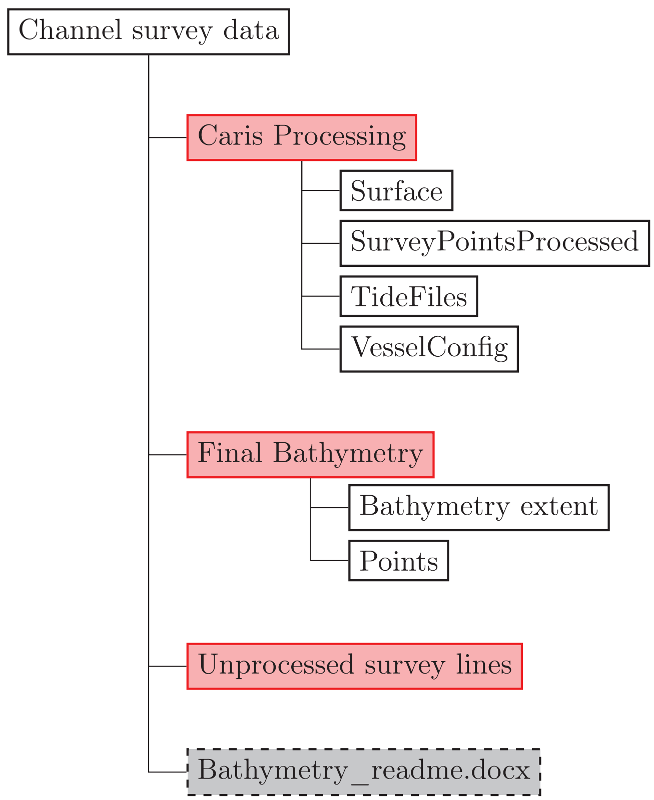

Figure 83: Bathymetric survey track lines

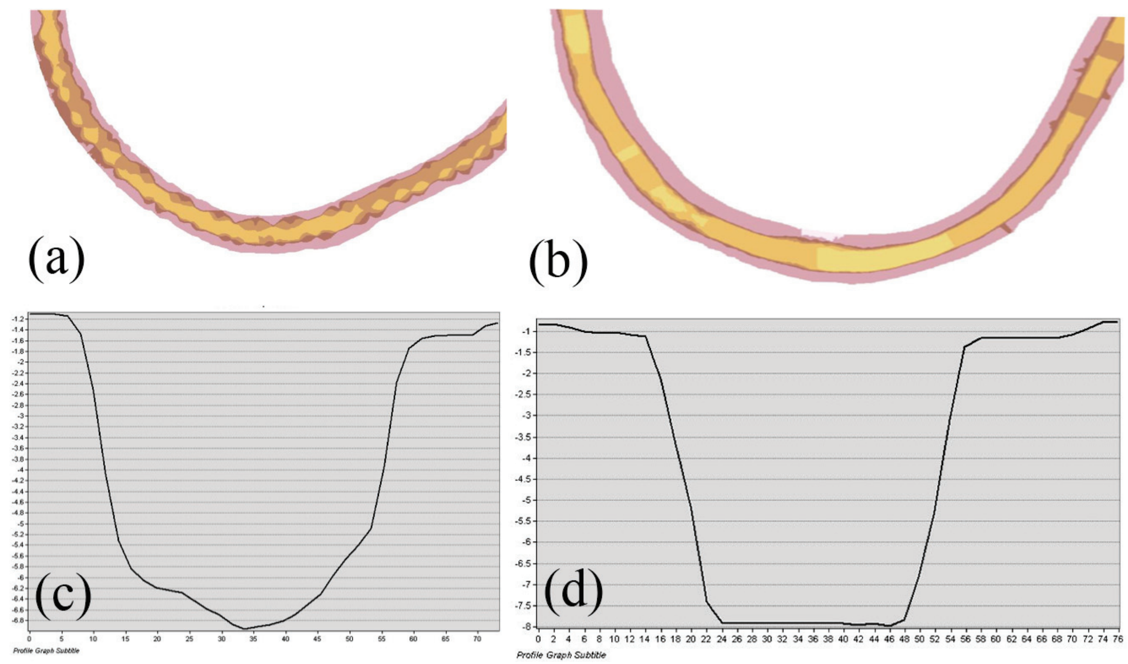

Figure 84: Original bathymetric data: a) Horizontal view, c) transect; Modified bathymetric data b) Horizontal view, d) transect

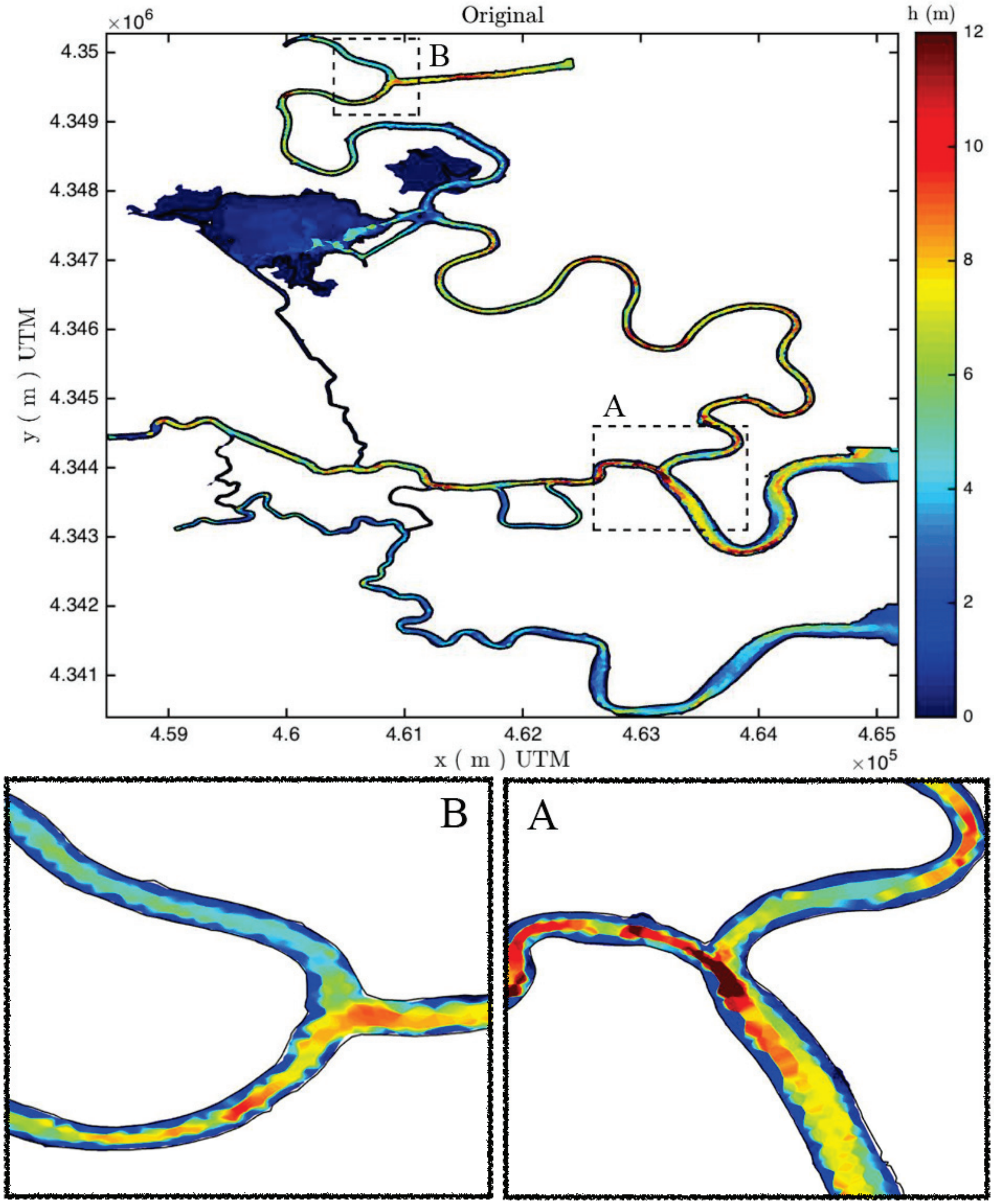

Figure 85: Original Bathymetric data, interpolated within channel boundaries

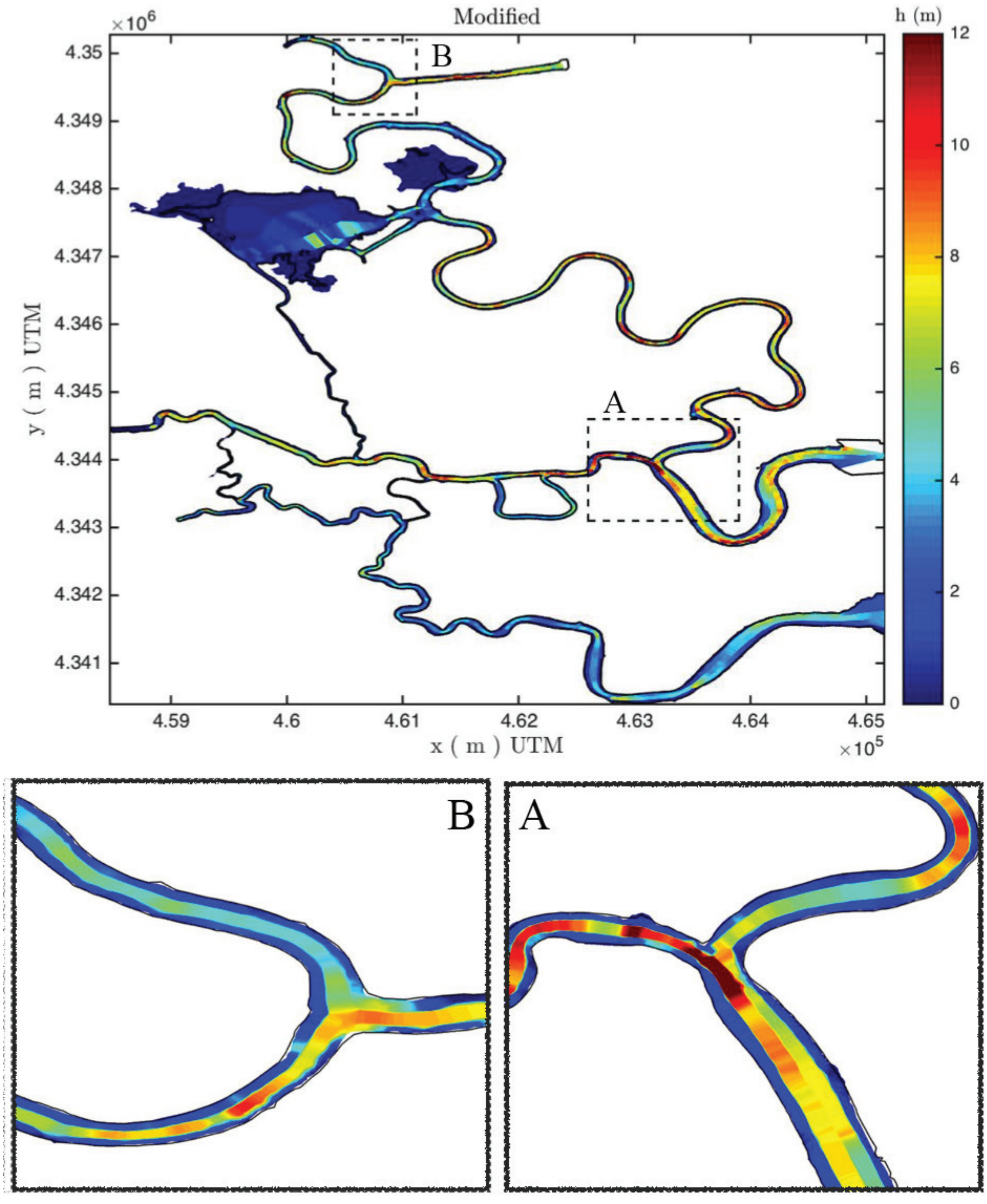

Figure 86: Modified Bathymetric data, interpolated within channel boundaries

6 Sediment coring and accretion analysis.

The collection of sediment cores and tabulated results of core analysis are presented separately in McDowell (2017). The reader is referred to that document for the full description.

A Technical specifications of Onset Hobo tide gauge

The basic features of an HOBO gauges are mentioned here from the instrument documentation website (http://www.onsetcomp.com/products/data-loggers/u20-001-01):

Pressure and Water Level Measurements

Water Level Accuracy: ± 0.05 FS, 0.5 cm (0.015 ft) water

Maximum error: ± 0.1 FS, 1.0 cm (0.03 ft) water

Raw Pressure Accuracy: ± 0.3 FS, 0.62 kPa (0.09 psi) maximum error

Resolution: ≤ 0.02 kPa (0.003 psi), 0.21 cm (0.007 ft) water

Temperature Measurements

Raw temperature Accuracy: ± 0.44°C from 0°to 50°C (± 0.79°F from 32°to 122°F)

Resolution: 0.10°C at 25°C (0.18°F at 77°F)

File type collected at Hobo 1 (39.247685 -75.464983) from May to July, 2015:

`Hobo1July23.csv`

The file has pressure data recorded at every 5 minutes. Column header in the .csv file:

Time | Pressure Data (kPa) | Temperature (°C)

* The first columns in all the time series are Matlab time, so to see the date, use: formatOut = 'mmmm-dd-yyyy HH:MM:SS'; datestr(766666666...)

B Technical specifications of RBRsolo wave gauge

The basic features of an RBRsolo are mentioned here from the instrument documentation website (https://rbr-global.com/products/compact-loggers/compact-tide-wave):

Temperature Sensor

1. Range: -5°C to 35°C
2. Initial accuracy: ± 0.002°C
3. Resolution: ≤ 0.00005°C

Pressure (Depth) Sensor

1. Range OSP: 20 / 50m (dbar)
2. Initial accuracy: ± 0.05
3. Resolution: ≤ 0.001

File type collected at location RBR 1 (39.271750, -75.4837) from April to May, 2015:

`RBR1_20150423.mat`

The file has pressure data recorded at a rate of 16 Hz. Column header in the .mat file:

Time | Pressure Data (dBar) | Temperature (°C)

* The first columns in all the time series are Matlab time, so to see the date, use: formatOut = 'mmmm-dd-yyyy HH:MM:SS'; datestr(766666666...)

C Technical specifications of Aquadopp current profiler

Some basic features of an Aquadopp HR-Profiler are mentioned here from the instrument documentation website (http://nortekusa.com/usa/products/current-profilers/aquadopp-hr-profiler):

1. Measures 3D velocity profiles with 1 – 5 cm vertical resolution.

2. Can sample in continuous mode (1 Hz) or burst mode (max 8 Hz).

3. Extended velocity range mode for use in energetic environments.

4. Software-configurable number of beams to sample: 1, 2 or 3.

5. Blanking distance reduced to 3 – 5 cm.

6. Measures to within a few cm from the bottom in down-looking mode.

7. Recording of data to internal recorder (352 MB) for stand-alone use.

8. Accuracy: 1% of measured value ±0.5 cm/s

Files types collected from location A (Sluice Ditch):

AquaA_20150612.dep; AquaA_20150612.txt; AquaA_20150612.a1; AquaA_20150612.a1; AquaA_20150612.a
AquaA_20150612.csv; AquaA_20150612.dat; AquaA_20150612.hdr; AquaA_20150612.nmea; AquaA_20150612.p
AquaA_20150612.sen; AquaA_20150612.ssl; AquaA_20150612.v1; AquaA_20150612.v2; AquaA_20150612.v3;

File column header (AquaA_20150612.csv):

DateTime | Battery | Heading | Pitch | Roll | Pressure | Temperature | AnalogIn1 | AnalogIn2 | Speed | Dir

* The first columns in all the time series are Matlab time, so to see the date, use: formatOut = 'mmmm-dd-yyyy HH:MM:SS'; datestr(766666666...)

References

Deb M, Abdolali A, Kirby JT, Shi F (2018) Hydrodynamics, sediment transport and wind waves in an eroding salt marsh environment. Bombay Hook National Wildlife Refuge, Delaware. Research Report CACR-18-04, Center for Applied Coastal Research, Department of Civil and Environmental Engineering, University of Delaware, Newark, DE

McDowell C (2017) Marsh sediment accumulation and accretion on a rapidly retreating estuarine coast. Ms, University of Delaware